Crystalline color superconductors

Roberto Anglani[*]

Institute of Intelligent Systems for Automation, National Research Council, CNR-ISSIA, Via Amendola 122/D-O, I-70126 Bari, Italy

Roberto Casalbuoni[†]

Department of Physics, University of Florence and INFN Via G. Sansone 1, 50019 Sesto Fiorentino (FI), Italy

Marco Ciminale[‡]

Ministero dell'Istruzione, dell'Università e della Ricerca (MIUR), Viale Trastevere 76/a, 00153 Roma, Italy

Nicola Ippolito[§]

INFN, Sezione di Bari, Via E. Orabona 4, 70126 Bari, Italy

Raoul Gatto[‖]

Departement de Physique Theorique, Universite de Geneve, CH-1211 Geneve 4, Switzerland

Massimo Mannarelli[¶]

INFN, Laboratori Nazionali del Gran Sasso, Via G. Acitelli 22, 67100 Assergi (AQ), Italy

Marco Ruggieri[**]

Department of Physics and Astronomy, University of Catania, Via S. Sofia 64, I-95125 Catania, Italy

(published 30 April 2014)

Inhomogeneous superconductors and inhomogeneous superfluids appear in a variety of contexts including quark matter at extreme densities, fermionic systems of cold atoms, type-II cuprates, and organic superconductors. In the present review the focus is on properties of quark matter at high baryonic density, which may exist in the interior of compact stars. The conditions realized in these stellar objects tend to disfavor standard symmetric BCS pairing and may favor an inhomogeneous color superconducting phase. The properties of inhomogeneous color superconductors are discussed in detail and in particular of crystalline color superconductors. The possible astrophysical signatures associated with the presence of crystalline color superconducting phases within the core of compact stars are also reviewed.

DOI: 10.1103/RevModPhys.86.509 PACS numbers: 12.38.−t, 21.65.Qr, 97.60.Jd, 74.20.−z

CONTENTS

[*]anglani@ba.issia.cnr.it
[†]casalbuoni@fi.infn.it
[‡]marco.ciminale@ba.infn.it
[§]nicola.ippolito@ba.infn.it
[‖]Raoul.Gatto@unige.ch
[¶]massimo@lngs.infn.it
[**]marco.ruggieri@lns.infn.it

I. INTRODUCTION

Ideas about color superconducting (CSC) matter date back to more than 30 years ago (Collins and Perry, 1975; Barrois, 1977; Frautschi, 1978; Bailin and Love, 1984), but this phenomenon has only recently received a great deal of consideration [for recent reviews, see Hsu (2000), Rajagopal and Wilczek (2000), Alford (2001), Hong (2001), Nardulli (2002), Schafer (2003b), Rischke (2004), and Alford *et al.* (2008)]. Color superconductivity is the quark matter analog of the standard electromagnetic superconductivity and is believed to be the ground state of hadronic matter at sufficiently large baryonic densities. At very high density the naive expectation, due to asymptotic freedom, is that quarks form a Fermi sphere of almost free fermions. However, Bardeen, Cooper, and Schrieffer (BCS) (Cooper, 1956; Bardeen, Cooper, and Schrieffer, 1957a, 1957b) have shown that the Fermi surfaces of free fermions are unstable in presence of an attractive, arbitrary small, interaction between fermions. In quantum chromodynamics (QCD) the attractive interaction between quarks can be due to instanton exchange (Schafer and Shuryak, 1998), at intermediate densities, or to gluon exchange in the $\bar{3}$ color channel, at higher densities. Therefore, one expects that at high densities quarks form a coherent state of Cooper pairs.

It should be noted that the older papers (Collins and Perry, 1975; Barrois, 1977; Frautschi, 1978; Bailin and Love, 1984) were based on the existence of the attractive $\bar{3}$ color channel and on analogies with ordinary superconductors. The main result of these analyses was that quarks form Cooper pairs with a gap of order a few MeV. In more recent times two papers (Rapp *et al.*, 1998; Alford, Rajagopal, and Wilczek, 1998) have brought this result to question. They considered diquark condensation arising from instanton-mediated interactions and although their approximations are not under rigorous quantitative control, the result was that gaps can be as large as 100 MeV.

Color superconductivity offers a clue to the behavior of strong interactions at very high baryonic densities, an issue of paramount relevance for the understanding of the physics of compact stars and of heavy ion collisions. In the asymptotic regime it is possible to understand the structure of the quark condensate from basic considerations. Consider the matrix element

$$\langle 0|\psi^{\alpha}_{is}\psi^{\beta}_{jt}|0\rangle, \tag{1}$$

where ψ^{α}_{is}, ψ^{β}_{jt} represent the quark fields, and $\alpha,\beta = 1,2,3$, $s,t = 1,2$, $i,j = 1,\ldots,N_f$ are color, spin, and flavor indices, respectively. For a sufficiently large quark chemical potential μ, assuming the orbital angular momentum state be in a s wave, the color, spin, and flavor structure can be completely fixed by the following arguments:

- Antisymmetry in color indices (α,β) in order to have attraction.
- Antisymmetry in spin indices (s,t) in order to have a spin zero condensate.
- Given the structure in color and spin, Fermi statistics requires antisymmetry in flavor indices.

The isotropic structure of the condensate with vanishing total angular momentum is favored with respect to higher spin or higher orbital angular momentum condensates because a larger portion of the phase space around the Fermi surface is available for pairing. Since the quark spin and momenta in the pair are opposite, it follows that the left- (right-) handed quarks can pair only with left- (right-) handed quarks. Considering three-flavor quark matter at large baryonic density, the so-called color-flavor locked (CFL) phase (Alford, Rajagopal, and Wilczek, 1999) turns out to be thermodynamically favored, with condensate

$$\langle 0|\psi^{\alpha}_{iL}\psi^{\beta}_{jL}|0\rangle = -\langle 0|\psi^{\alpha}_{iR}\psi^{\beta}_{jR}|0\rangle \propto \Delta_{\mathrm{CFL}}\sum_{I=1}^{3}\varepsilon^{\alpha\beta I}\epsilon_{ijI}, \tag{2}$$

where Δ_{CFL} is the pairing gap and $\varepsilon^{\alpha\beta\gamma}$ and ϵ_{ijk} are the completely antisymmetric Levi-Civita symbols in color and flavor space, respectively. We have suppressed spinorial indices and neglected pairing in the color sextet channel. Pairing in the color sextet channel is automatically induced by the quark color structure (Alford, Berges, and Rajagopal, 1999; Alford, Rajagopal, and Wilczek, 1999), but the condensate in this channel is much smaller than in the color

antitriplet channel (Shovkovy and Wijewardhana, 1999; Schafer, 2000a) and in most cases it can be neglected (Rajagopal and Wilczek, 2000).

The reason behind the name "color-flavor locked" is that only simultaneous transformations in color and in flavor spaces leave the condensate invariant. The corresponding symmetry breaking pattern is, indeed, the following:

$$\mathrm{SU}(3)_c \otimes \mathrm{SU}(3)_L \otimes \mathrm{SU}(3)_R \otimes \mathrm{U}(1)_B \rightarrow \mathrm{SU}(3)_{c+L+R} \otimes Z_2, \tag{3}$$

where $\mathrm{SU}(3)_{c+L+R}$ is the diagonal global subgroup of the three SU(3) groups and the Z_2 group means that the quark fields can still be multiplied by -1. According to the symmetry breaking pattern, the 17 generators of chiral symmetry, color symmetry, and $\mathrm{U}(1)_B$ symmetry are spontaneously broken. The 8 broken generators of the color gauge group correspond to the 8 longitudinal degrees of freedom of the gluons and according to the Higgs-Anderson mechanism these gauge bosons acquire a Meissner mass. The diquark condensation induces a Majorana-like mass term in the fermionic sector which is not diagonal in color and flavor indices. Thus, the fermionic excitations consist of gapped modes with mass proportional to Δ_{CFL}. (This is a feature of all homogeneous superconducting phases: the fermionic excitations which are charged with respect to the condensate acquire a Majorana-like mass term proportional to the pairing gap.) The low-energy spectrum consists of 9 Nambu-Goldstone bosons (NGB) organized in an octet, associated with the breaking of the flavor group, and in a singlet, associated with the breaking of the baryonic number. For nonvanishing quark masses the octet of NGBs becomes massive, but the singlet NGB is protected by the $\mathrm{U}(1)_B$ symmetry; it remains massless and determines the superfluid properties of the CFL phase. The effective theory describing the NGBs for the CFL phase has been studied in Casalbuoni and Gatto (1999), Son and Stephanov (2000a), and Son (2002). The CFL condensate also breaks the axial $\mathrm{U}(1)_A$ symmetry; given that at very high densities the explicit axial symmetry breaking is weak, one has to include the corresponding pseudo-NGB in the low-energy spectrum.

After the first attempts with instanton-induced interaction many tried various approaches for calculating the magnitude of the gap parameters in the CSC phases [for references see Rajagopal and Wilczek (2000)]. Dealing with QCD, the ideal situation would be if this kind of calculation could fall within the scope of lattice gauge theories. Unfortunately, lattice methods rely on Monte Carlo sampling techniques that are unfeasible at finite density because the fermion determinant becomes complex. Although various approximation schemes have been developed, for instance, Taylor expansion in the chemical potential (Allton *et al.*, 2003), reweighing techniques (Fodor and Katz, 2002), analytical continuation of calculation employing imaginary baryonic chemical potential (Roberge and Weiss, 1986; Alford, Kapustin, and Wilczek, 1999), or heavy Wilson quarks (Fromm *et al.*, 2012), no definite results have been obtained so far for large values of the baryonic chemical potential and physical quark masses.

In the absence of suitable lattice methods, quantitative analyses of color superconductivity have followed two distinct paths. The first path is semiphenomenological, and based on simplified models. The main feature of these models is that they should incorporate the most important physical effects while being at the same time tractable within present mathematical techniques. All these models have free parameters that are adjusted to give rise to a reasonable vacuum physics.

Examples of these kinds of techniques include Nambu-Jona–Lasinio (NJL) models in which the interaction between quarks is replaced by a four-fermion interaction originating from instanton exchange (Alford, Rajagopal, and Wilczek, 1998; Rapp *et al.*, 1998; Berges and Rajagopal, 1999) or where the four-fermion interaction is modeled by that induced by single-gluon exchange (Alford, Rajagopal, and Wilczek, 1998; Alford, Berges, and Rajagopal, 1999). Random matrix models have been studied by Vanderheyden and Jackson (2000) and instanton liquid models have been investigated by Carter and Diakonov (1999), Rapp *et al.* (2000), and Rapp, Shuryak, and Zahed (2001). Although none of these methods has a firm theoretical basis, all of them yield results in fairly qualitative agreement. This is probably due to the fact that what really matters is the existence of an attractive interaction between quarks and that the parameters of the various models are chosen in such a way to reproduce the chirally broken ground state. The gap parameter evaluated within these models varies between tens of MeV up to 100 MeV. The critical temperature is typically the same found in normal superconductivity, that is about one-half of the gap.

The second path starts from first principles and relies on the property of asymptotic freedom of QCD. Various results have been obtained starting from the QCD action, employing renormalization group techniques, or through the Schwinger-Dyson equation (Evans, Hsu, and Schwetz, 1999; Schafer and Wilczek, 1999b, 1999c; Son, 1999; Brown, Liu, and Ren, 2000; Evans *et al.*, 2000; Hong *et al.*, 2000; Pisarski and Rischke, 2000a). In particular, Son (1999), using the renormalization group near the Fermi surface obtained the asymptotic form of the gap and corrections have been evaluated by Brown, Liu, and Ren (2000).

The result of the above-mentioned methods is that the CFL phase is the thermodynamically favored state of matter at asymptotic densities. Qualitatively one can understand this result considering that in the CFL phase quarks of all three flavors participate coherently in pairing. Since superconductivity is a cooperative phenomenon, the larger the number of fermions that participate in pairing, more energetically favored is the superconducting phase.

In the description of color superconductivity one has to deal with various scales, the chemical potential μ, the gap parameter, which we generically indicate with Δ, the constituent strange quark mass M_s, and the screening or damping scale $g_s\mu$, where g_s is the QCD coupling. One typically has that $\mu \gg g_s\mu \gg \Delta$, whereas the strange quark mass can be considered as a free parameter, although in some models it can be computed self-consistently.

Quantum chromodynamics at high density is conveniently studied through a hierarchy of effective field theories, schematically depicted in Fig. 1. The starting point is the

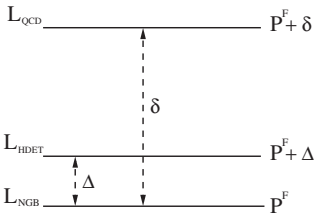

FIG. 1. Schematic representation of the hierarchy of effective Lagrangians characteristic of high-density QCD.

fundamental QCD Lagrangian, then one can obtain the low-energy effective Lagrangian through different methods. One way is to integrate out high-energy degrees of freedom as shown by Polchinski (1992). The physics is particularly simple for energies close to the Fermi energy where all interactions are irrelevant except for a four-fermion interaction coupling pair of fermions with opposite momenta. This is nothing but the interaction giving rise to BCS condensation, which can be described using the high-density effective theory (HDET) (Beane, Bedaque, and Savage, 2000; Hong, 2000a, 2000b; Casalbuoni, Gatto, and Nardulli, 2001; Nardulli, 2002; Schafer, 2003a). The HDET is based on the fact that at vanishing temperature and large chemical potentials antiparticle fields decouple and the only relevant fermionic degrees of freedom are quasiparticles and quasiholes close to the Fermi surface. In the HDET Lagrangian the great advantage is that the effective fermionic fields have no spin structure and therefore the theory is particularly simple to handle.

This description is supposed to hold up to a cutoff $P^F + \delta$, with δ smaller than the Fermi momentum P^F, but bigger than the gap parameter, i.e., $\Delta \ll \delta \ll P^F$. Considering momenta much smaller than Δ all gapped particles decouple and one is left with the low-energy modes as NGBs, ungapped fermions and holes, and massless gauge fields according to the symmetry breaking scheme. In the case of CFL and other CSC phases, such effective Lagrangians have been derived by Casalbuoni and Gatto (1999), Casalbuoni, Duan, and Sannino (2000), and Rischke, Son, and Stephanov (2001). The parameters of the effective Lagrangian can be evaluated at each step of the hierarchy by matching the Green's functions with the ones evaluated at the upper level. For the CFL phase the effective Lagrangian of the superfluid mode associated with the breaking of $\mathrm{U}(1)_B$ may also be determined by symmetry arguments alone as done by Son (2002).

In the high-density limit one neglects the quark masses, and the CFL is believed to be the favored phase. On the other hand, considering a quark chemical potential of the same order of magnitude of the strange quark mass tends to disfavor the CFL pairing. The reason is that the typical effect of quark masses is to produce a mismatch between Fermi surfaces. Neglecting light quark masses and assuming, for simplicity, that quarks have all the same chemical potentials, the Fermi spheres have different radii

$$P_s^F = \sqrt{\mu^2 - M_s^2}, \qquad P_u^F = P_d^F = \mu. \tag{4}$$

Thus, increasing M_s for a fixed value of μ increases the mismatch between the Fermi surface of strange quarks and the Fermi surfaces of up and down quarks (which in this simplistic case are equal).

The standard BCS mechanism assumes that the Fermi momenta of the fermionic species that form Cooper pairs are equal. When there is a mismatch it is not guaranteed that BCS pairing takes place, because the condensation of fermions with different Fermi momenta has a free energy cost. As first shown for weakly interacting two-level systems (Chandrasekhar, 1962; Clogston, 1962), for mismatches below the Chandrasekhar-Clogston (CC) limit there is still condensation and in the case at hand it means that the CFL phase is favored. However, for large values of the strange quark mass the assumptions leading to prove that the favored phase is CFL should be reconsidered. According to Eq. (4) if the strange quark mass is about the quark chemical potential, then strange quarks decouple, and the corresponding favored condensate should consist of only up and down quarks. With only two flavors of quarks, and due to the antisymmetry in color, the condensate must necessarily choose a direction in color space and one possible pairing pattern is

$$\langle 0|\psi_{iL}^{\alpha}\psi_{jL}^{\beta}|0\rangle = -\langle 0|\psi_{iR}^{\alpha}\psi_{jR}^{\beta}|0\rangle \propto \Delta_{2\mathrm{SC}}\varepsilon^{\alpha\beta 3}\epsilon_{ij3},$$
$$\alpha,\beta \in \mathrm{SU}_c(2) \qquad i,j \in \mathrm{SU}(2)_L. \tag{5}$$

This phase of matter is known as two-flavor color superconductor (2SC) and $\Delta_{2\mathrm{SC}}$ is the corresponding gap parameter. This phase is characterized by the presence of two ungapped quarks q_{ub}, q_{db} and four gapped quasiparticles given by the combinations $q_{dr} - q_{ug}$ and $q_{ur} - q_{dg}$ of the quark fields, where the color indices of the fundamental representation 1, 2, 3 have been identified with r, g, b (red, green, and blue). In case massive strange quarks are present the corresponding phase is named 2SC + s and eventually strange quarks may by themselves form a spin-1 condensate (Pisarski and Rischke, 2000b).

In the 2SC phase the symmetry breaking pattern is completely different from the three-flavor case and it turns out to be

$$\mathrm{SU}(3)_c \otimes \mathrm{SU}(2)_L \otimes \mathrm{SU}(2)_R \otimes \mathrm{U}(1)_B$$
$$\to \mathrm{SU}(2)_c \otimes \mathrm{SU}(2)_L \otimes \mathrm{SU}(2)_R \otimes \mathrm{U}(1)_{\tilde{B}} \otimes Z_2. \tag{6}$$

The chiral group remains unbroken, meaning that there are no NGBs. The original color symmetry group is broken to $\mathrm{SU}(2)_c$ and since three color generators are unbroken, only five gluons acquire a Meissner mass. Even though $\mathrm{U}(1)_B$ is spontaneously broken there is an unbroken $\mathrm{U}(1)_{\tilde{B}}$ global symmetry, with $\tilde{B}$ given by a combination of B and of the eighth color generator, playing the same role of the original baryonic number symmetry. In particular, this means that unlike CFL matter, 2SC matter is not superfluid. One can construct an effective theory describing the emergence of the unbroken subgroup $\mathrm{SU}(2)_c$ and the low-energy excitations, much in the same way as one builds a chiral effective Lagrangian with effective fields at zero density. This development can be found in Casalbuoni, Duan, and Sannino (2000) and Rischke, Son, and Stephanov (2001).

The CFL phase and the 2SC phase have been the first phases to be proposed and have been extensively studied. These are homogeneous phases, meaning that the condensate is not space dependent. The arising of inhomogeneous condensates for imbalanced Fermi momenta in quark matter has only lately attracted the interest of the high-energy community. Actually, this is quite a general problem arising not only in high-density QCD but also in condensed matter systems and in ultracold atom systems. There are several similarities between these systems; see Casalbuoni and Nardulli (2004) for a review and discussion of two-flavor QCD with imbalanced Fermi momenta. In the present review we focus on high-density QCD giving a detailed and self-contained presentation of the various properties of two- and three-flavor quark matter with mismatched Fermi spheres.

Studying the pairing mechanisms of quark matter in systems with mismatched Fermi spheres is relevant when considering realistic conditions, i.e., conditions that can be realized in a compact stellar object (CSO). This is a real possibility since the central densities for these stars is very large, conceivably reaching 10^{15} g/cm^3, whereas the temperature is of the order of tens of keV, much less than the critical temperature for color superconductivity. The various processes taking place in CSOs produce a more complicated mismatch than the one presented in Eq. (4). The reason is that matter inside a CSO should be electrically neutral, in β equilibrium and in a color singlet state. If electrons are present (as generally required by electrical neutrality), the β-equilibrium condition forces the chemical potentials of quarks with different electric charges to be different. As far as color is concerned, it is possible to impose a simple condition, that is color neutrality, because in Amore *et al.* (2002) it has been shown (in the two-flavor case) that there is a small free energy cost in projecting color singlet states out of color neutral ones. Since the condensate is in general not diagonal in color indices, the requirement of color neutrality determines a mismatch between the chemical potentials of quarks with different colors. Thus, the effect of the strange quark mass, β equilibrium, and color and electric neutrality is to produce a stress on the Fermi spheres of quarks with different flavor and color, trying to pull them apart. If the stress is sufficiently large the CFL phase cannot be realized, but condensation can still take place in different channels, depending on the parameters of the system. Besides the above-mentioned standard 2SC and 2SC + s phases, the two-flavor superconducting phase 2SCus, with pairing between up and strange quarks, can be favored; see, e.g., Iida *et al.* (2004) and Ruester *et al.* (2006a) for different pairing patterns. For very large mismatches among the three flavors of quarks only the interspecies single-flavor spin-1 pairing may take place (Bailin and Love, 1979; Alford, Rajagopal, and Wilczek, 1998; Schafer, 2000b; Schmitt, Wang, and Rischke, 2002; Alford *et al.*, 2003; Buballa, Hosek, and Oertel, 2003; Schmitt, 2005); see, e.g., Alford *et al.* (2008) for an extended discussion on these topics.

In the 2SC phase, β-equilibrium and neutrality conditions tend to induce a chemical potential mismatch $\delta\mu$ between up and down quarks. A remarkable property is that for $|\delta\mu| = \Delta_{2SC}$ gapless fermionic modes appear and therefore the corresponding phase has been named g2SC (Huang and Shovkovy, 2003; Shovkovy and Huang, 2003), with "g" standing for gapless. The g2SC phase has the same condensate of the 2SC phase reported in Eq. (5), and consequently the ground states of the 2SC and g2SC phases share the same symmetry. However, these two phases have a different low-energy spectrum, due to the fact that in the g2SC phase only two fermionic modes are gapped. The g2SC phase is energetically favored with respect to the 2SC phase and unpaired quark matter in a certain range of values of the four-fermion interaction strength when one considers β equilibrium, color, and electrical neutrality (Shovkovy and Huang, 2003).

Pinning down the correct ground state of neutral quark matter in β equilibrium is not simple because another difficulty emerges. This problem, already present in simple two-level systems [see, e.g., Gubankova, Mannarelli, and Sharma (2010)] has a rather general character (Alford and Wang, 2005), and is due to an instability connected to the Meissner mass. For sufficiently large chemical potential differences, the system becomes *magnetically* unstable, meaning that the Meissner mass becomes imaginary. In the 2SC phase the color group is broken to $\mathrm{SU}(2)_c$ and five out of eight gluons acquire a mass. Four of these masses turn out to be imaginary in the 2SC phase for $\Delta_{2SC}/\sqrt{2} < \delta\mu < \Delta_{2SC}$, thus in this range of $\delta\mu$ the 2SC phase is *chromomagnetically* unstable (Huang and Shovkovy, 2004a, 2004b). Increasing the chemical potential difference the instability gets worse, because at the phase transition from the 2SC phase to the g2SC phase all five gluon masses become pure imaginary.

An analogous phenomenon arises in three-flavor quark matter in the gapless CFL (gCFL) phase (Alford, Kouvaris, and Rajagopal, 2004, 2005; Alford, Jotwani *et al.*, 2005; Fukushima, Kouvaris, and Rajagopal, 2005). The gapless color-flavor locked phase has been proposed as the favored ground state for sufficiently large mismatch between up, down and strange quarks and occurs in color and electrically neutral quark matter in β equilibrium for $M_s^2/2\mu \gtrsim \Delta_{CFL}$. However, this phase turns out to be chromomagnetically unstable (Casalbuoni, Gatto, Mannarelli *et al.*, 2005; Fukushima, 2005), because when gapless fermionic modes appear the Meissner masses of some gluons become imaginary.

Quite generally, the imaginary value of the Meissner mass can be understood as a tendency of the system toward an inhomogeneous phase (Hong, 2005; Iida and Fukushima, 2006; Gubankova, Mannarelli, and Sharma, 2010). This can be easily seen in a toy model system for the case of a $\mathrm{U}(1)$ symmetry, in which one can show that the coefficient of the gradient term of the low-energy fluctuations around the ground state of the effective action is proportional to the Meissner mass squared (Gubankova, Mannarelli, and Sharma, 2010).

There is a variety of solutions that have been proposed for the chromomagnetic instability and that can be realized depending on the particular conditions considered. As discussed, the chromomagnetic instability is a serious problem not only for the gapless phases (g2SC and gCFL) but also for the 2SC phase. In the latter case, the vector condensates of

gluons with a value of about 10 MeV can cure the instability (Fukushima, 2006; Gorbar, Hashimoto, Miransky, and Shovkovy, 2006; Gorbar, Hashimoto, and Miransky, 2006a; Kiriyama, Rischke, and Shovkovy, 2006, 2007). The corresponding phase has been named gluonic phase and is characterized by the nonvanishing value of some gluon condensates and the spontaneous breakdown of the color, electromagnetic, and rotational symmetries down to the SO(2) rotational symmetry. As discussed by Gorbar, Hashimoto, Miransky, and Shovkovy (2006) and Gorbar, Hashimoto, and Miransky (2007), the chromomagnetic instabilities of the 4–7th gluons and the 8th gluon might be related to two different phenomena. The 4–7th instability seems to indicate the Bose-Einstein condensation of a plasmon, which can be taken to be $\langle \boldsymbol{A}^6 \rangle$, inducing a nonvanishing value of $\langle \boldsymbol{A}^3 \rangle$ and $\langle A_0^3 \rangle$. On the other hand, the existence of gapless fermionic modes in the g2SC phase may indicate the existence of a $\langle \boldsymbol{A}^8 \rangle$ condensate. The chromomagnetic instability of the gapped 2SC phase can also be removed by the formation of an inhomogeneous condensate of charged gluons (Ferrer and de la Incera, 2007). The finite temperature case has been discussed by Kiriyama (2006) and He, Jin, and Zhuang (2007), finding that, in the weak and intermediate coupling regimes, the 2SC and g2SC phases are stabilized by temperatures of the order of tens of MeV.

For cases in which the chromomagnetic instability is related to the presence of gapless modes, Hong (2005) studied the possibility that a secondary gap opens at the Fermi surface. The solution of the instability is due to a mechanism that stabilizes the system preventing the appearance of gapless modes. This solution represents one of the few cases in which the instability may be cured by means of a different homogeneous condensate. However, the secondary gap turns out to be extremely small and at temperatures typical of CSOs it is not able to fix the chromomagnetic instability (Alford and Wang, 2006).

For three-flavor quark matter two inhomogeneous superconducting phases have been proposed. If kaon condensation takes place in the CFL phase (Bedaque and Schafer, 2002; Kaplan and Reddy, 2002), the chromomagnetic instability might drive the system toward an inhomogeneous state in which a kaon condensate current is generated, balanced by a counterpropagating current in the opposite direction carried by gapless quark quasiparticles. This phase of matter, named curCFL-K^0, has been studied by Kryjevski (2008) and turns out to be chromomagnetically stable.

The second possibility is the crystalline color superconducting (CCSC) phase (Alford, Bowers, and Rajagopal, 2001; Bowers *et al.*, 2001; Casalbuoni, Gatto, Mannarelli, and Nardulli, 2001; Leibovich, Rajagopal, and Shuster, 2001; Bowers and Rajagopal, 2002; Casalbuoni, Fabiano *et al.*, 2002; Casalbuoni, Gatto *et al.*, 2002a; Kundu and Rajagopal, 2002; Casalbuoni *et al.*, 2003; 2004; Casalbuoni, Gatto, Ippolito *et al.*, 2005; Mannarelli, Rajagopal, and Sharma, 2006), which is the QCD analog of a form of non-BCS pairing first proposed by Larkin, Ovchinnikov, Fulde, and Ferrell (LOFF) (Fulde and Ferrell, 1964; Larkin and Ovchinnikov, 1964). The condensate characteristic of this phase is given by

$$\langle 0|\psi_{iL}^{\alpha}\psi_{jL}^{\beta}|0\rangle = -\langle 0|\psi_{iR}^{\alpha}\psi_{jR}^{\beta}|0\rangle \propto \sum_{I=1}^{3} \Delta_I \varepsilon^{\alpha\beta I}\epsilon_{ijI} \sum_{\boldsymbol{q}_I^m \in \{\boldsymbol{q}_I\}} e^{2i\boldsymbol{q}_I^m \cdot \boldsymbol{x}}, \tag{7}$$

which is similar to the condensate reported in Eq. (2) but now there are three gap parameters, each having a periodic modulation in space. The modulation of the Ith condensate is defined by the vectors $\boldsymbol{q}_I^m$, where m is the index which identifies the elements of the set $\{\boldsymbol{q}_I\}$. In position space, this corresponds to condensates that vary as $\sum_m \exp(2i\boldsymbol{q}^m \cdot \boldsymbol{x})$, meaning that the $\boldsymbol{q}^m$'s are the reciprocal vectors which define the crystal structure of the condensate.

The case of two-flavor CCSC, first proposed by Alford, Bowers, and Rajagopal (2001), corresponds to the vanishing of all but one gap parameter in Eq. (7) and represents a candidate phase for curing the chromomagnetic instability in the two-flavor case. Indeed, the chromomagnetic stability of a simple two-flavor periodic structure with a gap parameter modulated by a single plane wave with wave vector $\boldsymbol{q}$ [hereafter we refer to this phase as Fulde-Ferrell (FF) structure (Fulde and Ferrell, 1964)] has been considered by Giannakis, Hou, and Ren (2005) and Giannakis and Ren (2005a, 2005b), where the following has been shown:

- The presence of the chromomagnetic instability in g2SC is exactly what one needs in order that the FF phase is energetically favored (Giannakis and Ren, 2005a).
- The FF phase in the two-flavor case has no chromomagnetic instability (though it has gapless modes) at least in the weak coupling limit (Giannakis, Hou, and Ren, 2005; Giannakis and Ren, 2005b).

The stability of the FF phase in the strong coupling case has been studied by Gorbar, Hashimoto, and Miransky (2006b), in which it is shown that for large values of the gap parameter the FF phase cannot cure the chromomagnetic instability. Nickel and Buballa (2009) questioned whether among the possible one-dimensional periodic modulations the LOFF solution is the favored one. According to Nickel and Buballa (2009), for two-flavor quark matter a solitonic ground state is favored with respect to FF in the range of values $0.7\Delta \lesssim \delta\mu \lesssim 0.78\Delta$. However, at least in weak coupling, the FF phase is not the crystalline structure one should compare to. The FF phase is slightly energetically favored with respect to unpaired quark matter and 2SC quark matter for $\Delta/\sqrt{2} < \delta\mu < 0.754\Delta$, but more complicated crystalline structures have larger condensation energies in a larger range of values of $\delta\mu$ (Bowers and Rajagopal, 2002).

The stability analysis of the three-flavor CCSC phase has only been performed for a simple structure made of two plane waves by a Ginzburg-Landau (GL) expansion (Ciminale *et al.*, 2006). This particular three-flavor CCSC phase turns out to be chromomagnetically stable, but the stability of more complicated crystalline structures has not been studied, although by general arguments they are expected to be stable, at least in the weak coupling limit.

Whether or not the crystalline color superconducting phase is the correct ground state for quark systems with mismatched Fermi surfaces has not been proven yet. In any case it represents an appealing candidate because in this phase quark

pairing has no energy cost proportional to $\delta\mu$. The reason is that pairing occurs between quarks living on their own Fermi surfaces. However, this kind of pairing can take place only if Cooper pairs have nonzero total momentum $2\boldsymbol{q}$ and therefore it has an energy cost corresponding to the kinetic energy needed for the creation of quark currents. Moreover, pairing can take place only in restricted phase space regions, meaning that the condensation energy is smaller than in the homogeneous phase. The vector $\boldsymbol{q}$ has a magnitude proportional to the chemical potential splitting between Fermi surfaces, whereas its direction is spontaneously chosen by the system. In case one considers structures composed by a set of vectors $\{\boldsymbol{q}_I\}$, one has to find the arrangement that minimizes the free energy of the system (Bowers and Rajagopal, 2002; Rajagopal and Sharma, 2006). This is a rather complicated task that is achieved by analyzing some ansatz structures and comparing the corresponding free energy.

The presence of CCSC matter within CSOs may lead to a number of observable signatures associated with

(1) gravitational wave emission,
(2) anomalies in the rotation frequency (known as "glitches"),
(3) cooling processes,
(4) mass-radius relation.

Point (1) relies on the observation that pulsars can be continuous sources of gravitational waves if their mass distribution is not axis symmetric. The large shear modulus characteristic of the CCSC phase allows the presence of big deformations of the star, usually called "mountains," making CSOs with a CCSC core strong sources of gravitational waves. A different source of gravitational waves are the unstable oscillations of CSOs with a crystalline crust.

Regarding point (2), the large rigidity of the CCSC phase makes the crystalline phases of quark matter unique among all forms of matter proposed as candidates for explaining stellar glitches.

Regarding point (3), one of the interesting properties of the CCSC phase is that some quarks at their respective Fermi surfaces are unpaired. For this reason their neutrino emissivity and heat capacity are only quantitatively smaller than those of unpaired quark matter, not parametrically suppressed. This suggests that neutron stars with crystalline quark matter cores will cool down by the direct Urca reactions, i.e., more rapidly than in standard cooling scenarios.

Point (4) is related to the fact that recent observations of very massive compact stars seem to challenge the possibility that CSOs have a CCSC core.

Summarizing, the state of matter at asymptotic densities is well defined and should correspond to the CFL condensate. At intermediate and more realistic densities it is not clear which is the ground state of matter. Our knowledge of the phases of matter can be represented in the so-called QCD phase diagram, schematically depicted in Fig. 2. At low density and low temperature quarks are confined in hadrons but increasing the energy scale quarks and gluons degrees of freedom are liberated. At high temperature this leads to the formation of a plasma of quarks and gluons, while at large densities matter should be in a color superconducting phase. If the conditions realized in CSOs favor the presence of inhomogeneous CSC phase, there might be distinctive astrophysical signatures of its presence.

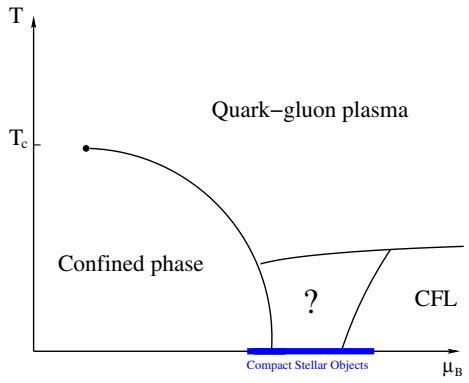

FIG. 2 (color online). Schematic phase diagram of strongly interacting matter as a function of the baryonic chemical potential and temperature. At low temperatures and low densities matter consists of confined hadrons. At high temperatures quark and gluons degrees of freedom are liberated forming the quark-gluon plasma. At low temperatures and very high densities, the CFL phase is favored. At densities and temperatures relevant for compact stellar objects, the CFL phase may be superseded by some different color superconducting phase or by some other phase of matter. The thick segment represents the possible range of baryonic chemical potential reachable in compact stars.

Apart from the phases we discussed other possibilities may be realized in the density regime relevant for CSOs. Here we mention only that one more candidate phase has recently been proposed, the so-called quarkyonic phase (McLerran and Pisarski, 2007), which is characterized by a nonvanishing baryon number density and found to be a candidate phase at least for a large number of colors. The possibility that the quarkyonic phase also shows a crystalline structure, in the so-called quarkyonic chiral spiral state, has been discussed by Kojo, Pisarski, and Tsvelik (2010). Another possibility is that the constituent value of the strange quark mass is so small that the CFL phase is the dominant one down to the phase transition to the hadronic phase. In this case, an interesting possibility is that there is no phase transition between the CFL phase and the hadronic phase (hypernuclear matter), in the so-called quark-hadron continuity scenario (Schafer and Wilczek, 1999a).

This review is organized as follows. Section II is devoted to the study of the two-flavor inhomogeneous phases. Here we go from mismatched Fermi spheres, discussed in Sec. II.A, to the analysis of the gapless 2SC phases of QCD in Sec. II.B, and a detailed study of the crystalline phase in Sec. II.C. An approximate method based on the Ginzburg-Landau expansion is introduced in Sec. II.C.2. A different approximation based on an expansion around the gapless modes is discussed in Sec II.D and applied to the analysis of the dispersion laws of fermionic quasiparticles and of the corresponding specific heats. A third approximation method based on a smearing procedure is discussed in Sec. II.E. Low-energy phonon excitations and their contributions to the specific heat are discussed in Sec. II.F. The stability analysis of the CCSC phase is considered in Sec. II.G. A discussion of the solitonic ground state is presented in Sec. II.H. In Sec. II.I we briefly

report on relevant results obtained in condensed matter and ultracold fermionic systems. In Sec. III we turn to the three-flavor case. In particular, in Sec. III.A we discuss the gapless CFL phase and its instability. In Sec. III.B various aspects of the three-flavor CCSC phase made of two plane waves are discussed. Section III.C is dedicated to the Ginzburg-Landau analysis of three-flavor crystalline structures. In Sec. III.D the Nambu-Goldstone and the phonon modes are studied and we report an analysis of the shear modulus of the two energetically favored crystalline phases. In Sec. IV we discuss whether the presence of an inhomogeneous color superconducting phase within the core of a compact star may lead to observable effects. Gravitational wave emission is discussed in Sec. IV.A; glitches are discussed in Sec. IV.B and the cooling of toy model compact stars with a CCSC core is discussed in Sec. IV.C; the mass-radius relation for some models of hybrid CSO with a CCSC core is discussed in Sec. IV.D. In Sec. V we draw our conclusions and outlook.

II. THE TWO-FLAVOR INHOMOGENEOUS PHASES

The inhomogeneous two-flavor crystalline color superconducting (CCSC) phase is an extension to QCD of the phase proposed in condensed matter systems by Fulde and Ferrell (1964) and Larkin and Ovchinnikov (1964) (LOFF). Some aspects of this phase have been previously reviewed by Casalbuoni and Nardulli (2004), in which the analogy between high-density QCD and condensed matter systems has been discussed as well. Therefore, we focus here on recent results, and in particular we discuss one of the main properties of this phase, namely, its *chromomagnetic* stability. This important property is not shared with homogeneous gapless color superconducting (CSC) phases (at least in weak coupling), and therefore strongly motivates its study.

A. Mismatched Fermi spheres

Before discussing the case of two-flavor quark matter, we show how gapless superconductivity may arise considering the simpler case of a nonrelativistic two-level fermionic gas, thus avoiding the formal complications due to flavor and color degrees of freedom. For definiteness, we review the system discussed by Gubankova, Mannarelli, and Sharma (2010) consisting of two unbalanced populations of fermionic species ψ_1 and ψ_2, with opposite spin, at vanishing temperature, having the Hamiltonian density

$$\mathcal{H} = \sum_{s=1,2} \psi_s^\dagger \left(-\frac{\nabla^2}{2m} - \mu_s \right) \psi_s - g \psi_1^\dagger \psi_2^\dagger \psi_2 \psi_1, \tag{8}$$

where $g > 0$ is the four-fermion coupling constant. The chemical potentials of the two species can be written as $\mu_1 = \mu + \delta\mu$ and $\mu_2 = \mu - \delta\mu$, so that μ is the average of the two chemical potentials and $2\delta\mu$ their difference. The effect of the attractive interaction between fermions is to induce the difermion condensate

$$\langle \psi_s(x) \psi_t(x) \rangle = \frac{\Delta(x)}{g} i(\sigma_2)_{st}, \tag{9}$$

which spontaneously breaks the global symmetry corresponding to particle number conservation. As a result the fermionic excitation spectrum consists of two Bogolyubov modes with dispersion laws

$$E_a = \delta\mu + \sqrt{\xi^2 + \Delta_0^2}, \qquad E_b = -\delta\mu + \sqrt{\xi^2 + \Delta_0^2}, \tag{10}$$

with $\xi = -\mu + p^2/2m$ and Δ_0 is the homogeneous mean field solution. Without loss of generality we take $\delta\mu > 0$, then from Eq. (10) we infer that tuning the chemical potential difference to values $\delta\mu \geq \Delta_0$ the mode b becomes gapless. This phase corresponds to a superconductor with one gapped and one gapless fermionic mode and is named gapless homogeneous superfluid.

In the above discussion we did not take into account that increasing $\delta\mu$ the difference between the free energy of the superfluid phase Ω_s and the normal phase Ω_n decreases; eventually the normal phase becomes energetically favored for sufficiently large $\delta\mu$. In weak coupling it is possible to show that the two free energies become equal at $\delta\mu_1 = \Delta_0/\sqrt{2}$ [corresponding to the so-called Chandrasekhar-Clogston limit (Chandrasekhar, 1962; Clogston, 1962)], that is before the fermionic excitation spectrum becomes gapless. At this critical value of $\delta\mu$ a first-order transition to the normal phase takes place and the superfluid phase becomes metastable. The reason for this behavior can be qualitatively understood as follows. Pairing results in an energy gain of the order of Δ_0, however, BCS pairing takes place between fermions with equal and opposite momenta. When a mismatch between the Fermi spheres is present it tends to disfavor the BCS pairing, because for having equal momenta fermions must pay an energy cost of the order of $\delta\mu$. Therefore, when $\delta\mu > c\Delta_0$, where c is some number, pairing cannot take place. In the weak coupling limit, one finds that $c = 1/\sqrt{2}$. This behavior is depicted in Fig. 3.

Considering homogeneous phases, a metastable superconducting phase exists for $\delta\mu \geq \delta\mu_1$, but still the system cannot develop fermionic massless modes, because at $\delta\mu = \Delta_0$ various instabilities appear (Wu and Yip, 2003; Gubankova, Schmitt, and Wilczek, 2006; Mannarelli, Nardulli, and Ruggieri, 2006; Pao *et al.*, 2006; Sheehy and Radzihovsky, 2006; Gubankova, Mannarelli, and Sharma, 2010). To explain what happens, consider the low-energy spectrum of the system, which can be described considering the fluctuations of $\Delta(x)$ around the mean field solution Δ_0. The oscillations in the magnitude of the condensate are described by the Higgs mode $\lambda(x)$, while the phase fluctuations are described by the Nambu-Goldstone (or Andersson-Bogolyubov) mode $\phi(x)$. Integrating out the fermionic degrees of freedom results in the Lagrangian density (Gubankova, Mannarelli, and Sharma, 2010)

$$\mathcal{L}_{\lambda,\phi} = A(\partial_t \phi)^2 - \frac{B}{3}(\boldsymbol{\nabla}\phi)^2 - C\lambda^2 + D(\partial_t \lambda)^2 - \frac{E}{3}(\boldsymbol{\nabla}\lambda)^2. \tag{11}$$

The stability of the system is guaranteed when all the coefficients A, B, C, D, and E are positive. A and D turn out to be always positive, then we define the following three stability conditions:

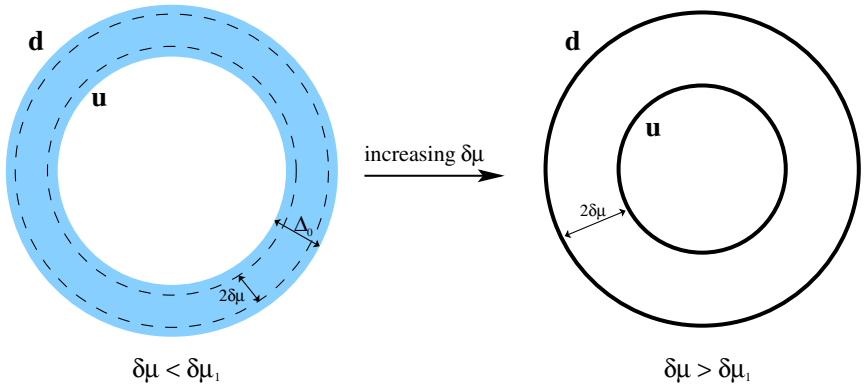

FIG. 3 (color online). Pictorial description of the behavior of the Fermi spheres of two different populations of fermions, with up (**u**) and down (**d**) spins, with increasing $\delta\mu$. Left panel: the dashed black lines correspond to the Fermi spheres of the two populations in the noninteracting case. In the presence of a weak attractive interaction the BCS pairing produces a smearing of the Fermi spheres corresponding to the gray region. Right panel: for $\delta\mu > \delta\mu_1 = \Delta_0/\sqrt{2}$ the Fermi spheres of the two populations (solid black lines) are widely separated and the BCS homogeneous phase is no more energetically favored.

(1) The Higgs has a positive squared mass: $C > 0$.
(2) The space derivative of the Higgs must be positive: $E > 0$.
(3) The space derivative of the NGB must be positive: $B > 0$.

Condition (1) is not satisfied if we are expanding around a maximum of the free energy, because the Higgs mass is proportional to the curvature of the free energy at the stationary point. The fact that condition (2) is not satisfied signals that the system is unstable toward space fluctuations of the absolute value of the condensate, while condition (3) is not fulfilled when the system is unstable toward space fluctuations of the phase of the condensate. Clearly conditions (2) and (3) are related and tell us that when a large mismatch between the Fermi sphere is present, the system prefers to move to a phase in which the translation symmetry is spontaneously broken. In other words, the fact that the homogeneous phase is unstable toward space fluctuations of the condensate means that the energetically favored condensate is the one having a spacial modulation, that is an inhomogeneous condensate. For this aspect one may actually think of $\delta\mu$ as the control parameter for the transition from a homogeneous phase to an inhomogeneous phase. We further elaborate on this point in Sec. II.G.1, when discussing the momentum susceptibility.

The results of the analysis concerning the stability conditions of the two-level model considered are reported in Fig. 4. The three conditions above are simultaneously violated in weak coupling for $\delta\mu/\Delta_0 \geq 1$, but they are violated at different values of this ratio in the strong coupling regime. The most stringent is condition (1), excluding the region above the dot-dot-dashed line. Conditions (2) and (3) exclude the region above the dot-dashed and dotted lines, respectively. The region above the dashed line corresponds to $\Omega_s > \Omega_n$. Therefore in weak coupling (that is, for $\Delta_0 \ll \mu$) the homogeneous phase is metastable for $\Delta_0/\sqrt{2} \leq \delta\mu \leq \Delta_0$. With increasing coupling strength it is possible to force the system into a stable homogeneous gapless phase (corresponding to the region between the solid and dashed lines at the bottom of Fig. 4), but this happens when $\mu \sim -\Delta_0$, deep in the Bose-Einstein condensate (BEC) limit.

In weak coupling the homogeneous BCS phase can be energetically favored for $\delta\mu > \delta\mu_1$ if there is a way of reducing $\Omega_s - \Omega_n$, and this is indeed what happens in some CSC phases in which the color and electrical neutrality conditions may disfavor the normal phase. On the other hand, this does not imply that the system has gapless modes. Indeed, in weak coupling the stability of the region with gapless modes is controlled by conditions (2) and (3). Decreasing $\Omega_s - \Omega_n$ does not *per se* guarantee that these constraints are satisfied. In fact, it turns out that the gapless homogeneous phase is in general not accessible in weak coupling, because when $\delta\mu > \Delta_0$, both conditions (2) and

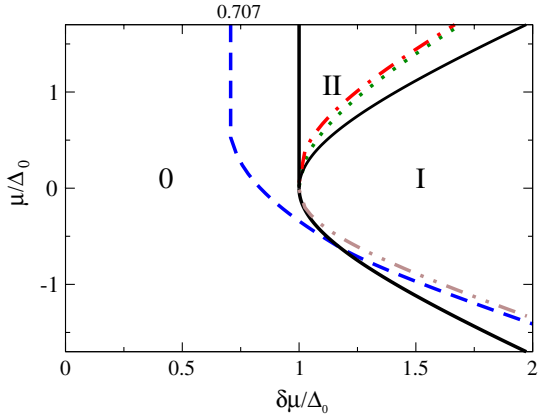

FIG. 4 (color online). Exclusion plot in the $(\delta\mu/\Delta_0, \mu/\Delta_0)$ plane according to conditions (1), (2), and (3) (see text). Condition (1) excludes the region above the dot-dot-dashed line; condition (2) excludes the region above the dot-dashed line; and condition (3) excludes the region above the dotted line. The region above the dashed line corresponds to $\Omega_s > \Omega_n$ and is therefore metastable or unstable. On the top of the figure the Chandrasekhar-Clogston limit $\delta\mu/\Delta_0 = 1/\sqrt{2} \simeq 0.707$ is indicated. Regions featuring zero (0), one (I), or two (II) gapless surfaces in momentum space are separated by solid lines. These lines are determined by finding the zeros of E_b, given in Eq. (10). Adapted from Gubankova, Mannarelli, and Sharma, 2010.

(3) are not satisfied, meaning that the solution with $\Delta_0 \neq 0$ is unstable.

Gauging the U(1) global symmetry, it is possible to show that the condition $B < 0$ is equivalent to the condition that the Meissner mass squared of the gauge field becomes negative, which corresponds to a *magnetic* instability. Therefore the magnetic instability is related to the fact that we are expanding the free energy around a local maximum. This statement is rather general and indeed in Sec. II.G we see that an analogous conclusion can be drawn for the 2SC phase. Notice that increasing the temperature of the system does not help to recover from this instability (Alford and Wang, 2005). Indeed, the effect of the temperature is to produce a smoothing of the dispersion law, which has the effect of increasing the instability region to values $\delta\mu < \Delta_0$.

Summarizing, for the simplest case of a weakly interacting two-flavor system, for $\delta\mu > \delta\mu_1$ the superfluid homogeneous phase is metastable, while for $\delta\mu > \Delta_0$, Ω_s does not have a local minimum in $\Delta_0 \neq 0$ and it is unstable toward fluctuations of the condensate. In general, the three conditions above should be simultaneously satisfied for having a stable (or metastable) vacuum. The gapless phase is only accessible for homogeneous superfluids deep in the strong coupling regime, for negative values of the chemical potential.

A different possibility is that gapless modes arise at weak coupling in an inhomogeneous superfluid. As we see in the following sections, the inhomogeneous LOFF phase is energetically favored for a certain range of values of $\delta\mu$ larger than the CC limit (see Sec. II.C), it has gapless fermionic excitations (see Sec. II.D), and it is (chromo)magnetically stable (see Sec. II.G). It is important to note that the presence of a gapless fermionic spectrum is not in contrast with the existence of superconductivity (de Gennes, 1966), e.g., type-II superconductors have gapless fermionic excitations for sufficiently large magnetic fields (de Gennes, 1966; Saint-James *et al.*, 1969).

B. Gapless 2SC phase of QCD

The gapless 2SC phase (g2SC) of QCD was proposed by Shovkovy and Huang (2003) [see also Huang and Shovkovy (2003)] as a CSC phase which may sustain large Fermi surface mismatches. However, they soon realized that this phase is chromomagnetic unstable (Huang and Shovkovy, 2004a, 2004b), meaning that the masses of some gauge fields become imaginary. In the following we briefly discuss the properties of the g2SC phase at vanishing temperature, and then we deal with the problem of the chromomagnetic instability.

We consider neutral two-flavor quark matter at finite chemical potential described by the following Lagrangian density:

$$\mathcal{L} = \bar{\psi}(i\gamma_\mu \partial^\mu - m + \boldsymbol{\mu}\gamma_0)\psi + \mathcal{L}_{\text{int}}, \tag{12}$$

where $\psi \equiv \psi_i^\alpha$, $i = 1, 2$, and $\alpha = 1, 2, 3$ corresponds to a quark spinor of flavor i and color α. The current quark mass is denoted by m (we take the isospin symmetric limit $m_u = m_d = m$), and $\mathcal{L}_{\text{int}}$ is an interaction Lagrangian that will be specified later.

In Eq. (12), $\boldsymbol{\mu}$ is the quark chemical potential matrix with color and flavor indices, given by

$$\boldsymbol{\mu} \equiv \mu_{ij,\alpha\beta} = (\mu\delta_{ij} - \mu_e Q_{ij})\delta_{\alpha\beta} + \frac{2}{\sqrt{3}}\mu_8 (T_8)_{\alpha\beta}\delta_{ij}, \tag{13}$$

where the quark electric charge matrix and the SU(3) color generators are, respectively,

$$Q_{ij} = \text{diag}(Q_u, Q_d), \qquad T_a = \frac{\lambda_a}{2}, \tag{14}$$

with λ_a the Gell-Mann matrices for $a = 1, \ldots, 8$. With μ_e and μ_8 we denote, respectively, the electron and the color chemical potential. Since $\boldsymbol{\mu}$ is diagonal in color and flavor spaces, we can indicate its element with $\mu_{i\alpha}$, e.g., μ_{ub} is the chemical potential of up blue quarks. A chemical potential along the third direction of color μ_3 can be introduced besides μ_8, but, for all the cases that we discuss in this section, we require the ground state to be invariant under the $\text{SU}(2)_c$ color subgroup; this makes the introduction of μ_3 unnecessary.

As interaction Lagrangian density we consider the NJL-like model

$$\begin{aligned}\mathcal{L}_{\text{int}} = {} & G_S[(\bar{\psi}\psi)^2 + (\bar{\psi} i\gamma_5 \boldsymbol{\tau}\psi)^2] \\ & + G_D[(\bar{\psi}^C \epsilon\varepsilon i\gamma_5 \psi)_{k\gamma}(i\bar{\psi}\epsilon\varepsilon i\gamma_5 \psi^C)_{k\gamma}],\end{aligned} \tag{15}$$

where $\psi^C = C\bar{\psi}^T$ denotes the charge-conjugate spinor, with $C = i\gamma_2\gamma_0$ the charge conjugation matrix. The matrices ε and ϵ denote the antisymmetric tensors in flavor and color space, respectively; we used in the second term on the right hand side of Eq. (15) the shorthand notation

$$(\bar{\psi}^C \epsilon\varepsilon i\gamma_5 \psi)_{k\gamma} \equiv (\bar{\psi}_i^{\alpha C} \epsilon_{ijk} \varepsilon^{\alpha\beta\gamma} i\gamma_5 \psi_j^\beta), \tag{16}$$

and an analogous expression for the other bilinear. For the 2SC phase considered in this section we assume condensation takes place only in the $k = \gamma = 3$ channel. In Eq. (15) two coupling constants are introduced in the scalar-pseudoscalar quark-antiquark channel, denoted by G_S, and in the scalar diquark channel, denoted by G_D. Huang and Shovkovy (2003) chose the parameters of the model to reproduce the pion decay constant in the vacuum $f_\pi = 93$ MeV and the vacuum chiral condensate $\langle \bar{u}u \rangle^{1/3} = \langle \bar{d}d \rangle^{1/3} = -250$ MeV. Moreover, an ultraviolet cutoff Λ is introduced to regularize the divergent momentum integrals. The parameter set of Huang and Shovkovy (2003) is given by

$$\Lambda = 653.3 \text{ MeV}, \qquad G_S = 5.0163 \text{ GeV}^{-2}. \tag{17}$$

The relative strength between the couplings in the quark-antiquark and quark-quark channels could be fixed by a Fierz rearranging of the quark-antiquark interaction; see, e.g., Buballa (2005). For example, considering interactions with the quantum numbers of the one gluon exchange, the Fierz transformation gives $G_D/G_S = 0.75$. However, nonperturbative in-medium effects might change this value. Therefore, in Huang and Shovkovy (2003) the ratio of G_D to G_S is considered as a free parameter.

At high density Huang and Shovkovy (2003) consider only the case $m = 0$ and vanishing chiral condensate. When $m \neq 0$ the chiral condensate in the ground state does not vanish, but its effects are presumably negligible, giving a small shift of the quark Fermi momenta. This shift might change the numerical value of the electron chemical potential only of some few percent. Hence, the main results of Huang and Shovkovy (2003) should not change much if a nonvanishing value of the current quark mass is considered.

Once the Lagrangian density is specified, the goal is to compute the thermodynamic potential. In the mean field (and one loop) approximation, this can be done easily using standard techniques. The mean field Lagrangian density can be written within the Nambu-Gorkov formalism, in the compact form

$$\mathcal{L} = \chi^\dagger S^{-1} \chi - \frac{\Delta_{2SC}^2}{4G_D}, \tag{18}$$

where

$$\chi = \begin{pmatrix} \psi \\ \psi^C \end{pmatrix}, \tag{19}$$

is the Nambu-Gorkov spinor and the gap parameter $\mathbf{\Delta} \equiv \Delta_{2SC} \epsilon^{\alpha\beta 3} \varepsilon_{ij3} C\gamma_5$ is included in the inverse propagator

$$S^{-1} = \begin{pmatrix} i\gamma_\mu \partial^\mu + \boldsymbol{\mu}\gamma_0 & \Delta \\ \Delta^\dagger & i\gamma_\mu \partial^\mu - \boldsymbol{\mu}\gamma_0 \end{pmatrix} \tag{20}$$

as an off-diagonal term in the "Nambu-Gorkov space."

We focus on the zero temperature regime [for a discussion of the rather uncommon temperature behavior of the g2SC phase see Huang and Shovkovy, 2003], which is relevant for astrophysical applications. The one loop expression of the thermodynamic potential can be determined from the inverse propagator in Eq. (20); for vanishing temperature it is given by

$$\Omega = \frac{\Delta_{2SC}^2}{4G_D} - \frac{\mu_e^4}{12\pi^2} - \sum_n \int \frac{d\boldsymbol{p}}{(2\pi)^3} |E_n|. \tag{21}$$

For a derivation, see, e.g., Buballa (2005). The second addendum corresponds to the electron free energy (electron masses have been neglected). The last addendum is the contribution due to the quark determinant. The sum runs over the twelve fermion propagator poles, six of them corresponding to quarks and the other six corresponding to antiquarks,

$$E_{1,2} = |\boldsymbol{p}| \mp \mu_{ub}, \tag{22}$$

$$E_{3,4} = |\boldsymbol{p}| \mp \mu_{db}, \tag{23}$$

$$E_{5,6} = \delta\mu + \sqrt{(|\boldsymbol{p}| \mp \bar{\mu})^2 + \Delta_{2SC}^2}, \tag{24}$$

$$E_{7,8} = -\delta\mu + \sqrt{(|\boldsymbol{p}| \mp \bar{\mu})^2 + \Delta_{2SC}^2}, \tag{25}$$

and $E_9 = E_5$, $E_{10} = E_6$, $E_{11} = E_7$, $E_{12} = E_8$. Here we have introduced the shorthand notation

$$\bar{\mu} = \mu - \frac{\mu_e}{6} + \frac{\mu_8}{3}, \qquad \delta\mu = \frac{\mu_e}{2}. \tag{26}$$

Using the explicit form of the dispersion laws, the free energy can be written as

$$\begin{aligned} \Omega = &- \frac{\mu_e^4}{12\pi^2} - \frac{\mu_{ub}^4}{12\pi^2} - \frac{\mu_{db}^4}{12\pi^2} - \frac{\Lambda^4}{2\pi^2} - 2\int_0^\Lambda \frac{p^2 dp}{\pi^2} \\ &\times \left(\sqrt{(p-\bar{\mu})^2 + \Delta_{2SC}^2} + \sqrt{(p+\bar{\mu})^2 + \Delta_{2SC}^2} \right) \\ &- 2\theta(\delta\mu - \Delta_{2SC}) \int_{\mu_-}^{\mu_+} \frac{p^2 dp}{\pi^2} \left(\delta\mu - \sqrt{(p-\bar{\mu})^2 + \Delta_{2SC}^2} \right), \end{aligned} \tag{27}$$

where $\mu_\pm = \bar{\mu} \pm \sqrt{\delta\mu^2 - \Delta_{2SC}^2}$.

The value of Δ_{2SC} is determined by the solution of the following equation:

$$\frac{\partial\Omega}{\partial\Delta_{2SC}} = 0, \tag{28}$$

with the neutrality constraints,

$$n_8 = -\frac{\partial\Omega}{\partial\mu_8} = 0, \qquad n_Q = -\frac{\partial\Omega}{\partial\mu_e} = 0, \tag{29}$$

which fix the values of μ_e and μ_8.

The numerical analysis of Huang and Shovkovy (2003) shows that μ_8 is much smaller than μ_e and Δ_{2SC}, both for $\Delta_{2SC} \geq \delta\mu$ and for $\Delta_{2SC} < \delta\mu$. As a consequence, it is possible to simplify the equations for the gap parameter and the electron chemical potential, Eqs. (28) and (29), respectively, by putting $\mu_8 = 0$. Therefore, the properties of the system depend only on the values Δ_{2SC} and μ_e and on the couplings G_D and G_S. The result of Huang and Shovkovy (2003) can be summarized as follows:

- For $G_D/G_S \gtrsim 0.8$, strong coupling, the 2SC phase is the only homogeneous stable phase.
- For $0.7 \lesssim G_D/G_S \lesssim 0.8$, intermediate coupling, the g2SC phase is allowed for $\delta\mu > \Delta_{2SC}$.
- For $G_D/G_S \lesssim 0.7$, weak coupling, only unpaired quark matter is favored.

In the g2SC phase the quasiparticle fermionic spectrum consists of four gapless modes and two gapped modes, whereas in the 2SC phase there are two gapless fermionic modes and four gapped fermionic modes. In the latter case the only gapless modes correspond to the up and down blue quarks that do not participate in pairing.

1. Meissner masses of gluons in the g2SC phase

The diquark condensate of the 2SC phase induces the symmetry breaking pattern reported in Eq. (6); in particular, the group $SU(3)_c \otimes U(1)_{em}$ is broken down to

$SU(2)_c \otimes \tilde{U}(1)_{em}$, where $\tilde{U}(1)_{em}$ is the gauge group corresponding to the rotated massless photon associated with the unbroken generator

$$\tilde{Q} = Q\cos\theta - \frac{g_s}{e}T_8\sin\theta, \tag{30}$$

where g_s and e denote the strong and the electromagnetic couplings, respectively, and Q and T_8 are defined in Eq. (14). The mixing coefficients have been determined by Alford, Berges, and Rajagopal (2000b) [see also Gorbar (2000)] and are given by

$$\cos\theta = \frac{\sqrt{3}g_s}{\sqrt{3g_s^2+e^2}}, \qquad \sin\theta = \frac{e}{\sqrt{3g_s^2+e^2}}. \tag{31}$$

The linear combination

$$T_{\bar{8}} = T_8\cos\theta + \frac{g_s}{e}Q\sin\theta \tag{32}$$

is orthogonal to $\tilde{Q}$ and gives the broken generator; the corresponding gauge field, which we refer to as the $\bar{8}$ mode, acquires a Meissner mass. Actually, the NJL-like Lagrangian in Eqs. (12) and (15) has only global symmetries, but gauging the $SU(3)_c$ group and the $U(1)$ subgroup of $SU(2)_L \times SU(2)_R$, one has that the spontaneous symmetry breaking leads to the generation of Meissner masses for the five gluons associated with the broken generators. To compute these masses, we define the gauge boson polarization tensor [see, e.g., Le Bellac (2000)],

$$\Pi^{\mu\nu}_{ab}(p) = -\frac{i}{2}\int\frac{d^4q}{(2\pi)^4}\,\mathrm{Tr}[\Gamma^\mu_a S(q)\Gamma^\nu_b S(q-p)], \tag{33}$$

where $S(p)$ is the quark propagator in momentum space, which can be obtained from Eq. (20), and

$$\Gamma^\mu_a = g_s\gamma^\mu \mathrm{diag}(T_a, -T_a^T), \tag{34}$$

$$\Gamma^\mu_9 = e\gamma^\mu \mathrm{diag}(Q, -Q), \tag{35}$$

are the interaction vertex matrices. The trace in Eq. (33) is taken over Dirac, Nambu-Gorkov, color, and flavor indices; a, $b = 1, \ldots, 8$ indicate the adjoint color and we use the convention that the component with a, $b = 9$ corresponds to the photon.

The screening masses of the gauge bosons are defined in terms of the eigenvalues of the polarization tensor and in the basis in which $\Pi^{\mu\nu}_{ab}$ is diagonal the Debye masses and the Meissner masses are, respectively, defined as

$$\mathcal{M}^2_{D,a} = -\lim_{p\to 0}\Pi^{00}_{aa}(0,\boldsymbol{p}), \tag{36}$$

$$\mathcal{M}^2_{M,a} = -\frac{1}{2}\lim_{p\to 0}\left(g_{ij} + \frac{\boldsymbol{p}_i\boldsymbol{p}_j}{|\boldsymbol{p}|^2}\right)\Pi^{ij}_{aa}(0,\boldsymbol{p}). \tag{37}$$

Both masses have been evaluated in the 2SC phase by Rischke (2000b, 2004), Rischke and Shovkovy (2002), and Schmitt, Wang, and Rischke (2004). The Debye masses of all gluons are related to the chromoelectric screening and are always real, therefore do not affect the stability of the 2SC and g2SC phases. The Meissner masses of the gluons with adjoint color $a = 1, 2, 3$ are always zero, because they are associated with the unbroken color subgroup $SU(2)_c$. It is interesting to note that in the 2SC phase Π^{00}_{ab} is diagonal in the a, b indices and therefore there is no need to diagonalize it (Rischke (2004), and Schmitt, Wang, and Rischke (2004). This happens because of a cancellation between the contribution of the blue ungapped quarks with that of the gapped excitations. The magnetic components of the 8th gluon and the photon do instead mix and the polarization tensor has to be diagonalized for extracting the Meissner mass. In contrast, in the CFL phase both the electric and magnetic sectors mix because of the absence of ungapped excitations (Schmitt, Wang, and Rischke, 2004).

For nonvanishing values of $\delta\mu$ the Meissner masses have been evaluated by Huang and Shovkovy (2004a, 2004b). Gluons with adjoint color $a = 4, 5, 6, 7$ are degenerate and in the limit $\mu_8 = 0$ their Meissner masses are given by

$$\mathcal{M}^2_{M,4} = \frac{4\alpha_s\bar{\mu}^2}{\pi}\left[\frac{\Delta^2_{2SC}-2\delta\mu^2}{2\Delta^2_{2SC}} + \frac{\delta\mu}{\Delta^2_{2SC}}\sqrt{\delta\mu^2-\Delta^2_{2SC}}\,\theta(\delta\mu-\Delta_{2SC})\right]. \tag{38}$$

The squared Meissner mass turns out to be negative not only in the gapless phase $\Delta_{2SC}/\delta\mu < 1$ but also in the gapped phase, when $\Delta_{2SC}/\delta\mu < \sqrt{2}$. This result seems in contrast with the result of the previous section, where an imaginary Meissner mass was related to the existence of a local maximum of the free energy arising at $\delta\mu = \Delta$. However, from the analysis of the 2SC free energy of the system, one can see that when $\Delta_{2SC}/\delta\mu = \sqrt{2}$ the state with $\Delta_{2SC} \neq 0$ corresponds to a saddle point in the Δ-$\delta\mu$ plane. The neutrality condition transforms this saddle point into a local minimum. However, as explained in the previous section, the gauge fields can be related to the fluctuations of the gap parameter. These fluctuations can probe all directions in the Δ-$\delta\mu$ plane around the stationary point and would result in a low-energy Lagrangian with dispersion laws akin to those discussed in Eqs. (11) with the coefficients E and B negative.

Finally, we consider the $\bar{8}$ mode, which is associated with the broken generator defined in Eq. (32). The corresponding Meissner mass can be obtained diagonalizing the polarization tensor in Eq. (33) in the subspace a, $b \in \{8, 9\}$ or, more directly, by substituting $T_a \to T_{\bar{8}}$ in the vertex factors of the polarization tensor. The squared Meissner mass of the $\bar{8}$ mode turns out to be

$$\mathcal{M}^2_{M,\bar{8}} = \frac{4(3\alpha_s+\alpha)\bar{\mu}^2}{27\pi}\left(1 - \frac{\delta\mu}{\sqrt{\delta\mu^2-\Delta^2_{2SC}}}\theta(\delta\mu-\Delta_{2SC})\right), \tag{39}$$

and becomes negative for $\Delta_{2SC}/\delta\mu < 1$. As shown by Gatto and Ruggieri (2007), the instability in this sector is transmitted to a gradient instability of the pseudo-Goldstone boson related

to the $U(1)_A$ symmetry which is broken by the diquark condensate. Although in vacuum the $U(1)_A$ symmetry is explicitly broken by instantons, at finite chemical potential instantons are Debye screened and $U(1)_A$ can be considered as an approximate symmetry, which is then spontaneously broken by the diquark condensate.

C. The two-flavor crystalline color superconducting phase

Since the homogeneous g2SC phase is chromomagnetically unstable, the question arises of the possible existence of a different superconducting phase for large mismatch between the Fermi spheres. There are several candidate phases, which include the gluonic phase (Gorbar, Hashimoto, and Miransky, 2006a; Gorbar, Hashimoto, Miransky, and Shovkovy, 2006), the solitonic phase (see Sec. II.H), and the CCSC phase.

In this section we review some of the main results on the two-flavor CCSC phase. First, we describe the one plane wave ansatz in the framework of the simple model discussed in Sec. II.A; then, we turn to the CCSC phase and report on the Ginzburg-Landau (GL) analysis of various crystalline structures. We relax the constraint of electrical and color neutrality, and treat the difference of chemical potentials between u and d quarks $2\delta\mu$ as a free parameter.

1. From one plane wave to the crystalline phase

In Sec. II.A we showed that in weak coupling the CC limit signals that the standard BCS phase becomes metastable, but does not forbid the existence of different forms of superconductivity. In particular, it does not forbid the existence of Cooper pairs with nonvanishing total momentum. It was shown by Larkin and Ovchinnikov (1964) and Fulde and Ferrell (1964), in the context of electromagnetic superconductors, that in a certain range of values of $\delta\mu$ it might be energetically favored the realization of Cooper pairs with nonzero total momentum. For the simple two-level system discussed in Sec. II.A, Cooper pairs with momentum $2\boldsymbol{q}$ can be described by considering the difermion condensate in Eq. (9) given by

$$\langle \psi_s(x)\psi_t(x)\rangle = \frac{\Delta}{g} i(\sigma_2)_{st} e^{2i\boldsymbol{q}\cdot\boldsymbol{x}}, \tag{40}$$

and we call this state of matter the FF phase.

Note that this ansatz breaks rotational symmetry because there is a privileged direction corresponding to $\boldsymbol{q}$. In the left panel of Fig. 5 the two Fermi spheres of fermions are pictorially shown and the gray ribbons correspond to the regions in momentum space where pairing occurs. Pairing between fermions of different spin can only take place in a restricted region of momentum space and this implies that $\Delta < \Delta_0$. The reason why the FF phase is energetically favored with respect to the normal phase is that no energy cost proportional to $\delta\mu$ has to be paid for allowing the formation of Cooper pairs. The only energetic price to pay is due to the kinetic energy associated with Cooper pairs: there is a spontaneous generation of a supercurrent in the direction of $\boldsymbol{q}$, which is balanced by a current of normal fermions in the opposite direction (Fulde and Ferrell, 1964). The gap parameter in Eq. (40) can be determined solving a gap equation under the constraint that the modulus of the Cooper momentum q minimizes the free energy. The result is that at $\delta\mu \approx \delta\mu_1 = \Delta_0/\sqrt{2}$ there is a first-order phase transition from the homogeneous BCS phase to the FF phase. Increasing further $\delta\mu$ results in a smooth decreasing of the gap function of the FF phase, until at a critical value $\delta\mu_2$ a second-order phase transition to the normal phase takes place. In the weak coupling limit $\delta\mu_2 = 0.754\Delta_0$; the range $[\delta\mu_1, \delta\mu_2]$ is called the LOFF *window*. In the LOFF window, the optimal value of q turns out to be approximately constant, $q \approx 1.2\delta\mu$.

Alford, Bowers, and Rajagopal (2001) presented the two-flavor QCD analog of the FF phase. In this case the condensate has the same color, spin, and flavor structure of the 2SC condensate, but with the plane wave space dependence characteristic of the FF phase, that is,

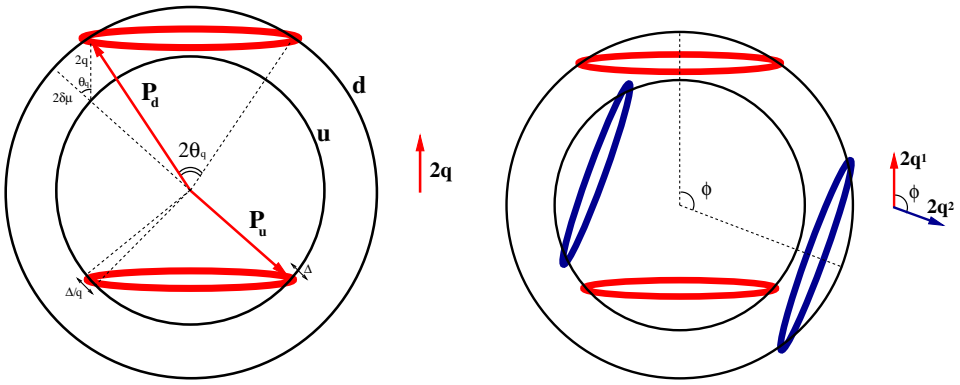

FIG. 5 (color online). Pictorial description of the LOFF pairing in the weak coupling approximation. When $\delta\mu > \Delta_0/\sqrt{2}$ the BCS homogeneous pairing is not energetically allowed, but pairing between fermions with total nonvanishing momentum can be realized. Left panel: In the FF phase pairing takes place in two ribbons on the top the Fermi spheres of up and down fermions, such that $\boldsymbol{P}_u + \boldsymbol{P}_d = 2\boldsymbol{q}$, having opening angle $2\vartheta_q \simeq 2\arccos(\delta\mu/q) \simeq 67^\circ$, thickness Δ, and angular width Δ/q; see Sec. II.E.1. Right panel: Structure obtained with two plane waves corresponding to two vectors $2\boldsymbol{q}^1$ (light gray) and $2\boldsymbol{q}^2$ (dark gray) with relative angle ϕ. The size and the opening angle of each ribbon is as in the FF phase. The structure with $\phi = 180^\circ$ is called the "strip." For illustrative purposes, we exaggerated the splitting between the Fermi surfaces, relative to the values used in the calculations reported in Sec. II.C.

$$\langle \psi_i^\alpha(x) C\gamma_5 \psi_j^\beta(x)\rangle \propto \Delta_{ij}^{\alpha\beta} = \Delta e^{i2\boldsymbol{q}\cdot\boldsymbol{x}} \varepsilon^{\alpha\beta 3}\epsilon_{ij3}. \tag{41}$$

As noted by Alford, Bowers, and Rajagopal (2001), the FF condensate induces a spin-1 condensate as well; however, its effect is found to be numerically small, and it will be neglected here. As in the simple two-level system, in the two-flavor FF phase it is possible to determine the free energy using a NJL-like model with the condensate given in Eq. (41). To this end it is convenient using the Nambu-Gorkov formalism discussed in Sec. II.B in a slightly different way. In the FF case we are considering pairing between u quarks with momentum $\boldsymbol{p}+\boldsymbol{q}$ and d quarks with momentum $-\boldsymbol{p}+\boldsymbol{q}$ so that the total momentum is $2\boldsymbol{q}$ as in Eq. (41). In momentum space, the standard two-flavor Nambu-Gorkov spinor reads

$$\chi(\boldsymbol{p}) = \begin{pmatrix} \psi_u(\boldsymbol{p}) \\ \psi_d(\boldsymbol{p}) \\ \psi_u^C(-\boldsymbol{p}) \\ \psi_d^C(-\boldsymbol{p}) \end{pmatrix}, \tag{42}$$

and thus the corresponding propagator has terms in it that are not only off-diagonal in the Nambu-Gorkov space, but also off-diagonal in *momentum* space. Thus any calculation looks complicated in this basis, but it simplifies changing the Nambu-Gorkov basis as follows (Bowers *et al.*, 2001):

$$\chi(\boldsymbol{p}) = \begin{pmatrix} \psi_u(\boldsymbol{p}+\boldsymbol{q}) \\ \psi_d(\boldsymbol{p}-\boldsymbol{q}) \\ \psi_u^C(-\boldsymbol{p}-\boldsymbol{q}) \\ \psi_d^C(-\boldsymbol{p}+\boldsymbol{q}) \end{pmatrix}. \tag{43}$$

The effect of this momentum shift is to eliminate the dependence on $\boldsymbol{q}$ in the off-diagonal terms in the Nambu-Gorkov propagator. Indeed, the pair condensate described by terms in the fermion propagator occurring in the ψ_u-ψ_d^C and ψ_d-ψ_u^C entries are now independent of $\boldsymbol{q}$, making the propagator diagonal in $\boldsymbol{p}$ space and the calculation tractable. Of course the above choice of the momentum shift is not unique: with $\boldsymbol{p}$ being an integration variable we can shift it, for example, by $\boldsymbol{p}\to\boldsymbol{p}-\boldsymbol{q}$ thus rewriting the Nambu-Gorkov spinor in the two-flavor phase as

$$\chi(\boldsymbol{p}) = \begin{pmatrix} \psi_u(\boldsymbol{p}) \\ \psi_d(\boldsymbol{p}-2\boldsymbol{q}) \\ \psi_u^C(-\boldsymbol{p}) \\ \psi_d^C(-\boldsymbol{p}+2\boldsymbol{q}) \end{pmatrix} \tag{44}$$

is always possible.

The inverse propagator in the shifted basis has formally the same expression given in Eq. (20), with space-independent off-diagonal terms, but now the derivatives act on spinors with shifted momenta; see Bowers *et al.* (2001) for more details. The gap parameter can then be determined solving the corresponding gap equation under the constraint that the favored value of q minimizes the free energy. The results are the same obtained in the two-level system; in particular, the LOFF window and q have the same expressions reported above (but now $2\delta\mu$ is the difference of chemical potentials between u and d quarks).

From Fig. 5, it should be clear that an immediate generalization of the FF phase can be obtained adding more ribbons on the top of the Fermi spheres, corresponding to different vectors $\boldsymbol{q}_m$, with $\boldsymbol{q}_m \in \{\boldsymbol{q}\}$, where $\{\boldsymbol{q}\}$ is some set of vectors to be determined by minimizing the free energy of the system and m is a label that identifies the vectors of the set. This in turn corresponds to considering inhomogeneous CSC phases with a more general ansatz than in Eq. (41), where the single plane wave is replaced by a superposition of plane waves, that is,

$$\Delta e^{2i\boldsymbol{q}\cdot\boldsymbol{x}} \to \sum_{\boldsymbol{q}^m\in\{\boldsymbol{q}\}} \Delta_{\boldsymbol{q}^m} e^{2i\boldsymbol{q}^m\cdot\boldsymbol{x}}. \tag{45}$$

To simplify the analysis, a set of assumptions are used. The vectors $\boldsymbol{q}^m$ are taken with equal length, thus we can write $\boldsymbol{q}^m = q\boldsymbol{n}^m$ and the set of vectors characterizing each condensate can be indicated with $\{\boldsymbol{n}\}$. The set of vectors $\{\boldsymbol{n}\}$ identifies the vertices of a crystalline structure, thus at each set $\{\boldsymbol{n}\}$ corresponds a particular crystalline phase. As a further simplifying assumption, the coefficients $\Delta_{\boldsymbol{q}^m}$ are taken independent of $\boldsymbol{q}^m$ and we indicate their common value with Δ. In other words, we consider condensates with

$$\Delta(\boldsymbol{x}) = \Delta \sum_{m=1}^{P} e^{2iq\boldsymbol{n}^m\cdot\boldsymbol{x}}, \tag{46}$$

where P is the number of vectors $\boldsymbol{n}^m$. The simplest example is clearly the FF condensate, depicted in the left panel of Fig. 5, characterized by a single plane wave, thus corresponding to $P=1$. The case with $P=2$ is reported in the right panel of Fig. 5, in this case the "crystalline" structure is completely determined by ϕ, the relative angle between $\boldsymbol{n}^1$ and $\boldsymbol{n}^2$; more complicated structures can be pictorially represented in a similar way.

It is important to stress that the crystalline structure is determined by the modulation of the condensate, but the underlying fermions are not arranged in an ordered pattern, indeed fermions are superconducting, that is they form a superfluid of charged carriers.

Computation of the spectrum and the free energy of a system with a general crystalline condensate cannot be obtained by the momentum shift technique discussed above. The reason is that by a momentum shift we can eliminate the dependence on only one of the vector $\boldsymbol{q}^m$ in the off-diagonal term of the Nambu-Gorkov propagator. As a consequence, the use of some approximation is necessary. In the next section we discuss the GL approximation for the evaluation of the free energy and in Sec. II.D we present a method for determining the low-energy fermionic spectrum. A different approximation method is discussed in Sec. II.E.

2. Ginzburg-Landau analysis

A viable method for the evaluation of the free energy of some crystalline structures is the GL expansion, which is obtained expanding Ω in powers of Δ

$$\Omega = \Omega_n + P\alpha\Delta^2 + \frac{\beta}{2}\Delta^4 + \frac{\gamma}{3}\Delta^6 + \mathcal{O}(\Delta^8), \tag{47}$$

where Ω_n is the free energy of the normal phase and the coefficients α, β, and γ have been computed, in the one-loop approximation, using as microscopic theory a NJL model by Bowers and Rajagopal (2002). The GL expansion is well suited for studying second-order phase transitions but might give reasonable results for *soft* first-order phase transitions as well. In the present case the expansion is under control for $\Delta/q \ll 1$ and if the coefficient γ is positive, meaning that the free energy is bounded from below.

For a given crystalline structure, the coefficients in Eq. (47) depend on $\delta\mu$ and q; the latter is fixed, in the calculation of Bowers and Rajagopal (2002), to the weak coupling value $q \simeq 1.2\delta\mu$. For any value of $\delta\mu$ the thermodynamic potential of a given structure is computed by minimization with respect to Δ and then the optimal crystalline structure is identified with that with the lowest free energy. It is possible to compute analytically the GL coefficients only for few structures. One example is the FF phase, in which

$$\alpha_{\mathrm{FF}}(q,\delta\mu) = \frac{2\mu^2}{\pi^2}\left(-1 + \frac{\delta\mu}{2q}\ln\left|\frac{q+\delta\mu}{q-\delta\mu}\right| + \frac{1}{2}\ln\left|\frac{4(q^2-\delta\mu^2)}{\Delta_{\mathrm{2SC}}^2}\right|\right), \tag{48}$$

$$\beta_{\mathrm{FF}}(q,\delta\mu) = \frac{\mu^2}{2\pi^2}\frac{1}{q^2-\delta\mu^2}, \tag{49}$$

$$\gamma_{\mathrm{FF}}(q,\delta\mu) = \frac{\mu^2}{16\pi^2}\frac{q^2+3\delta\mu^2}{(q^2-\delta\mu^2)^3}, \tag{50}$$

where Δ_{2SC} is the 2SC gap parameter. In general, the GL coefficients of more complicated structures have to be computed numerically; see the appendix of Bowers and Rajagopal (2002) for details. Bowers and Rajagopal (2002) studied twenty-three crystalline structures and among them those with $P > 9$ turn out to be largely disfavored. This has been nicely explained in the weak coupling regime: in this case, as shown in the left panel of Fig. 5 for the FF phase, the pairing regions of the inhomogeneous superconductor can be approximated as rings on the top of the Fermi surfaces; one ring per wave vector $\boldsymbol{n}$ in the set $\{\boldsymbol{n}\}$. The computation of the lowest order GL coefficients shows that the intersection of two rings is energetically disfavored (Bowers and Rajagopal, 2002). As a consequence, it is natural to expect that in the most favored structure no intersecting rings appear. Since each ring has an opening angle of approximately 67°, a maximum of nine rings can be accommodated on a spherical surface.

The fact that configurations with overlapping rings are disfavored can be quantitatively understood as follows. For the case of two plane waves (right panel of Fig. 5), in the weak coupling approximation there is one pairing ring for each of the two wave vectors. The quartic coefficient β depends on the angle ϕ between the two wave vectors and it diverges at

$$\phi_0 \approx 2\vartheta_q \approx 2\arccos\frac{\delta\mu}{q} \approx 67^\circ, \tag{51}$$

corresponding to the angle at which the two pairing rings are contiguous, meaning that for $\phi < \phi_0$ the two rings overlap. The latter case is energetically disfavored because, being β large and positive, the free energy gain would be smaller.

The divergence of the coefficient $\beta(\phi)$ at $\phi = \phi_0$ is due to the two limits that have been taken to compute the free energy, namely, the GL and weak coupling limits. A detailed explanation of what happens will be given in Sec. III.B when discussing a simple three-flavor crystalline structure. In any case it is clear that the divergency of a GL coefficient means that the expansion is not under control, or, more precisely, that the radius of convergence of the series in Eq. (47) tends to zero.

Among the crystals with no intersecting rings, seven are good candidates to be the most favored structure. Within these seven structures, the octahedron, which corresponds to a crystal with $P = 6$ and whose wave vectors point into the direction of a body-centered cube (bcc), is the only one with effective potential bounded from below (that is, with $\gamma > 0$). The remaining six structures, given by different configurations with $P = 7$, 8, and 9, are characterized by a potential which is unbounded from below, at least at the considered order Δ^6. Even if in this case the free energy cannot be computed, qualitative arguments given by Bowers and Rajagopal (2002) suggest that the favored structure is the one with $P = 8$ having wave vectors pointing toward the vertices of a face-centered cube (fcc).

Of course, as Bowers and Rajagopal admit, their study cannot be trusted quantitatively, because of the several limitations of the GL analysis. First, the GL expansion formally corresponds to an expansion in powers of Δ/q and therefore it is well suited for the study of second-order phase transitions, but the condition that $\Delta/q \ll 1$ is not satisfied by all crystalline structures considered by Bowers and Rajagopal (2002). In some cases the GL analysis predicts a strong first-order phase transition to the normal state, with a large value of the gap at the transition point. Moreover, it may happen that the local minimum for small values of Δ/q is not a global minimum of the system, as discussed in Sec. II.H. In this case the GL expansion in Eq. (47) underestimates the free energy gain of the system and is not able to reproduce the correct order of the phase transition. For a more reliable determination of the ground state one should consider terms of higher power in Δ, which are difficult to evaluate. Finally, the claimed favored crystalline structure, namely, the fcc, has $\gamma < 0$ and a global minimum cannot be found unless the coefficient $\mathcal{O}(\Delta^8)$ (or of higher order) is computed and found to be positive.

Because of these reasons, the quantitative predictions of the GL analysis should be taken with a grain of salt. One should not trust the order of the phase transition obtained by the GL expansion and the comparison among various crystalline structures may be partially incorrect, because it is not guaranteed that the corresponding free energies have been accurately determined.

On the other hand, the qualitative picture that we can draw from it, namely, the existence of crystalline structures with

lower free energy than the single plane wave, is quite reasonable: crystalline structures benefit of more phase space available for pairing, thus lowering the free energy. The symmetry argument is quite solid too, because it is based on the fact that configurations with overlapping pairing regions are disfavored, and as we see for one particular configuration in the three-flavor case in Sec. III.B, one can prove that this statement is correct without relying on the GL expansion. We also show an interesting point, that the GL expansion underestimates the free energy gain of the crystalline structures. And this happens not only in the presence of a global minimum different from the local minimum around which the GL expansion is performed (see Sec. II.H), but also comparing the GL free energy with the free energy evaluated without the Δ/q expansion.

D. Fermionic dispersion laws and specific heats

The thermal coefficients (specific heat, thermal conductivity, etc.) of quark matter at very low temperature are of fundamental importance for the transport properties and cooling mechanisms of compact stars. The largest contribution to the thermal coefficients comes from the low-energy degrees of freedom and it is therefore of the utmost importance to understand whether fermionic modes are gapped or gapless. Indeed, the absence of a gap in the spectrum of fermions implies that quasiquarks can be excited even at low temperature and therefore the corresponding thermal coefficients are not suppressed by a factor $\approx e^{-\Delta/T}$ (which is distinctive of homogeneous BCS superconductors).

In this section we discuss the fermion dispersion laws in the two-flavor CCSC phase for low values of momenta. Then, we use the obtained dispersion laws for the computation of the specific heat. A different contribution to the specific heat, due to phonons, will be presented in Sec. II.F. The results discussed below do not rely on the GL approximation but are obtained by an expansion around the zeros of the full inverse propagator (Larkin and Ovchinnikov, 1964; Casalbuoni *et al.*, 2003).

1. Fermi quasiparticle dispersion law: General settings

We consider a general difermion condensate $\Delta(\boldsymbol{x})$, and determine the quasiparticle dispersion laws looking at the zero modes of the inverse propagator of the system. Arranging the fields in the Nambu-Gorkov spinor as follows:

$$\chi_i^\alpha = \begin{pmatrix} \tilde{G}_i^\alpha \\ -i(\sigma_2)_{\alpha\beta}\tilde{F}_i^\beta \end{pmatrix}, \tag{52}$$

the inverse propagator is given by

$$(S^{-1})_{ij}^{\alpha\beta} = \begin{pmatrix} \delta^{\alpha\beta}[\delta_{ij}(E + iv\cdot\boldsymbol{\nabla}) + \delta\mu(\sigma_3)_{ij}] & -\varepsilon^{\alpha\beta 3}\varepsilon_{ij3}\Delta(\mathbf{x}) \\ -\varepsilon^{\alpha\beta 3}\varepsilon_{ij3}\Delta(\mathbf{x})^* & \delta^{\alpha\beta}[\delta_{ij}(E - iv\cdot\boldsymbol{\nabla}) + \delta\mu(\sigma_3)_{ij}] \end{pmatrix}, \tag{53}$$

where E is the quasiparticle energy and $\boldsymbol{v}$ is the Fermi velocity, that for massless quarks satisfies $v = |\boldsymbol{v}| = 1$. The quasiparticle spectrum can obtained by solving the eigenvalue equation

$$(S^{-1})_{ij}^{\alpha\beta}\chi_j^\beta = 0. \tag{54}$$

Performing the unitary transformation

$$\bar{G}_i^\alpha = (e^{i\delta\mu\sigma_3\boldsymbol{v}\cdot\boldsymbol{x}/v^2})_{ij}G_j^\alpha, \qquad \bar{F}_i^\alpha = (e^{-i\delta\mu\sigma_3\boldsymbol{v}\cdot x/v^2}\sigma_2)_{ij}F_j^\alpha, \tag{55}$$

it is possible to eliminate the dependence on $\delta\mu$ in the eigenvalue problem and this corresponds to measuring the energy of each flavor from its Fermi energy. The resulting equations for F_i^α and G_i^α are independent of color and flavor indices, and therefore these indices will be omitted below. The eigenvalue problem reduces to solve the coupled differential equations

$$\begin{aligned}(E + i\boldsymbol{v}\cdot\boldsymbol{\nabla})G - i\Delta(\boldsymbol{x})F = 0,\\ (E - i\boldsymbol{v}\cdot\boldsymbol{\nabla})F + i\Delta(\boldsymbol{x})^*G = 0.\end{aligned} \tag{56}$$

These equations can be used to find the dispersion laws for any inhomogeneous $\Delta(\boldsymbol{x})$, and we consider here the periodic structures of the form given in Eq. (46) determining whether gapless fermionic excitations are present. We prove that for any crystalline structure with real-valued periodic functions $\Delta(\boldsymbol{x})$ there exists a gapless mode if and only if the set $\{\boldsymbol{n}\}$ does not contain the vector $\boldsymbol{n} = \mathbf{0}$.

The proof is given below. Here we note that this theorem does not apply to the case in which $\Delta(\boldsymbol{x})$is not real. As a representative case of complex $\Delta(\boldsymbol{x})$, we consider the single plane wave (FF structure), explaining in which circumstances gapless modes arise. The theorem implies that any antipodal structure has a gapless mode, in particular, the "strip" (corresponding to the structure depicted in the right panel of Fig. 5 for $\phi = 180°$) and the cube have gapless modes. On the other hand, the set of vectors which identify a trihedral prism or a hexahedral prisms have a vector with $\boldsymbol{n} = \mathbf{0}$, and the corresponding dispersion laws are gapped.

Proof.—A periodic solution of the system in $\Delta(\boldsymbol{x})$ solution of the system in (56) is given by the Bloch functions

$$G(\boldsymbol{x}) = u(\boldsymbol{x})e^{i\boldsymbol{k}\cdot\boldsymbol{x}} \qquad F(\boldsymbol{x}) = w(\boldsymbol{x})e^{i\boldsymbol{k}\cdot\boldsymbol{x}}, \tag{57}$$

where $u(\boldsymbol{x})$ and $w(\boldsymbol{x})$ are periodic functions. These solutions are periodic if $\boldsymbol{k}$ is real. However, we can look for a generic solution of Eqs. (56) with k complex. If the solution with a complex k exists, it means that a gap is present in the excitation spectrum and the eigenfunctions decrease exponentially with x. In fact, suppose that the dispersion law has a gap $\Delta \neq 0$, then it can be written as $E = \sqrt{k^2 + \Delta^2}$. Since we are expanding around $E = 0$, then $k \approx \sqrt{-\Delta^2} +$ corrections,

making k complex. Clearly, the physical momentum is always real; the fact that we find a complex momentum only means that the spectrum is gapped.

Taking $E = 0$ in Eq. (56), the two solutions of the system of equations are given by $F_+ = G_+$ or $F_- = -G_-$, where

$$G_{\pm}(\boldsymbol{x}) = \exp\left(\pm \int_0^{x_\parallel} \Delta(\boldsymbol{x}')\frac{dx'_\parallel}{v^2}\right), \tag{58}$$

with $x_\parallel = \boldsymbol{x}\cdot\boldsymbol{v}$.

Comparing this expression with Eq. (57), it is clear that these solutions corresponds to Bloch functions with $\mathrm{Re}(k) = 0$. If $\Delta(\boldsymbol{x})$ has a term with $\boldsymbol{n} = \boldsymbol{0}$, it means that $\Delta(\boldsymbol{x}) = A + f(\boldsymbol{x})$, where A is a constant and $f(\boldsymbol{x})$ is a periodic nonconstant function. In this case Eq. (58) has an exponential behavior of the type $G(|\boldsymbol{x}|) \propto \exp(\pm A|\boldsymbol{x}|)$ and therefore the spectrum is gapped. On the other hand, if in the expansion of $\Delta(\boldsymbol{x})$ no term with $\boldsymbol{n} = \boldsymbol{0}$ is present then the imaginary part of k vanishes and the spectrum is gapless Q.E.D.

The fermion dispersion law for the gapless modes can be determined using degenerate perturbation theory for $\xi = p - \mu \ll q$, i.e., close to the Fermi sphere. At the lowest order in ξ/q one finds that

$$E(\boldsymbol{v},\xi) = \frac{\xi}{\sqrt{A_+(\boldsymbol{v})A_-(\boldsymbol{v})}} = c(\boldsymbol{v})\xi, \tag{59}$$

where $c(\boldsymbol{v})$ is the velocity of the excitations, and

$$A_{\pm}(\boldsymbol{v}) = \frac{1}{V_c}\int_{\mathrm{cell}} d\boldsymbol{x}\,\exp\left[\pm 2\int \Delta(\boldsymbol{x}')\frac{dx'_\parallel}{v^2}\right], \tag{60}$$

where V_c is the volume of a unit cell of the lattice. The energy of the fermionic excitations depends linearly on the residual momentum ξ, but the velocity of the excitations is not isotropic.

We now specialize Eq. (59) to the case of the strip,

$$\Delta(\boldsymbol{x}) = 2\Delta\cos(2\boldsymbol{q}\cdot\boldsymbol{x}), \tag{61}$$

which corresponds to the condensate in Eq. (46) with $m = 2$ and $\boldsymbol{n}^2 = -\boldsymbol{n}^1 = \boldsymbol{n}$ and strictly speaking does not describe a crystal, but a condensate that is modulated in the $\boldsymbol{n}$ direction. The coefficients in the dispersion law are given by

$$A_{\pm}^{(\mathrm{strip})} \equiv A^{(\mathrm{strip})} = I_0\left(\frac{2\Delta}{\boldsymbol{q}\cdot\boldsymbol{v}}\right), \tag{62}$$

where $I_0(z)$ is the modified Bessel function of the zeroth order. Therefore, the velocity of the fermionic quasiparticles has the analytic expression

$$c_{\mathrm{strip}}(\boldsymbol{v}) = \frac{1}{I_0(2\Delta/\boldsymbol{q}\cdot\boldsymbol{v})}, \tag{63}$$

which has the important property to vanish when $\boldsymbol{v}$ is orthogonal to $\boldsymbol{n}$. The reason is that in the direction orthogonal to $\boldsymbol{n}$ the gap is constant and its effect is equivalent to a potential barrier. Taking $\boldsymbol{n} = (0,0,1)$, the dispersion law is

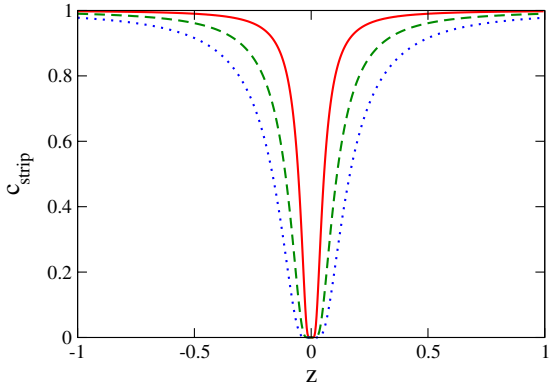

FIG. 6 (color online). Velocity of the fermionic quasiparticles as a function of $z = \cos\vartheta$ for $2\Delta/qv = 0.1$ (solid line), $2\Delta/qv = 0.2$ (dashed line), and $2\Delta/qv = 0.3$ (dotted line) for the strip structure given in Eq. (61).

symmetric for rotations around the z axis, for inversions with respect to the plane $z = 0$, and depends only on the polar angle ϑ, between $\boldsymbol{v}$ and the z axis. In Fig. 6 we report a plot of the velocity of fermionic quasiparticles as a function of $\cos\vartheta$, for three different values of the ratio Δ/qv. In the ultrarelativistic case, $v = 1$, the relevant case is $\Delta/q < 1$ and we see that the dispersion law of fermionic quasiparticles is not much affected by the condensate for $\cos\vartheta \gtrsim 0.2\Delta/q$ and it is the same of relativistic fermions. On the other hand, for small values of $\cos\vartheta$ the fermionic velocity is exponentially suppressed and vanishes for $\vartheta = \pi/2$, meaning that fermionic quasiparticles cannot propagate in the x-y plane, as discussed above.

The fact that the dispersion law is linear in ξ for small values of the momentum does not assure that it is linear for any value of the momentum. Considering $v_z \ll 1$, it is possible to solve the Eq. (56) for $\boldsymbol{k}$ in (57) along the z direction, without restricting to low momenta (Larkin and Ovchinnikov, 1964); the result is that

$$E^2 = \frac{4\Delta|v_z q|}{\pi}e^{-4\Delta/|v_z q|}\left(1 - \cos\frac{\pi k}{q}\right), \tag{64}$$

thus the dispersion law is linear in the residual momentum, only for $k/q \ll 1$.

For the octahedron, whose six wave vectors point into the direction of a bcc structure, the corresponding gap parameter can be written as

$$\Delta(\boldsymbol{x}) = 2\Delta[\cos(2\,qx) + \cos(2\,qy) + \cos(2\,qz)]. \tag{65}$$

It is easy to show that in this case the integral in Eq. (60) factorizes, and the dispersion law is gapless with velocity

$$c_{\mathrm{BCC}}(\boldsymbol{v}) = \frac{1}{I_0(2\Delta/qv_x)I_0(2\Delta/qv_y)I_0(2\Delta/qv_z)}. \tag{66}$$

The corresponding plot is reported in Fig. 7, left panel, where the unit vector $\boldsymbol{v}$ has been expressed by the polar angles ϑ and φ. The plot has been obtained for $2\Delta/qv = 0.3$ and considering $\vartheta \in [0,\pi]$ and $\varphi \in [0,2\pi]$. Note that according to

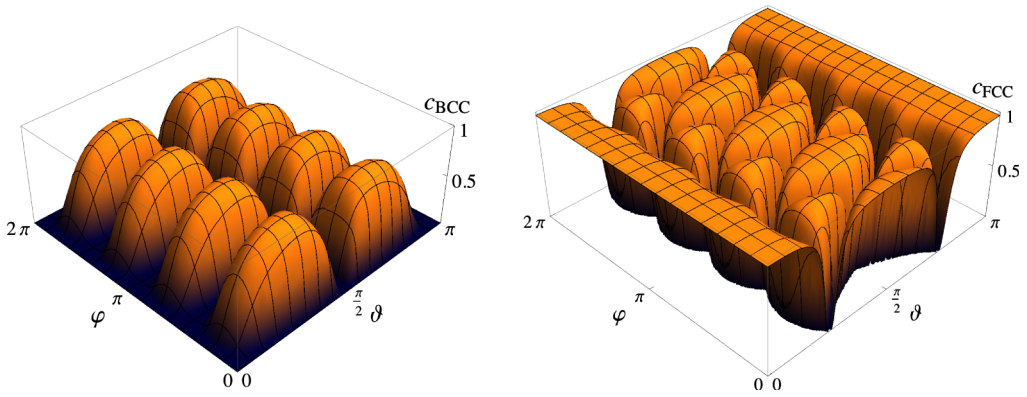

FIG. 7 (color online). Velocity of the fermionic quasiparticles in the BCC crystalline structure (left panel) and in the FCC crystalline structure (right panel) as a function of the polar angles ϑ and φ, for $2\Delta/(qv) = 0.3$.

Eq. (66) the velocity of the fermionic quasiparticles vanishes along the planes $v_x = 0$, $v_y = 0$, and $v_z = 0$.

Unfortunately, for more complicated crystalline structures it is not possible to have an analytic expression of the fermionic velocity. One notable example is the fcc structure which is defined by the condensate

$$\Delta(\boldsymbol{x}) = 2\Delta \sum_{m=1}^{4} \cos(2q\boldsymbol{n}^m \cdot \boldsymbol{x}), \tag{67}$$

where $\boldsymbol{n}^1 = \sqrt{\frac{1}{3}}(1,1,1)$, $\boldsymbol{n}^2 = \sqrt{\frac{1}{3}}(1,1,-1)$, $\boldsymbol{n}^3 = \sqrt{\frac{1}{3}}(1,-1,1)$, and $\boldsymbol{n}^4 = \sqrt{\frac{1}{3}}(-1,1,1)$. Upon plugging this expression in to Eq. (60) we obtain that

$$A_{\pm}^{(\rm fcc)} = \left(\frac{q}{\pi}\right)^3 \int_{\rm cell} dV \exp\left\{ \pm \frac{2\Delta}{qv} B \right\}, \tag{68}$$

where the integration is over the elementary cell of volume $(\pi/q)^3$ and

$$B = \sqrt{3} v \left(\frac{\sin 2q(x+y+z)}{v_x+v_y+v_z} + \frac{\sin 2q(x+y-z)}{v_x+v_y-v_z} + \frac{\sin 2q(x-y+z)}{v_x-v_y+v_z} + \frac{\sin 2q(-x+y+z)}{-v_x+v_y+v_z} \right). \tag{69}$$

It is then easy to show that $A_{+}^{(\rm fcc)} = A_{-}^{(\rm fcc)} \equiv A^{(\rm fcc)}$ and expressing the components of the unit vector $\boldsymbol{v}$ in B as functions of the polar angles ϑ and φ, and upon substituting in $A^{(\rm FCC)}$, one has that the quasiparticle velocity

$$c_{\rm fcc}(\vartheta,\varphi) = \frac{1}{A^{(\rm fcc)}(\vartheta,\varphi)} \tag{70}$$

has the behavior reported in Fig. 7, right panel. The plot of $c_{\rm fcc}(\vartheta,\varphi)$ has been obtained for $2\Delta/qv = 0.3$ and considering $\vartheta \in [0,\pi]$ and $\varphi \in [0,2\pi]$. The velocity of the fermionic quasiparticles is equal to 1 almost everywhere with the exclusion of a restricted region which corresponds to the zeros of $B(\vartheta,\varphi)$, given by the solutions of $\boldsymbol{v}\cdot\boldsymbol{n}^m = 0$.

In conclusion, we have shown that for various crystalline structures the fermionic spectrum is gapless. For $k/q \ll 1$ the dispersion law is linear in momentum and the fermionic velocity vanishes along the planes orthogonal to the direction of the vertices of the reciprocal lattice. This result remains valid also for massive quarks, since the effect of the quark mass can be accounted for by reducing v (Casalbuoni, De Fazio *et al.*, 2002).

Regarding the FF condensate we take the direction of the Cooper pair total momentum $2\boldsymbol{q}$ along the z axis. In this case, the quasiparticle spectrum has the analytical expression

$$E_{\pm} = qv_z \pm \sqrt{\xi^2 + \Delta^2}, \tag{71}$$

where the quasiparticle energies are computed from the corresponding Fermi energies $\mu_{u,d}$. Equation (71) is the dispersion law of quasiparticle ($E_{\pm} \geq 0$) or hole states ($E_{\pm} < 0$). As for the case of the strip and the fcc, the dispersion law depends on the considered direction in coordinate space. However, contrary to what happens for real crystalline structures, in the FF phase there are directions along which the dispersion laws are gapped and directions along which the dispersion laws are gapless.

The zeros of the dispersion laws are located, for a given value of $\cos\vartheta$, at

$$\xi_0 = \pm \sqrt{(qv\cos\vartheta)^2 - \Delta^2}, \tag{72}$$

and therefore for $\Delta/qv > 1$ both gapless modes disappear.

2. Specific heat of the Fermi quasiparticles

The contribution of the Fermi quasiparticles to the specific heat per unit volume is given by

$$c_V = 2\sum_j \int \frac{d^3p}{(2\pi)^3} E_j \frac{\partial n(E_j,T)}{\partial T}, \tag{73}$$

where $n(E_j,T)$ is the Fermi distribution function and the sum is over all fermionic modes. Considering the low temperature range, $T \ll \Delta$, which is relevant for astrophysical applications, and using Eq. (59) one obtains for a generic two-flavor crystalline structure

$$c_V = \frac{4\mu^2 T}{3}\int \frac{d\Omega}{4\pi}\frac{1}{c(\boldsymbol{v})} + \frac{2\mu^2}{3}T, \tag{74}$$

where the first and second addenda correspond to the contribution of the paired and unpaired quarks, respectively. Note that both contributions are linear in T, because all degrees of freedom have a linear dispersion law at small momenta. This expression can be evaluated in closed form for the strip (Casalbuoni *et al.*, 2003)

$$c_V^{(\mathrm{strip})} = \frac{4\mu^2 T}{3}{}_1F_2(-1/2;1/2,1;(\Delta/qv)^2) + \frac{2\mu^2}{3}T, \tag{75}$$

where ${}_1F_2$ denotes the generalized hypergeometric function (Gradshteyn and Ryzhik, 1980). Different from the analysis of Larkin and Ovchinnikov (1964), here v is not small and we can take $\Delta/qv \to 0$ near the second-order phase transition. Since for small Δ/qv one has ${}_1F_2(-1/2;1/2,1;(\Delta/qv)^2) \simeq 1-(\Delta/qv)^2$, it is easily seen that the normal Fermi liquid result is obtained for $\Delta = 0$. On the other hand, for nonvanishing Δ, the specific heat turns out to be smaller.

In the case of the FF state, the dispersion law of the quasiparticles is given by Eq. (71) and using Eq. (73) one obtains that in the small temperature limit ($T \ll \Delta$) and for $\Delta < q$

$$c_V^{(\mathrm{FF})} \simeq \frac{4\mu^2 T}{3}\sqrt{1-\frac{\Delta^2}{(qv)^2}} + \frac{2\mu^2}{3}T. \tag{76}$$

The paired quark contribution depends linearly on temperature because the quasiparticle dispersion law (71) gives rise to gapless modes when $\Delta/qv < 1$. There is also an additional contribution to the specific heat due to gapped modes, but this contribution is exponentially suppressed with the temperature and has not been reported in Eq. (76).

E. Smearing procedure and HDET approximation for two-flavor QCD

In Sec. II.C.2 we discussed the GL expansion of the free energy for various CCSC phases. Since the GL expansion has several limitations and is reliable when $\Delta/\delta\mu$ is small, it is useful to derive a different approximation scheme. In Sec. II.D.1 we presented an approximation allowing us to deal with the dispersion law of fermionic quasiparticles close to the gapless momentum. However, this method cannot be used for evaluating the free energy of the system or the low-energy Lagrangian. For these purposes a different approximation named the *smearing procedure* can be used. This approximation, developed by Casalbuoni *et al.* (2004) within the HDET framework, is valid when $\Delta/\delta\mu$ is large, and is thus complementary to the GL expansion.

1. Gap equations

The mean field Lagrangian term describing condensation in any CCSC phase can be written as follows:

$$\mathcal{L}_\Delta = -\frac{1}{2}[\psi_i^\alpha C\gamma_5\psi_j^\beta \Delta_{ij}^{\alpha\beta}(\boldsymbol{x}) + \mathrm{H.c.}] - \frac{\Delta^*(\boldsymbol{x})\Delta(\boldsymbol{x})}{G}, \tag{77}$$

where $\Delta_{ij}^{\alpha\beta}(\boldsymbol{x})$ is the pertinent gap parameter and hereafter we indicate the NJL coupling constant in the diquark channel with G. We define the smearing procedure considering in the first place the FF phase, with $\Delta_{ij}^{\alpha\beta}(\boldsymbol{x})$ given in Eq. (41). Although this case can be solved exactly, it is useful to consider it to fix the notation and to introduce some definitions to be used later on. We consider Cooper pairing of the massless up and down quarks, chemical potential μ_u, μ_d, and we define $\mu = (\mu_u+\mu_d)/2$ and $\delta\mu = |\mu_u-\mu_d|/2 \ll \mu$.

The calculation can be simplified using the HDET approximation (Beane, Bedaque, and Savage, 2000; Hong, 2000a, 2000b; Casalbuoni, Gatto, and Nardulli, 2001; Nardulli, 2002; Schafer, 2003a). We Fourier decompose the fermionic fields as follows:

$$\psi_i^\alpha(x) = \int \frac{d\Omega}{4\pi} e^{-i\mu\boldsymbol{v}\cdot\boldsymbol{x}}[\psi_{i,\boldsymbol{v}}^\alpha(x) + \psi_{i,\boldsymbol{v}}^{\alpha-}(x)], \tag{78}$$

where $\boldsymbol{v}$ is a unit three-dimensional vector whose direction is integrated over. $\psi_{i,\boldsymbol{v}}^\alpha(x)$ [$\psi_{i,\boldsymbol{v}}^{\alpha-}(x)$] are positive (negative) energy projections of the fermionic fields with flavor i and color α indices, as defined by Casalbuoni, Gatto, Mannarelli, and Nardulli (2001) and Nardulli (2002). Note that these fields are written in a mixed notation, meaning that they depend both on the space coordinates and on the unit vector $\boldsymbol{v}$, which points to a particular direction in momentum space. Since only quasiparticles and quasiholes live close to the Fermi surface, they are the only relevant degrees of freedom. Antiparticles decouple and their contribution is suppressed by powers of $1/\mu$. The three-dimensional momentum of a fermion is written as $(\mu+\xi)\boldsymbol{v}$, with ξ representing the "residual" momentum component. The integration over momentum space is separated into an angular integration over $\boldsymbol{v}$ and a radial integration over $-\delta \le \xi \le \delta$. The cutoff δ must be taken smaller than μ but much larger than the gap in the homogeneous phase and $\delta\mu$; see Fig. 1. At the leading order in $1/\mu$ the free Lagrangian can be written as

$$\mathcal{L} = \int \frac{d\Omega}{4\pi}[\psi_{i,\boldsymbol{v}}^{\alpha\dagger}(iV\cdot\partial + \delta\mu_i)\psi_{i,\boldsymbol{v}}^\alpha], \tag{79}$$

where $V^\nu = (1,\boldsymbol{v})$, and we also define for later use $\tilde{V}^\nu = (1,-\boldsymbol{v})$. In the HDET approximation the Lagrangian term in Eq. (77) for the FF phase turns into

$$\mathcal{L}_\Delta = -\frac{1}{2}\left(\int \frac{d\Omega}{4\pi}\Delta_{ij}^{\alpha\beta}\psi_{i,-\boldsymbol{v}}^{\alpha T}C\gamma_5\psi_{j,\boldsymbol{v}}^\beta + \mathrm{H.c.}\right) - \frac{\Delta^2}{G}, \tag{80}$$

and the zero-temperature gap equation can be written as

$$1 = \frac{G\rho}{2}\int \frac{d\Omega}{4\pi}\int_0^\delta \frac{d\xi}{\sqrt{\xi^2+\Delta^2}}[1-\theta(-E_u)-\theta(-E_d)], \tag{81}$$

where $\rho = 4\mu^2/\pi^2$ is the density of states in two-flavor QCD. The quasiparticle dispersion laws have been obtained in Eq. (71), but energies are now measured from the common energy level μ, and therefore

$$E_{u,d} = \pm\,\delta\mu \mp \boldsymbol{q}\cdot\boldsymbol{v} + \sqrt{\xi^2+\Delta^2}. \tag{82}$$

In Eq. (81) the contribution of hole excitations is taken into account simply multiplying the contribution of quasiparticles times 2. We observe that in general

$$1-\theta(-x)-\theta(-y)=\theta(x)\theta(y)-\theta(-x)\theta(-y), \tag{83}$$

and since E_u and E_d cannot be simultaneously negative, then

$$1-\theta(-E_u)-\theta(-E_d)=\theta(E_u)\theta(E_d), \tag{84}$$

so the integration in Eq. (81) is over a restricted region named the pairing region (PR), defined by

$$\mathrm{PR}=\{(\xi,\boldsymbol{v}\cdot\boldsymbol{n})|E_u>0 \quad \text{and} \quad E_d>0;\xi\le\delta\}. \tag{85}$$

More explicitly, the pairing region is defined by the condition

$$\max\left\{-1,z_q-\frac{\sqrt{\xi^2+\Delta^2}}{q}\right\} < \boldsymbol{v}\cdot\boldsymbol{n} < \min\left\{1,z_q+\frac{\sqrt{\xi^2+\Delta^2}}{q}\right\}, \tag{86}$$

with

$$z_q=\frac{\delta\mu}{q}. \tag{87}$$

From the above definition it follows that for small values of Δ and ξ the pairing region is centered at $\vartheta_q=\arccos z_q$, has an angular width of order Δ/q and a thickness of order Δ; see Fig. 5.

Thus, Eq. (81) can be written in a different way,

$$\Delta=\frac{G\rho}{2}\int\int_{\mathrm{PR}}\frac{d\Omega}{4\pi}d\xi\frac{\Delta}{\sqrt{\xi^2+\Delta^2}} =\frac{G\rho}{2}\int\frac{d\Omega}{4\pi}\int_0^{\delta}d\xi\frac{\Delta_{\mathrm{eff}}}{\sqrt{\xi^2+\Delta_{\mathrm{eff}}^2}}, \tag{88}$$

where $\Delta_{\mathrm{eff}}\equiv\Delta_{\mathrm{eff}}(\boldsymbol{v}\cdot\boldsymbol{n},\xi)$ is defined as

$$\Delta_{\mathrm{eff}}=\Delta\theta(E_u)\theta(E_d)=\begin{cases}\Delta & \text{for} \quad (\xi,\boldsymbol{v}\cdot\boldsymbol{n})\in\mathrm{PR}\\ 0 & \text{elsewhere.}\end{cases} \tag{89}$$

The above procedure defines the smearing procedure for the FF phase; it can be extended to the case of P plane waves, Eq. (46), generalizing the results of the previous equations, assuming that in the mean field Lagrangian one can substitute Δ with $\Delta_{\mathrm{E}}(\boldsymbol{v},p_0)$, where

$$\Delta_E(\boldsymbol{v},p_0)=\sum_{m=1}^{P}\Delta_{\mathrm{eff}}(\boldsymbol{v}\cdot\boldsymbol{n}^m,p_0), \tag{90}$$

meaning that $\Delta_E=n\Delta$, where $n=1,\ldots,P$. We can thus generalize the pairing region to

$$\mathcal{P}_n=\{(\boldsymbol{v},\xi)|\Delta_E(\boldsymbol{v},\epsilon)=n\Delta\}. \tag{91}$$

Note that in this equation we have made explicit the dependence on the energy p_0 instead of that on the residual momentum, because the pole position is in general in

$$\epsilon_n=\sqrt{\xi^2+n^2\Delta^2}. \tag{92}$$

Correspondingly, the gap equation is

$$P\Delta=i\frac{G\rho}{2}\int\frac{d\Omega}{4\pi}\int\frac{dp_0d\xi}{2\pi}\frac{\Delta_E(\boldsymbol{v},p_0)}{p_0^2-\xi^2-\Delta_E^2(\boldsymbol{v},p_0)}, \tag{93}$$

which generalizes Eq. (88). The origin of the factor P on the left-hand side of this equation is as follows. The Lagrangian contains the term

$$\frac{\Delta^*(\boldsymbol{x})\Delta(\boldsymbol{x})}{G}, \tag{94}$$

which, when averaged over the cell, gets nonvanishing contribution only from the diagonal terms in the double sum over the plane waves and each plane wave gives a separate contribution.

The energy integration is performed by the residue theorem and the phase space is divided into different regions according to the pole positions. Therefore the gap equation turns out to be given by

$$P\Delta\ \ln\frac{2\delta}{\Delta_{\mathrm{2SC}}}=\sum_{n=1}^{P}\int\int_{\mathcal{P}_n}\frac{d\Omega}{4\pi}d\xi\frac{n\Delta}{\sqrt{\xi^2+n^2\Delta^2}}, \tag{95}$$

where we have used the NJL gap equation

$$\Delta_{\mathrm{2SC}}=2\delta\ \exp\left\{-\frac{\pi^2}{2G\mu^2}\right\}, \tag{96}$$

for relating the NJL coupling G to the 2SC gap parameter and the momentum cutoff. The first term in the sum, corresponding to the region $\mathcal{P}_1$, has P equal contributions with a dispersion law equal to the FF case. This can be interpreted as a contribution from P noninteracting plane waves. In the other regions the different plane waves have an overlap. Since the definition of the regions $\mathcal{P}_n$ depends on the value of Δ, their determination is part of the problem of solving the gap equation.

Stated in a different way, in the smearing procedure the dispersion relation of the quasiparticles has several branches corresponding to the values $n\Delta$, $n=1,\ldots,P$. Therefore, the following interpretation of the gap equation (95) can be given. Each term in the sum corresponds to one branch of the dispersion law, i.e., to the propagation of a gapped quasiparticle with gap $n\Delta$, which is defined in the region $\mathcal{P}_n$. However, the regions $\mathcal{P}_n$ do not represent a partition of the phase space since it is possible to have at the same point quasiparticles with different gaps.

2. Numerical results: Free energy computation

In Table I we report the results obtained in the CC limit ($\delta\mu=\delta\mu_1=\Delta_{\mathrm{2SC}}/\sqrt{2}$) for four crystalline structures, respectively, the FF ($P=1$), the strip ($P=2$), the octahedron (bcc) ($P=6$), and the fcc ($P=8$). The table shows that, among the four considered structures, the favored one at $\delta\mu=\delta\mu_1$ is the octahedron, which, however, does not have the largest gap Δ. The gap parameter determines the extension of the pairing regions [see Eq. (86)], but a free energy gain may result from

TABLE I. The values of $z_q = \delta\mu/q$, the gap, and the free energy at $\delta\mu = \delta\mu_1 = \Delta_{2SC}/\sqrt{2}$ for different crystalline structures. See the text for more details. Adapted from Casalbuoni *et al.*, 2004.

P	z_q	$\frac{\Delta}{\Delta_{2SC}}$	$\frac{\Omega-\Omega_n}{\rho\Delta_{2SC}^2}$
1	0.78	0.24	-3.6×10^{-3}
2	1.0	0.75	−0.16
6	0.9	0.28	−0.22
8	0.9	0.21	−0.18

having many small nonoverlapping pairing regions, as well. Indeed, the strip has the largest gap parameter, but not the largest free energy, presumably because the pairing occurs only in four large ribbons (two for each vectors $\boldsymbol{q}^m$; see the right panel of Fig. 5). Indeed, as shown in the previous section, the width and the thickness of the ribbons are proportional to Δ. For example, in the octahedron pairing occurs in smaller ribbons, but there are twelve pairing regions, which give a large contribution to the free energy.

For the case $\delta\mu \neq \delta\mu_1$, we plot in Fig. 8 the free energy of the octahedron (dashed line) and the fcc (full line) structures as a function of $\delta\mu/\Delta_{2SC}$. The octahedron is the favored structure up to $\delta\mu \simeq 0.95\Delta_{2SC}$; the fcc structure is favored in the range $0.95\Delta_{2SC} \lesssim \delta\mu \lesssim 1.32\Delta_{2SC}$; for larger values of $\delta\mu$ the normal phase becomes favored. The fcc gap parameter is smaller than the octahedron gap parameter for any value of $\delta\mu$, but the fcc benefits of more pairing regions than the octahedron.

In Table II we report various numerical results for each crystalline structure at the transition point from the CCSC phase to the normal phase: the value of $\delta\mu_2$, the computed order of the phase transition between the crystalline phase and the normal phase, the value of z_q [see Eq. (87)], and of the discontinuity in Δ/Δ_{2SC} at $\delta\mu = \delta\mu_2 - 0^+$.

In the smearing approximation both the order of the transition and the point where the transition occurs are

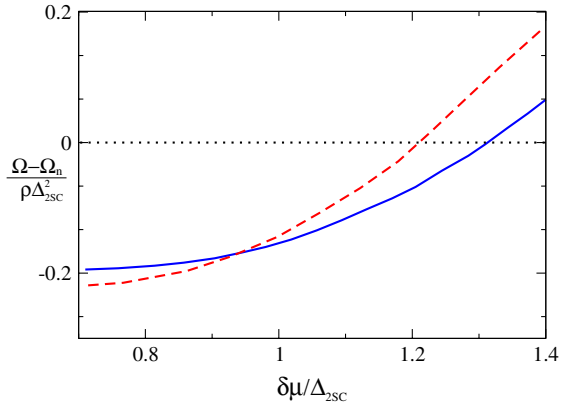

FIG. 8 (color online). Free energy as a function of $\delta\mu/\Delta_{2SC}$, for the octahedron (dashed line) and the fcc (solid line). Free energies are measured respect to the normal phase. The octahedron is the favored structure up to $\delta\mu \simeq 0.95\Delta_{2SC}$. In the range $0.95\Delta_{2SC} \lesssim \delta\mu \lesssim 1.32\Delta_{2SC}$ the fcc is favored. For larger values of $\delta\mu$ the normal phase is energetically favored. In this plot the values of $\delta\mu$, z_q, and Δ are those that minimize the free energy. Adapted from Casalbuoni *et al.*, 2004.

TABLE II. Values of $\delta\mu_2$, the order of the phase transition between the CCSC phase and the normal phase, $z_q = \delta\mu/q$, and the discontinuity of Δ/Δ_{2SC} at the phase transition point for different crystalline structures. See the text for more details. Adapted from Casalbuoni *et al.*, 2004.

P	$\delta\mu_2/\Delta_{2SC}$	Order	z_q	Δ/Δ_{2SC}
1	0.754	II	0.83	0
2	0.83	I	1.0	0.81
6	1.22	I	0.95	0.43
8	1.32	I	0.90	0.35

different from those obtained within the GL approximation. However, the difference in $\delta\mu_2$ is ∼10% and in z_q is ≃17% at most (in GL for any structure $z_q \approx 0.83$). On the other hand, in agreement with the GL results, the structure with six plane waves is energetically favored over the structure with two plane waves or with one plane wave. Therefore, increasing the pairing region leads to an increase of the free energy gain making the configuration more stable. An interesting result of the smearing procedure is that with increasing $\delta\mu$ the configuration with six plane waves is superseded by the structure with eight plane waves, which has a lower Δ but a larger number of pairing regions. This has to be contrasted with the result of the GL approximation (see Sec. II.C.2), where the octahedron is always disfavored with respect to the fcc (but one should consider that the GL free energy of the fcc is not bounded from below).

F. Effective Lagrangian of phonons and contribution to the specific heat

The low-energy spectrum of a periodically modulated condensate, besides Fermi quasiparticles, consists also of massless NGBs which originate from the spontaneous breaking of translational invariance. For two-flavor quark matter in any crystalline phase, these are the only NGBs, because no global symmetry of the system is spontaneously broken. Since the modulation of the condensate is associated with a crystalline structure, these NGBs describe the vibrations of the crystal and are for this reason called phonons. These phonons are not the standard pressure oscillations of a fluid, rather they are akin to second sound in standard superfluids, because they are related to chemical potential oscillations; see, e.g., Anglani, Mannarelli, and Ruggieri (2011). In more detail, phonons are small position and time dependent displacements of the condensate: in the presence of phonons, then,

$$\Delta(\boldsymbol{x}) \to \Delta^u(x) = \Delta(\boldsymbol{x} - \boldsymbol{u}(x)), \tag{97}$$

and one may define a set of three dimension-one scalar field $\phi^{(i)}$ by

$$\frac{\phi^{(i)}}{f_\phi} = 2q\boldsymbol{u}_i, \tag{98}$$

with $i = 1, 2, 3$, where f_ϕ is the corresponding decay constant. In the following we refer to both $\boldsymbol{u}$ and ϕ as the phonons. For any crystalline structure one can deduce the general expression of the phonon Lagrangian from the symmetries of the system, but the various coefficients have to

be evaluated with a microscopic theory. Calculation of the low-energy coefficients can be done using a NJL-like model with a smearing procedure, as in Casalbuoni, Gatto, Mannarelli, and Nardulli (2001) and Casalbuoni, Fabiano *et al.* (2002), or by a GL expansion, as in Mannarelli, Rajagopal, and Sharma (2007). These coefficients are related to the elastic properties of the crystalline structure. For the two-flavor CCSC phases the elastic properties do not seem to be of particularly interest, because not all quarks condense and thus the system should not behave as a crystal under an external stress. However, as we discuss in Sec. III.D, the shear modulus of various three-flavor crystalline structures is actually associated with a form of rigidity of quark matter.

The GL expansion of Mannarelli, Rajagopal, and Sharma (2007) provides an expression of the leading order (LO) Lagrangian density in the derivative expansion valid for a generic set $\{\boldsymbol{n}\}$ of unit vectors

$$\mathcal{L}^{\Delta^2}[\boldsymbol{u}] = \frac{1}{2}\frac{2\mu^2|\Delta|^2}{\pi^2(1-z_q^2)}\sum_m [\partial_0(\boldsymbol{n}^m\cdot\boldsymbol{u})\partial_0(\boldsymbol{n}^m\cdot\boldsymbol{u}) - (\boldsymbol{n}^m\cdot\partial)(\boldsymbol{n}^m\cdot\boldsymbol{u})(\boldsymbol{n}^m\cdot\partial)(\boldsymbol{n}^m\cdot\boldsymbol{u})], \tag{99}$$

with z_q given in Eq. (87). This $\mathcal{O}(\Delta^2)$ Lagrangian includes the displacement fields at the second order and therefore the interaction terms are missing. We see in Sec. III.D.1 how this expression can be derived from a NJL-like model in the more complicated case of the three-flavor CCSC phase.

In the FF phase there is one single phonon field ϕ and one privileged direction corresponding to $\boldsymbol{q}$. Given the space symmetries of the system, the LO Lagrangian density in the momentum expansion is given by

$$\mathcal{L} = \frac{C}{2f_\varphi^2}[\dot\varphi^2 - v_\parallel^2(\nabla_\parallel\varphi)^2 - v_\perp^2|\nabla_\perp\varphi|^2], \tag{100}$$

where $\nabla_\parallel = \boldsymbol{n}\cdot\boldsymbol{\nabla}$, $\boldsymbol{\nabla}_\perp = \boldsymbol{\nabla} - \boldsymbol{n}\nabla_\parallel$, and $\boldsymbol{n}$ is the unit vector parallel to $\boldsymbol{q}$. The breaking of the rotational symmetry in the underlying microscopic theory implies that the velocity of propagation in the direction parallel to $\boldsymbol{n}$, $v_\parallel$, can be different from the velocity of propagation in the direction orthogonal to $\boldsymbol{n}$, $v_\perp$. The dispersion law, relating the phonon quasimomentum $\boldsymbol{k}$ and energy ω, is given by

$$\omega(\boldsymbol{k}) = \sqrt{v_\perp^2(k_x^2+k_y^2) + v_\parallel^2 k_z^2}, \tag{101}$$

and the contribution of phonons to the specific heat at small temperatures turns out to be

$$c_V^{(\mathrm{FF})} = \frac{8\pi^2}{15 v_\perp^2 v_\parallel}T^3 \quad \text{(phonons)}. \tag{102}$$

Casalbuoni *et al.* (2003), using the smearing procedure, obtained that $C = \mu^2 k_r^2$, with $k_r \propto \delta\mu^2/q^2$ a coefficient arising within the smearing procedure. The obtained values of the velocities are

$$v_\parallel^2 = \cos^2\vartheta_q \simeq 0.7, \qquad v_\perp^2 = \tfrac{1}{2}\sin^2\vartheta_q \simeq 0.15, \tag{103}$$

with ϑ_q defined in Eq. (51).

Since the strip has the same space symmetries of the FF phase and one phonon field, the Lagrangian density has the same formal expression reported in Eq. (100), but the values of the longitudinal and transverse velocities can be different. Thus, for the strip the expression of the specific heat is formally the same reported above. From Eq. (99) we can see that the $\mathcal{O}(\Delta^2)$ GL expansion gives $v_\parallel = 1$ and $v_\perp = 0$ for both the FF and the strip. Unfortunately, higher order corrections in Δ of the phonon velocities have not been computed within the GL expansion, hindering the comparison with Eq. (103). Note, however, that both methods give a FF low-energy Lagrangian with the same O(2) symmetry of the microscopic system.

The low-energy oscillations of more complicated crystals can in principle be described in a similar way. As an example, for the FCC structure the oscillations are described by three phonon fields $\phi^{(i)}$ and the LO Lagrangian density compatible with the fcc symmetry is given by

$$\mathcal{L} = \frac{C}{2f_\phi^2}\left[\sum_{i=1,2,3}(\dot\phi^{(i)})^2 - a\sum_{i=1,2,3}|\boldsymbol{\nabla}\phi^{(i)}|^2 - b\sum_{i=1,2,3}\partial_i\phi^{(i)}\partial_i\phi^{(i)} - 2c\sum_{i,j=1,2,3}\partial_i\phi^{(i)}\partial_j\phi^{(j)}\right], \tag{104}$$

where a, b, and c are three coefficients to be determined by the microscopic theory. The smearing procedure gives

$$a = 1/12 \simeq 0.08, \qquad b = 0, \qquad c = (3\cos^2\vartheta_q - 1)/12 \simeq 0.09. \tag{105}$$

Since for vanishing b the Lagrangian in Eq. (104) is rotationally invariant, it has a larger symmetry than the underlying microscopic theory, which has the FCC symmetry. A possible explanation is that being phonons long wavelength fluctuations of the crystal, the low-energy parameters are given by an average over the cubic structure and thus are not sensitive to the local modulation of the condensate. On the other hand, substituting the appropriate unit vectors in the $\mathcal{O}(\Delta^2)$ GL in Eq. (99) one obtains $a = c = -b/2 = 1/3$. Thus, according to the GL analysis the low-energy theory and the microscopic theory have the same FCC symmetry. This might be an artifact of the GL expansion, indeed in the GL analysis the low-energy parameters are obtained first expanding the action in Δ and then in ϕ, but it is not obvious that the two expansions commute. Nevertheless, note that the smearing procedure gives $a \simeq c$, compatible with the GL result $a = c$. In principle the additional term $\partial_i\phi^{(j)}\partial_j\phi^{(i)}$ should be included [see, e.g., Leutwyler (1997)], but here it is assumed that it can be recast in the term proportional to c by integration by parts.

The specific heat contribution of the phonons in the fcc structure has been evaluated numerically by Casalbuoni *et al.* (2003), and the result is

$$c_V^{(\mathrm{fcc})} \approx 88\pi^2 T^3 \quad \text{(phonons)}. \tag{106}$$

G. Chromomagnetic stability of the two-flavor crystalline phase

As discussed in Sec. II.B.1, the 2SC phase is chromomagnetically unstable for $\delta\mu > \delta\mu_1$. This instability could be interpreted as the tendency of the system to generate a net momentum of the quark pair, as shown by Giannakis and Ren (2005a). Therefore, the chromomagnetic instability can be interpreted as a tendency to develop quark currents, which in turn is equivalent to the FF phase, where diquark carry momentum $2\boldsymbol{q}$.

In this section, we review the results of Giannakis and Ren (2005a), which relate the Meissner mass of the $\bar{8}$ mode of the 2SC to the momentum susceptibility and also the computation of the Meissner tensor in the crystalline phases (Giannakis, Hou, and Ren, 2005; Giannakis and Ren, 2005a, 2005b; Reddy and Rupak, 2005).

1. Momentum susceptibility

The response of the thermodynamic potential of the 2SC phase to a small momentum of the quark pair can be computed absorbing the phase of the condensate into the phase of the quark fields; the net effect is a shift of each quark momentum by $\boldsymbol{q}$; see Sec. II.C.1. Therefore, the one loop effective action (in the presence of background gauge fields) can be computed using the same steps that lead to Eq. (21); see also the discussion after Eq. (44). Expanding the thermodynamic potential around $q = 0$ one has, at the lowest order,

$$\Omega = \Omega_{2SC} + \tfrac{1}{2}\mathcal{K}q^2, \tag{107}$$

where the momentum susceptibility is given by

$$\mathcal{K} = \frac{i}{6}\sum_{i=1}^{3}\int \frac{d^4p}{(2\pi)^4}\,\mathrm{Tr}[\Gamma_i S(p)\Gamma_i S(p)], \tag{108}$$

with $S(p)$ the quark propagator in momentum space and $\mathbf{\Gamma} = \mathrm{diag}(\boldsymbol{\gamma}, -\boldsymbol{\gamma})$ the appropriate vertex factor. Note that we are considering an expansion of the thermodynamic potential for small q, therefore the momentum susceptibility does not depend on q, meaning that $S(p)$ is the 2SC quark propagator, which can be obtained inverting Eq. (20). The momentum susceptibility has an expression similar to the space component of the 2SC polarization tensor [see Eq. (33)], at vanishing momentum. In particular, it is possible to show that it is proportional to the squared Meissner mass of the $\bar{8}$ mode. The reason is that the only nonvanishing contribution both to the momentum susceptibility and to the Meissner mass of the $\bar{8}$ mode are determined from the red-green color sector (blue quarks do not carry a condensate and do not mix with red and green quarks). But in this color sector $T_{\bar{8}}$ is proportional to the identity and thus the corresponding vertex factor is proportional to $\mathbf{\Gamma}$. A more detailed discussion can be found in Giannakis and Ren (2005a), where it was shown that

$$\mathcal{M}^2_{M,\bar{8}} = \frac{1}{12}\left(g_s^2 + \frac{e^2}{3}\right)\mathcal{K}, \tag{109}$$

where the mass of the $\bar{8}$ mode in the 2SC phase is given in Eq. (39).

At the transition point between the 2SC and g2SC phases, $\delta\mu = \Delta$, one finds $M^2_{M,\bar{8}} < 0$ and thus Eq. (109) implies that the system is unstable toward the formation of pairs with nonvanishing net momentum; indeed a negative $\mathcal{K}$ in Eq. (107) implies that there is a gain in free energy if $q \neq 0$. Therefore, the chromomagnetic instability of the $\bar{8}$ mode leads naturally to the FF state.

Before turning to the computation of the Meissner tensor in the crystalline phase, we briefly comment on the absence of total currents induced by the net momentum of the quark pair. The value of the total momentum is determined by minimizing the free energy, thus $\partial\Omega/\partial q = 0$, and the stationarity condition is equivalent to

$$\langle\bar{\psi}\boldsymbol{\gamma}\psi\rangle = 0, \tag{110}$$

which implies that no baryon matter current is generated in the ground state. Analogously, one can show (Giannakis and Ren, 2005a) that electric and color currents vanish as well. In particular, the residual $\mathrm{SU}(2)_c \otimes \mathrm{U}(1)_{\tilde{Q}}$ symmetry implies that $\langle\bar{\psi}\Gamma_A\psi\rangle = 0$ for $A \neq 8$, with $\mathbf{\Gamma}_A$ defined in Eqs. (34) and (35); moreover, for $A = 8$ one finds

$$\boldsymbol{J}_8 = \frac{\sqrt{3g_s^2 + e^2}}{6}\langle\bar{\psi}\boldsymbol{\gamma}\psi\rangle, \tag{111}$$

which vanishes because of the stationary condition, Eq. (110). Therefore, no total current is generated in the FF state.

2. Meissner masses in the FF phase

Since the FF phase has the same gauge symmetry breaking pattern of the 2SC phase, it has five massive gluons. Computation of the Meissner tensor of gluons in the two-flavor FF phase has been done by Giannakis, Hou, and Ren (2005) and Giannakis and Ren (2005b), neglecting neutrality conditions and considering the isospin chemical potential $\delta\mu = \mu_e/2$ as a free parameter. Since there exists a privileged direction, the Meissner mass becomes direction dependent and is in general decomposed into longitudinal and transverse components with respect to $\boldsymbol{q}$. The Meissner tensors of the gluon fields with adjoint color $a = 4, \ldots, 7$ are all equal and can be written as

$$(\mathcal{M}^2_{M,4})_{ij} = A\left(\delta_{ij} - \frac{q_i q_j}{q^2}\right) + B\frac{q_i q_j}{q^2}. \tag{112}$$

The Meissner tensor of the $\bar{8}$ mode can be decomposed in a similar way

$$(\mathcal{M}'^2_{M,\bar{8}})_{ij} = C\left(\delta_{ij} - \frac{q_i q_j}{q^2}\right) + D\frac{q_i q_j}{q^2}. \tag{113}$$

The coefficients A and C are called the *transverse* Meissner masses; similarly, B and D are the *longitudinal* Meissner masses. As discussed in the previous section, the mass of the rotated eighth gluon is related to the variation of the free energy with respect to q. In the FF phase it has been shown by Giannakis, Hou, and Ren (2005) that the precise relation is the following:

$$C = \frac{1}{12}\left(g_s^2 + \frac{e^2}{3}\right)\frac{1}{q}\frac{\partial\Omega}{\partial q}, \tag{114}$$

$$D = \frac{1}{12}\left(g_s^2 + \frac{e^2}{3}\right)\frac{\partial^2\Omega}{\partial q^2}. \tag{115}$$

If the phase with $q \neq 0$ is a minimum of the free energy, then both the conditions $\partial\Omega/\partial q = 0$ and $\partial^2\Omega/\partial q^2 > 0$ must be satisfied. Thus, $C = 0$ and $D > 0$ at the minimum. As a consequence, the Meissner tensor of the $\bar{8}$ mode is purely longitudinal and positively defined.

The coefficients A, B, and D can be computed analytically. We refer the interested reader to the original article (Giannakis and Ren, 2005b). Here it is enough to consider the small gap expansion (Giannakis and Ren, 2005b; Ciminale *et al.*, 2006); in this approximation scheme one has

$$A = \frac{g_s^2\mu^2}{96\pi^2}\frac{\Delta^4}{\delta\mu^4(z_q^{-2}-1)^2}, \tag{116}$$

$$B = \frac{g_s^2\mu^2}{8\pi^2}\frac{\Delta^2}{\delta\mu^2(z_q^{-2}-1)}, \tag{117}$$

$$D = \frac{g_s^2\mu^2}{6\pi^2}\left(1 + \frac{e^2}{3g_s^2}\right)\frac{\Delta^2}{\delta\mu^2(z_q^{-2}-1)}. \tag{118}$$

The message of the above equations is that the Meissner tensor is positively defined for the one plane wave phase, within the small gap parameter approximation. Giannakis and Ren (2005b) argued that for a multiple plane wave structure the situation will be better (within the small gap expansion). As a matter of fact, at the $\Delta^2/\delta\mu^2$ order, the Meissner tensor is purely longitudinal, and the longitudinal components are positive at the minimum of the free energy. Therefore, if the expansion in plane waves contains at least three linearly independent momenta, the Meissner tensor will be positive definite, being additive with respect to different terms of the plane wave expansion to order $\Delta^2/\delta\mu^2$. This has been explicitly checked by Ciminale *et al.* (2006).

Besides, Giannakis and Ren (2005b) performed the numerical computation of the Meissner masses, beyond the small gap expansion. The results can be summarized as follows. First, the FF phase is found to be more stable than the 2SC phase in the LOFF window

$$0.706\Delta_{2SC} \lesssim \delta\mu \lesssim 0.754\Delta_{2SC}. \tag{119}$$

Within this range, the LOFF gap window is

$$0 < \Delta \lesssim 0.242\Delta_{2SC}, \tag{120}$$

and the longitudinal Meissner masses B and D turn out to be positive within the range

$$0 < \Delta \lesssim 0.84\Delta_{2SC}; \tag{121}$$

moreover, the transverse mass A of the gluons with $a = 4, \ldots, 7$ turns out to be positive within the range

$$0 < \Delta \lesssim 0.38\Delta_{2SC}. \tag{122}$$

Since the LOFF window for the FF state (120) is contained in both the intervals (121) and (122), the FF state is free from the chromomagnetic instability, as long as it is energetically favored with respect to the homogeneous phase.

H. Solitonic ground state

The analysis of various crystalline phases has shown that a periodic structure is energetically favored for mismatched Fermi spheres. Nickel and Buballa (2009) proposed a generalization of the crystalline structure for exploring whether the more complicated periodic condensate [we do not report the color-flavor structure because it is the same as Eq. (41)]

$$\Delta(z) = \sum_{k\in\mathbb{Z}} \Delta_{\boldsymbol{q},k} e^{2\,ikqz}, \tag{123}$$

may be energetically favored with respect to standard crystalline structures. The wave vector $\boldsymbol{q}$ is taken along the z axis, thus the condensate corresponds to a band structure along the z direction. Assuming that the condensate is real [which is the assumption of Nickel and Buballa (2009)], one has $\Delta_{\boldsymbol{q},k} = \Delta^*_{\boldsymbol{q},-k}$ and Eq. (123) can be rewritten as

$$\Delta(z) = 2\sum_{n=1}^{\infty} \Delta_n \cos(2nqz). \tag{124}$$

Hereafter we refer to this phase as the solitonic phase. Written in this form, it is clear that the ansatz is a generalization of the strip structure and amounts to considering higher harmonics contributions to the gap function, which are not included in the strip.

For any value of $\delta\mu$, the ground state in Nickel and Buballa (2009) is determined using a two-step procedure. First, the magnitude of q in Eq. (124) is fixed, and the profile $\Delta(z)$ is determined by solving the gap equation. Then, among several choices for q, the physical value corresponds to the one minimizing the free energy. In the left panel of Fig. 9, which is from Nickel and Buballa (2009), the plotted profile $\Delta(z)$ is obtained with the numerical solution of the gap equation at fixed value of q. In the plot, $\delta\mu$ is fixed to the numerical value $0.7\Delta_{2SC}$ with $\Delta_{2SC} = 80$ MeV; but changing $\delta\mu$ does not change the picture qualitatively. For q of the same order of Δ_{2SC}, the shape of the gap function is very close to that of the strip. In this case, the largest contribution to the gap comes from the lowest order harmonic $n = 1$ in Eq. (124). However, for small values of q/Δ_{2SC}, the solution of the gap equation has a solitonic shape. This is evident in the case $q = 0.1\Delta_{2SC}$, in which $\Delta(z) \approx \pm\,\Delta_{2SC}$ for one half period, then suddenly changes its sign in a narrow interval. In this case, the higher order harmonics play a relevant role in the gap function profile.

In the right panel of Fig. 9, the physical value of q as a function of $\delta\mu$ is plotted. In the window in which $q = 0$, the ground state is the homogeneous BCS state. At the critical value $\delta\mu \equiv \delta\mu_c \approx 0.695\Delta_{2SC}$, the ground state has $q \neq 0$. This

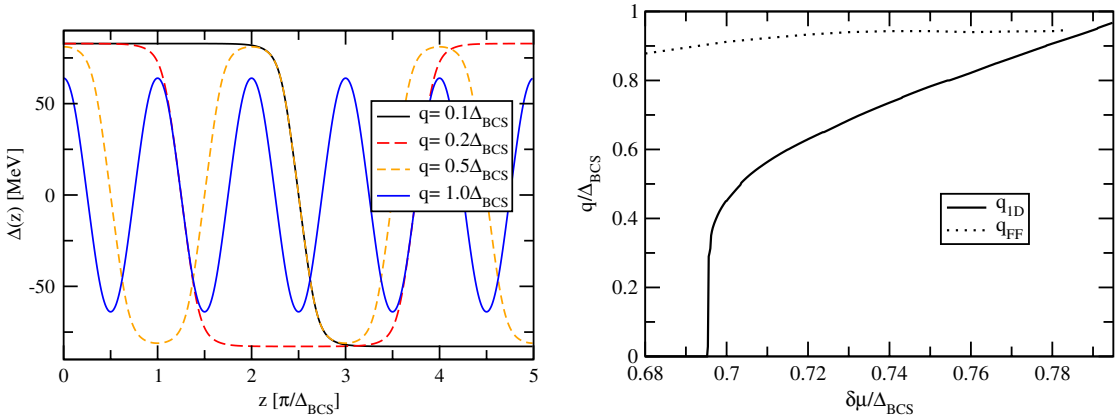

FIG. 9 (color online). Left panel: Profile for the gap function, at several values of q, obtained from the self-consistent solution of the gap equation, at $\delta\mu = 0.7\Delta_{\rm BCS}$. Right panel: Physical wave vector magnitude as a function of $\delta\mu$. In both plots $\Delta_{\rm BCS} \equiv \Delta_{\rm 2SC}$. From Nickel and Buballa, 2009.

signals the transition to the inhomogeneous phase. Since q can be arbitrarily small in proximity to the transition point, from the left panel of Fig. 9 we see that the ground state will consist of a solitonic structure for $\delta\mu \approx \delta\mu_c$. As $\delta\mu$ is increased, the physical value of q increases as well. Therefore, again from the left panel of the figure, we see that the solitonic structure will continuously evolve into the strip structure.

In Fig. 10, from Nickel and Buballa (2009), the BCS free energy (solid line) and the solitonic phase (dashed line) are plotted as a function of $\delta\mu$. The dotted line corresponds to the free energy of the FF phase. The baseline corresponds to the free energy of the normal phase. With increasing mismatch a second-order phase transition takes place from the BCS to the solitonic structure at a value $\delta\mu/\Delta_{\rm BCS} \simeq 0.7$ which is smaller than the value at which the transition from the BCS phase to the FF phase takes place. On the other hand, the transition from the solitonic phase to the normal one takes place almost simultaneously with the transition from the FF phase to the normal one.

In the case of the FF phase, the transition to the BCS state is first order and to the normal phase is second order. On the other hand, the transition from the solitonic phase to the BCS phase is second order. This is possible because the gap

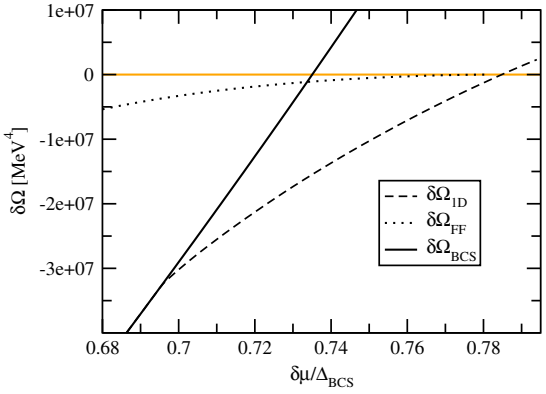

FIG. 10 (color online). Free energy as a function of $\delta\mu$, for the BCS phase (solid line), FF phase (dotted line), and solitonic phase (dashed line). Free energies are measured with respect to the normal phase. From Nickel and Buballa, 2009.

function (124) naturally interpolates between the homogeneous state, corresponding to a single soliton with infinite period, and the cosine-shaped solution.

The transition from the solitonic phase to the normal phase is found to be of the first order, in agreement with the results of the smearing procedure for the strip (Casalbuoni *et al.*, 2004); see Table II. At this transition point, the profile of the gap function is of the cosine type, i.e., the strip profile discussed above.

The results of this analysis are in disagreement with those of the GL expansion (Larkin and Ovchinnikov, 1964; Bowers and Rajagopal, 2002), which predicts that the transition from the strip to the normal phase is second order. Since the GL expansion is expected to be exact in proximity of a second-order phase transition, it is important to understand the origin of the discrepancy among the GL result and that of Nickel and Buballa (2009) and the smearing procedure. To this end, Nickel and Buballa (2009) computed the free energy for a gap function $\Delta(z) = \Delta\cos(2qz)$ with a fixed value of q, as is customary in the GL studies. Their analysis reveals that in this case, beside the local minimum of Ω located at small values of Δ, and which is captured by the GL expansion, a global minimum appears for larger values of Δ. Then they argued that to capture this true minimum, which is responsible for the first-order transition to the normal phase, terms of at least eighth order in the GL expansion, which are usually neglected, should be included. In a subsequent paper Nickel (2009) discussed the emergence of a solitonic phase for lower dimensional modulations in the NJL model and the quark-meson model. His results confirm the replacement of the first-order transition of the phase diagram of the homogeneous NJL phase by two transition lines of second order. These lines are the borders of an inhomogeneous phase and they intersect at the critical point. An interesting point is the relation to the chiral Gross-Neveu model (Gross and Neveu, 1974). A more complete program would require the inclusion of higher dimensional modulations of the inhomogeneity [as done by Abuki, Ishibashi, and Suzuki (2012) for the chiral condensates], and, as pointed out by Buballa and Nickel (2010), simultaneous study of both superconducting and chiral condensates.

I. Condensed matter and ultracold fermionic systems

Fermionic systems consisting of two different "flavors" with mismatched Fermi surfaces and inhomogeneous condensates are quite generic and appear in various contexts. Particularly interesting are the population imbalanced superfluid (or superconducting) systems that can be realized and studied in laboratory. Examples of these type are gases of cold atoms, type-II cuprates, and organic superconductors. The study of these systems is helpful for shedding light on various aspects of superfluidity of asymmetric systems in a framework under experimental control.

Of considerable importance for their similarity to quark matter are ultracold systems consisting of fermions of two different species corresponding to two hyperfine states of a fermionic atom; see Giorgini, Pitaevskii, and Stringari (2008), Ketterle and Zwierlein (2008), Radzihovsky and Sheehy (2010), and Gubbels and Stoof (2012) for reviews. These fermions have opposite spin and one can change the number of up and down fermions at will. One of the most intriguing aspects of these systems is that the interaction between fermions can be tuned by employing a Feshbach resonance (Chin *et al.*, 2010), and therefore the crossover between the BCS and BEC superfluid phases can be studied. This research field has grown in an impressive way in the last two decades and continuous progress in understanding and characterizing the properties of these systems is under way; see, e.g., Muther and Sedrakian (2002), Bedaque, Caldas, and Rupak (2003), Gubankova, Vincent Liu, and Wilczek (2003), Liu and Wilczek (2003), Carlson and Reddy (2005), Castorina *et al.* (2005), Forbes McNeil *et al.* (2005), Yang (2005), Bulgac, Forbes McNeil, and Schwenk (2006), Gubankova, Schmitt, and Wilczek (2006), Mannarelli, Nardulli, and Ruggieri (2006), Pao *et al.* (2006), Partridge *et al.* (2006), Sheehy and Radzihovsky (2006), Son and Stephanov (2006), Yang (2006), Zwierlein and Ketterle (2006), Zwierlein *et al.* (2006), Bulgac and Forbes (2008), Rizzi *et al.* (2008), Sharma and Reddy (2008), and Shin *et al.* (2008).

A mismatch between the populations of electrons in a superconductor can also be produced by Zeeman splitting. The magnetic field that couples with the spins of the electrons can be an external one or an exchange field. However, an external magnetic field couples with the orbital motion of the electrons as well, destroying superconductivity or leading to the creation of a vortex lattice structure.

In order to reduce the orbital effect one employs 2D superconductors, i.e., films of superconducting material or systems with a layered structure, and an in-plane magnetic field (Bulaevskiĭ, 1973). Good candidates for LOFF superconductors of this type are heavy-fermion compounds like $CeRu_2$ (Huxley *et al.*, 1993). Recently, interesting results have also been obtained with $CeCOIN_5$ (Matsuda and Shimahara, 2007). Quasi-two-dimensional organic superconductors (Uji *et al.*, 2006) like κ-(ET) or λ-(ET) salts, in particular, λ-$(BETS)_2F_eCl_4$, are promising candidates for realizing the LOFF phase, as well. High-T_c superconductors are good candidates as well.

As a final remark, we recall that the gapless CSC phases are the QCD analog of a condensed matter phase, known as the Sarma phase (Sarma, 1963; Gubankova, Vincent Liu, and Wilczek, 2003; Liu and Wilczek, 2003; Forbes McNeil *et al.*, 2005), which are found to be unstable (Wu and Yip, 2003; Gubankova, Schmitt, and Wilczek, 2006; Mannarelli, Nardulli, and Ruggieri, 2006; Pao *et al.*, 2006; Sheehy and Radzihovsky, 2006; Gubankova, Mannarelli, and Sharma, 2010) in the weak coupling limit.

III. THE THREE-FLAVOR INHOMOGENEOUS PHASES

In Sec. II we discussed the crystalline inhomogeneous phases that can be realized in two-flavor quark matter. A plethora of possible structures have been analyzed by a Ginzburg-Landau expansion and by the so-called smearing procedure for determining the favored thermodynamic state.

Here we extend the analysis to the three-flavor case which is relevant if the effective strange quark mass M_s is not too heavy. In compact stars M_s will lie somewhere between its current mass of order 100 MeV and its vacuum constituent mass of order 500 MeV, and therefore is of the order of the quark number chemical potential μ, which is expected to be in the range 400–500 MeV. Furthermore, deconfined quark matter, if present in compact stars, must be in weak equilibrium and must be electrically and color neutral. All these factors work to separate the Fermi momenta of the quarks and thus disfavor the cross-species BCS pairing. Actually, as discussed in Sec. I, quark matter must be in a color singlet, however, it has been shown by Amore *et al.* (2002) that projecting out color singlet states into color neutral states does not lead to a large change of the free energy.

As a means to understand how the mismatch among Fermi momenta is linked to β equilibrium and neutrality, consider quark matter composed of u, d, and s quarks with no strong interactions. We treat the strange quark mass as a parameter considering sufficiently long time scales for which weak equilibrium and electrical neutrality are relevant.

Since we are assuming that color interactions are absent, the chemical potential of quarks is diagonal in the color indices and the free energy of the system is given by

$$\begin{aligned}\Omega_{\text{unpaired}}(\mu,\mu_e,M_s) = {}& \frac{3}{\pi^2}\int_0^{P_u^F}(p-\mu_u)p^2dp \\ & + \frac{3}{\pi^2}\int_0^{P_d^F}(p-\mu_d)p^2dp \\ & + \frac{3}{\pi^2}\int_0^{P_s^F}(\sqrt{p^2+M_s^2}-\mu_s)p^2dp \\ & + \frac{1}{\pi^2}\int_0^{\mu_e}(p-\mu_e)p^2dp, \end{aligned} \tag{125}$$

where the Fermi momenta are given by

$$P_u^F = \mu_u, \qquad P_d^F = \mu_d, \qquad P_s^F = \sqrt{\mu_s^2 - M_s^2}. \tag{126}$$

Weak equilibrium relates the chemical potentials of quarks with different flavors as follows:

$$\mu_u = \mu - \tfrac{2}{3}\mu_e \qquad \mu_d = \mu + \tfrac{1}{3}\mu_e \qquad \mu_s = \mu + \tfrac{1}{3}\mu_e, \tag{127}$$

and the electrical chemical potential is obtained from the neutrality constraint

$$\frac{\partial\Omega}{\partial\mu_e}=0. \tag{128}$$

Solving Eq. (128) one determines μ_e and using Eqs. (126) and (127) one obtains the values of P_u^F, P_d^F, and P_s^F for the electrically neutral unpaired phase. The effect of M_s is to reduce the number of strange quarks, which must be compensated by a larger number of down quarks to ensure electrical neutrality. It follows that there is a hierarchy of Fermi momenta

$$P_s^F \le P_u^F \le P_d^F, \tag{129}$$

and in Fig. 11 we report the difference of the Fermi momenta $P_d^F - P_u^F$ and $P_u^F - P_s^F$ as a function of M_s, for $\mu = 500$ MeV.

For $M_s \ll \mu$, the effect of a nonzero strange quark mass can be taken into account by treating the strange quark as massless, but with a chemical potential that is lowered by $M_s^2/(2\mu)$ from $\mu + \mu_e/3$. To the order M_s^2/μ electric neutrality, Eq. (128), requires that $\mu_e \simeq M_s^2/4\mu$. In this case $P_d^F - P_u^F \simeq P_u^F - P_s^F$, and we need no longer to be careful about the distinction between P_F and μ, as we can simply think of the three flavors of quarks as if they have chemical potentials

$$\mu_d = \mu_u + 2\delta\mu, \qquad \mu_u = p_F^u, \qquad \mu_s = \mu_u - 2\delta\mu, \tag{130}$$

with

$$\delta\mu \equiv \frac{M_s^2}{8\mu}, \tag{131}$$

and we can write the chemical potential matrix as

$$\mu_{ij,\alpha\beta} = \delta_{\alpha\beta} \otimes \mathrm{diag}(\mu_u, \mu_d, \mu_s)_{ij}. \tag{132}$$

The above results are strictly valid for unpaired matter; indeed, if BCS pairing between quarks with different flavors takes place, their Fermi momenta must be equal and the electron chemical potential vanishes. As discussed in the two-flavor case, the cross-species homogeneous pairing between quarks on split Fermi spheres has a free energy cost proportional to the corresponding chemical potential difference.

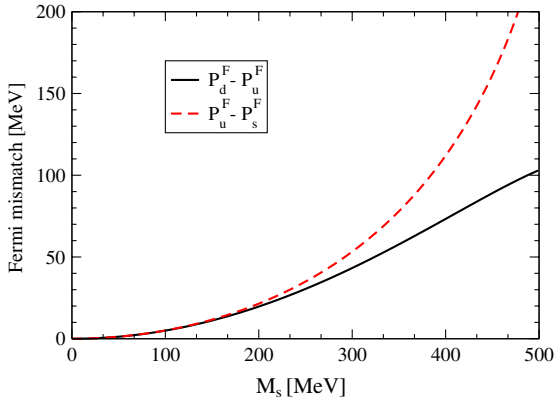

FIG. 11 (color online). Fermi momenta differences $P_d^F - P_u^F$ (black solid line) and $P_u^F - P_s^F$ (dashed line) as a function of M_s, for $\mu = 500$ MeV.

Since in the CFL phase quarks of all flavors and all colors pair according with the condensate in Eq. (2), increasing the value of $\delta\mu$ makes the CFL phase less energetically favored. However, small values of the chemical potential difference, i.e., of M_s, cannot disrupt the BCS pairing and the CFL phase will be energetically favored. Nevertheless, when M_s is sufficiently large, the mismatch between the Fermi momenta becomes large disfavoring CFL pairing.

As shown in Fig. 11, for values of M_s comparable with μ the strange quarks decouple; in this case only the 2SC phase with the pairing between up and down quarks seems realizable. However, as pointed out by Alford and Rajagopal (2002), once the constraints of electrical and color neutrality and β equilibrium are imposed, the 2SC phase turns out to be strongly disfavored or even excluded at least at zero temperature [for finite temperature evaluations see, e.g., Abuki (2003)]. Alford and Rajagopal (2002), performing an expansion in terms of the strange quark mass (at the leading nontrivial order), found that whenever the 2SC phase is more favored than unpaired matter, then the CFL is even more favored. The point is that the CFL phase is extremely robust, because it allows pairing between all the three-flavor species. This analysis has been redone by Steiner, Reddy, and Prakash (2002) evaluating the density-dependent strange quark mass self-consistently. The results of Steiner, Reddy, and Prakash (2002) almost confirm previous conclusions, finding the 2SC favored in a very narrow region of density, that is likely to disappear once the hadronic phase boundary is properly taken into account. Note that these results are valid in the weak-coupling approximation. Computations using NJL-like models with a stronger coupling (Abuki and Kunihiro, 2006; Ruester *et al.*, 2006a) (see also Sec. II.B) show that a large portion of the phase diagram is occupied by the 2SC phase.

A. The gapless CFL phase

Given that the effect of nonzero strange quark mass and electrical neutrality constraints is to pull apart the Fermi spheres of different quark flavors, there is little motivation for assuming the symmetric CFL pairing reported in Eq. (2). Indeed, one might expect that a mismatch between the Fermi momenta reflects in a reduction of the interaction channel and thus in a reduction of the corresponding gap parameter. Therefore, the gap parameters should now be flavor dependent and one can consider the generalized pairing ansatz

$$\langle 0|\psi_{iL}^{\alpha}\psi_{jL}^{\beta}|0\rangle = -\langle 0|\psi_{iR}^{\alpha}\psi_{jR}^{\beta}|0\rangle \propto \sum_{I=1}^{3}\Delta_I\epsilon_{ijI}\epsilon^{\alpha\beta I}, \tag{133}$$

where Δ_1, Δ_2, and Δ_3 describe d-s, u-s, and u-d Cooper pairing, respectively. Alford, Kouvaris, and Rajagopal (2004), (2005) studied the superconducting phase characterized by the ansatz (133) with a NJL-like model at zero temperature [see Fukushima, Kouvaris, and Rajagopal (2005) for a study at nonvanishing temperature], considering the in-medium strange quark mass as a free parameter, while the light quarks are taken massless. The gap equations, coupled to the neutrality conditions, have been solved and the corresponding free energy has been determined. Besides the strange quark mass, the final results depend on the quark chemical potential, which

is fixed to the numerical value $\mu = 500$ MeV; moreover, the strength of the NJL-like interaction is fixed by the value of the homogeneous CFL gap Δ_{CFL}. The numerical value $\Delta_{\mathrm{CFL}} = 25$ MeV, corresponding to the weak-coupling regime, has been chosen.

Some of the results of Alford, Kouvaris, and Rajagopal (2004), (2005) are summarized in Fig. 12. In the left panel of the figure, the solutions of the gap equations as a function of M_s^2/μ are plotted. As can be inferred from the figure, at $M_s^2/\mu \approx 47.1$ MeV, there is a continuous phase transition between the CFL phase and a phase characterized by $\Delta_3 > \Delta_2 > \Delta_1 > 0$. Note that the hierarchy of the gap parameters is in agreement with the hierarchy of the Fermi momenta splitting reported in Fig. 11, which substantiates the reasoning presented above about the relation between mismatched Fermi momenta and gap parameters. Actually, the mismatches of chemical potential are not only due to the finite value of the strange quark mass, but as well as to the nonzero values of the color chemical potentials μ_3 and μ_8, which, however, do not overturn the hierarchy in Fig. 11.

The phase appearing at $M_s^2/\mu \approx 47.1$ MeV is called the gapless CFL, or gCFL, phase, and is the three-flavor analog of the g2SC phase discussed in Sec. II.B. The symmetry breaking pattern is the same of the CFL phase [see Eq. (3)], but the spectra of some fermionic excitations are gapless (Alford, Kouvaris, and Rajagopal, 2004, 2005; Kryjevski and Schfer, 2005). The possibility of a gapless CFL superconductor was first argued by Alford, Berges, and Rajagopal (2000a), where a toy model was used to infer the effect of a heavy M_s on the quasiparticle spectrum and it was found that if the condensates of light and strange quarks are below a certain critical value, there is not a minimum excitation energy in the quasiparticle spectrum. As discussed in Sec. II.A, the mechanism at the origin of gapless modes in a superconductor is quite general, and is due to a mismatch $\delta\mu$ between condensing fermions of the order of Δ.

In three-flavor quark matter the situation is complicated by the presence of several interaction channels and three chemical potential differences proportional to μ_e, μ_3, and μ_8. Thus, in the gCFL phase the dispersion laws are more complicated than those reported in Eq. (10). However, the qualitative result is rather similar, as gapless excitations appear in the spectrum for sufficiently large mismatches between the Fermi momenta of the various species.

Comparing the free energy of the gCFL with other candidate phases, e.g., the 2SC phase, or the 2SC + s, which is a three-flavor model in which the decoupled strange quark is taken in to account, or the so-called 2SCus in which only the u-s pairing survives (i.e., $\Delta_2 > 0$, $\Delta_1 = \Delta_3 = 0$) or the g2SC discussed in Sec. II.B, the gCFL phase turns out to be energetically favored in a quite large window of the control parameter (Alford, Kouvaris, and Rajagopal, 2004, 2005). The comparison of the gCFL free energy with the free energy of some of theses phases is reported in Fig. 12. Besides the considered phases, other pairing patterns have been proposed (Iida *et al.*, 2004), corresponding to the uSC phase (with $\Delta_1 = 0$ and Δ_2, $\Delta_3 \neq 0$) and the dSC phase (with $\Delta_2 = 0$ and Δ_1, $\Delta_3 \neq 0$); see Fukushima, Kouvaris, and Rajagopal (2005) and Ruester *et al.* (2006a) for a comparison of the thermodynamic potentials of the various phases.

However, as discussed for the two-flavor case, the fact that a phase is energetically favored with respect to other phases is not a sufficient condition to ensuring its stability. Indeed, the analysis of fluctuations around the mean field solutions may reveal that the phase does not correspond to a minimum of the free energy. As in the case of the g2SC phase, the gCFL phase is indeed chromomagnetically unstable, because four of the eight Meissner masses of gluons become imaginary when gapless modes appear (Casalbuoni, Gatto, Mannarelli *et al.*, 2005; Fukushima, 2005). Further increasing the mismatch among the Fermi surfaces, the masses of the remaining four gluons become imaginary as well. The effects of temperature on the Meissner masses in the gCFL phase has been studied by Fukushima (2005), in which it was found that for sufficiently high temperatures [of about 10 MeV for the parameter choice of Fukushima (2005)] the gCFL phase becomes stable. However, such a temperature is much larger than the typical temperature of compact stars and

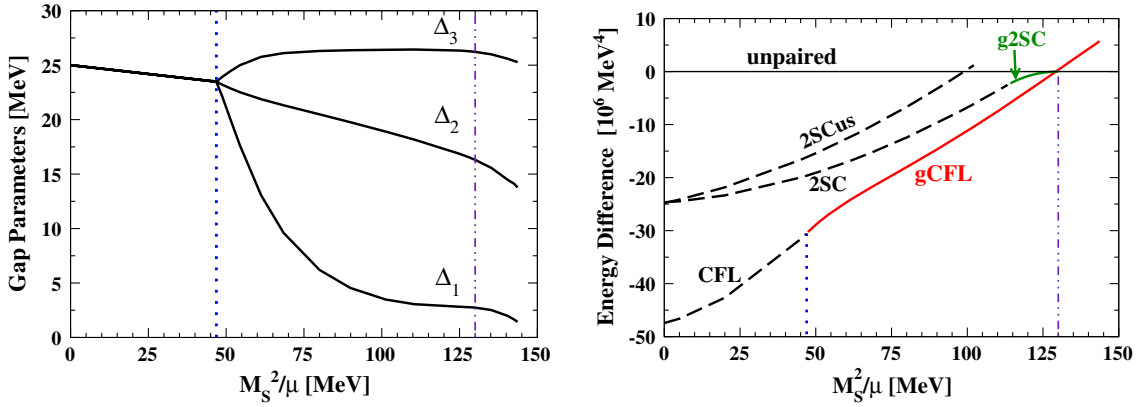

FIG. 12 (color online). Left panel: Gap parameters Δ_3, Δ_2, and Δ_1 as a function of M_s^2/μ for $\mu = 500$ MeV, in a model where $\Delta_{\mathrm{CFL}} = 25$ MeV (see text). Right panel: Free energy of the CFL-gCFL phase, relative to that of neutral noninteracting quark matter and that of the 2SC-g2SC and 2SCus phases. At $M_s^2/\mu \approx 47.1$ MeV (vertical dotted line) there is a continuous phase transition between the CFL and gCFL phases. Above $M_s^2/\mu \approx 130$ MeV (vertical dash-dotted line) unpaired quark matter has a lower free energy than the gCFL phase. From Alford, Kouvaris, and Rajagopal, 2005.

therefore cannot be used as an argument in favor of the gCFL phase.

Since the gCFL is chromomagnetically unstable but is energetically favored with respect to both unpaired quark matter and the two-flavor CSC phases, there must exist a phase with a lower free energy. Interestingly, at vanishing temperature the gCFL phase is favored with respect to the other phases even at weak coupling, whereas the g2SC phase is energetically favored with respect to unpaired quark matter and the 2SC phase only in the intermediate coupling regime; see Sec. II.B.

As discussed for the two-flavor case, the chromomagnetic instability can be associated with the tendency of the system to develop supercurrents, that is to realize a FF-like state. Then, as done for the two-flavor case, one can generalize the FF state to more complicated structures trying to single out the favored ground state among various crystalline phases. We investigate various crystalline patterns in the following sections.

B. Three-flavor crystalline phase: Two plane waves

In this section we present the evaluation of the simplest nontrivial three-flavor CCSC phase using a modified Nambu-Gorkov formalism. The approach presented is based on the high-density effective theory (HDET) of Casalbuoni, Gatto, Mannarelli, and Nardulli (2001) and Nardulli (2002) and the evaluation is performed with and without making a GL expansion.

1. Nambu-Gorkov and HDET formalisms for the three-flavor crystalline phase

As discussed in Sec. II.C.1 one can properly choose the Nambu-Gorkov basis for simplifying the calculation in the FF phase. Here we extend that reasoning to the three-flavor case. In the three-flavor case the simplest form of inhomogeneous pairing corresponds to the condensate

$$\Delta_{ij}^{\alpha\beta} = \sum_{I=1}^{3} \Delta_I e^{2i\boldsymbol{q}_I\cdot\boldsymbol{x}} \epsilon_{ijI}\epsilon^{\alpha\beta I}, \tag{134}$$

meaning that for each pairing channel we assume a FF ansatz, with $2\boldsymbol{q}_I$ representing the momentum of the pair.

In this case it is not possible to diagonalize the propagator in $\boldsymbol{p}$ space, because three different fields are locked together in pairs and thus one can only eliminate in the off-diagonal terms of the propagator two independent momenta. However, as shown in Eqs. (130) and (131), the separation between the s and d Fermi spheres is twice the separation between the d and s Fermi spheres and the u and s Fermi spheres, thus it is reasonable to expect $\Delta_1 \ll \Delta_2, \Delta_3$. As a first approximation one can consider $\Delta_1 = 0$ and in this case it is possible to diagonalize the propagator in momentum space.

The form of the two-flavor Nambu-Gorkov spinor (44) immediately suggests that we analyze the three-flavor crystalline phase with condensate (134) with Δ_1 set to zero by introducing the Nambu-Gorkov spinor

$$\chi(\boldsymbol{p}) = \begin{pmatrix} \psi_u(\boldsymbol{p}) \\ \psi_d(\boldsymbol{p}-2\boldsymbol{q}_3) \\ \psi_s(\boldsymbol{p}-2\boldsymbol{q}_2) \\ \psi_u^C(-\boldsymbol{p}) \\ \psi_d^C(-\boldsymbol{p}+2\boldsymbol{q}_3) \\ \psi_s^C(-\boldsymbol{p}+2\boldsymbol{q}_2) \end{pmatrix}. \tag{135}$$

It is clear that it would not be possible to use this calculation method if Δ_1 were kept nonzero, except for the special case, in which $\boldsymbol{q}_1 = \boldsymbol{q}_2 - \boldsymbol{q}_3$. (That is, except in this special case which is far from sufficiently generic, it will not be possible to choose a Nambu-Gorkov basis such that one obtains a propagator that is diagonal in some momentum variable $\boldsymbol{p}$.) Moreover, it seems unlikely that this method can be employed to analyze more complicated crystal structures. Indeed, it seems that the pairing with $\Delta_1 = 0$ and Δ_2 and Δ_3 each multiplying a single plane wave is the most complex example that is currently known how to analyze without using the GL expansion.

We now implement the calculation in the basis (135) using the HDET formalism. We generalize the discussion presented in Sec. II.E including the shifts of the quasiparticle momenta. To this end we Fourier decompose the fermionic fields as follows:

$$\psi_i^\alpha(x) = e^{-i\boldsymbol{k}_i\cdot\boldsymbol{x}} \int \frac{d\Omega}{4\pi} e^{-i\mu\boldsymbol{v}\cdot\boldsymbol{x}} [\psi_{i,\boldsymbol{v}}^\alpha(x) + \psi_{i,\boldsymbol{v}}^{\alpha-}(x)], \tag{136}$$

which differs from Eq. (78) by the presence of the three vectors $\boldsymbol{k}_i$, one for each flavor, that we specify below. In the standard HDET approximation $\boldsymbol{k}_i \equiv 0$ and the field $\psi_{i,\boldsymbol{v}}^\alpha(x)$ is used to describe a quark in a patch in momentum space in the vicinity of momentum $\boldsymbol{p} = \mu\boldsymbol{v}$. The introduction of the $\boldsymbol{k}_i$ vectors means that now $\psi_{i,\boldsymbol{v}}^\alpha(x)$ describes a quark with momentum in a patch in the vicinity of momentum $\mu\boldsymbol{v} + \boldsymbol{k}_i$ and the chemical potential differences with respect to the average value μ are then given by

$$\delta\mu_i(\boldsymbol{v}) = \mu_i - \mu - \boldsymbol{k}_i\cdot\boldsymbol{v}. \tag{137}$$

At the leading order in $1/\mu$ (i.e., neglecting the contribution of antiparticles) the free Lagrangian can be written as in Eq. (79), but with a velocity dependent chemical potential difference

$$\mathcal{L} = \int \frac{d\Omega}{4\pi} \{\psi_{i,\boldsymbol{v}}^{\alpha\dagger}[iV\cdot\partial + \delta\mu_i(\boldsymbol{v})]\psi_{i,\boldsymbol{v}}^\alpha\}. \tag{138}$$

To take into account diquark condensation, we add to Eq. (138) a term similar to Eq. (80), which, however, takes into account the $\boldsymbol{k}_i$ shifts in the momenta, that is,

$$\mathcal{L}_\Delta = -\frac{1}{2}\int \frac{d\Omega}{4\pi} \Delta_{ij}^{\alpha\beta} \psi_{i,-\boldsymbol{v}}^{\alpha T} C\gamma_5 \psi_{j,\boldsymbol{v}}^\beta e^{-i(\boldsymbol{k}_i+\boldsymbol{k}_j)\cdot\boldsymbol{x}} + \text{H.c.}, \tag{139}$$

where the condensate $\Delta_{ij}^{\alpha\beta}$ is given in Eq. (134) and we have omitted the term proportional to Δ^2. In the three-flavor case it

is convenient to work in a new basis for the spinor fields defined by

$$\psi_i^\alpha = \sum_{A=1}^{9} (F_A)_i^\alpha \psi_A, \tag{140}$$

where the matrices F_A are given by

$$F_1 = \frac{1}{3}I + T_3 + \frac{1}{\sqrt{3}}T_8, \qquad F_2 = \frac{1}{3}I - T_3 + \frac{1}{\sqrt{3}}T_8,$$
$$F_3 = \frac{1}{3}I - \frac{2}{\sqrt{3}}T_8, \qquad F_{4,5} = T_1 \pm iT_2,$$
$$F_{6,7} = T_4 \pm iT_5, \qquad F_{8,9} = T_6 \pm iT_7,$$

with T_a the SU(3) generators defined in Eq. (14) and I the 3×3 identity matrix. Introducing the velocity dependent Nambu-Gorkov fields

$$\chi_{\boldsymbol{v}}^A = \frac{1}{\sqrt{2}} \begin{pmatrix} \psi_{\boldsymbol{v}} \\ C\psi_{-\boldsymbol{v}}^* \end{pmatrix}_A, \tag{141}$$

and replacing any matrix M in color-flavor space with $M_{AB} = \mathrm{Tr}[F_A^T M F_B]$, the NJL Lagrangian density can be written in the compact form

$$\mathcal{L} = \frac{1}{2}\int \frac{d\Omega}{4\pi} \chi_{\boldsymbol{v}}^{A\dagger} S_{AB}^{-1}(\boldsymbol{v}) \chi_{\boldsymbol{v}}^B, \tag{142}$$

where the inverse propagator is given by

$$S_{AB}^{-1} = \begin{pmatrix} [V\cdot\ell + \delta\mu_A(\boldsymbol{v})]\delta_{AB} & -\Delta_{AB} \\ -\Delta_{AB} & [\bar{V}\cdot\ell - \delta\mu_A(-\boldsymbol{v})]\delta_{AB} \end{pmatrix}, \tag{143}$$

where $\ell^\nu = (p_0, \xi\boldsymbol{v})$. As discussed in Sec. II.E for the standard HDET, the integration over momentum space is separated into an angular integration over $\boldsymbol{v}$ and a radial integration over $-\delta \le \xi \le \delta$. The cutoff δ must be taken smaller than μ but much larger than the homogeneous gap parameter (that is, Δ_{CFL} in the three-flavor case) and $\delta\mu$; see Fig. 1.

If $\Delta_1 = 0$, the space dependence in the anomalous terms of the propagator can be eliminated by choosing

$$\boldsymbol{k}_u + \boldsymbol{k}_d = 2\boldsymbol{q}_3, \qquad \boldsymbol{k}_u + \boldsymbol{k}_s = 2\boldsymbol{q}_2, \tag{144}$$

and the calculation is technically simplified. It has been numerically checked by Mannarelli, Rajagopal, and Sharma (2006) that different choices of $\boldsymbol{k}_u$, $\boldsymbol{k}_d$, and $\boldsymbol{k}_s$ satisfying Eq. (144) yield the same results for the gap parameter and free energy. The different choices yield quite different intermediate stages to the calculation; the fact that the final results are the same is a nontrivial check of the numerics.

From the Lagrangian (142), following a derivation analogous to that by Alford, Kouvaris, and Rajagopal (2005), the free energy can be evaluated to be

$$\Omega = -\frac{\mu^2}{4\pi^2}\sum_{a=1}^{18}\int_{-\delta}^{+\delta} d\xi \int \frac{d\Omega}{4\pi}|E_a(\boldsymbol{v},\xi)| + \frac{2\Delta^2}{G} - \frac{\mu_e^4}{12\pi^2}, \tag{145}$$

where we have set $\Delta_2 = \Delta_3 = \Delta$ and G is the NJL coupling constant. The dependence on G can be eliminated by using the CFL gap equation

$$\Delta_{\mathrm{CFL}} = 2^{2/3}\delta \exp\left\{-\frac{\pi^2}{2G\mu^2}\right\}, \tag{146}$$

where Δ_{CFL} is the CFL gap parameter for $M_s = 0$ and $\mu_e = 0$. As discussed, for example, by Nardulli (2002), although the value of the free energy and the gap parameter depend on δ, the energetically favored phase is independent of it. Alternatively, one can use a coupling constant which explicitly depends on the momentum cutoff as in Ippolito, Nardulli, and Ruggieri (2007).

In Eq. (145), the E_a are the energies of the fermionic quasiparticles, which are given by the 18 roots of $\det S^{-1} = 0$, given in Eq. (143). The doubling of degrees of freedom in the Nambu-Gorkov formalism means that the 18 roots come in pairs whose energies are related by $E_a(\boldsymbol{v},\xi) = E_b(-\boldsymbol{v},\xi)$. One set of nine roots describes $(\psi_{d,\boldsymbol{v}}, \psi_{u,-\boldsymbol{v}})$ and $(\psi_{s,\boldsymbol{v}}, \psi_{u,-\boldsymbol{v}})$ pairing, while the other set describes $(\psi_{u,\boldsymbol{v}}, \psi_{d,-\boldsymbol{v}})$ and $(\psi_{u,\boldsymbol{v}}, \psi_{s,-\boldsymbol{v}})$ pairing (color indices have been omitted for simplicity). Since $\boldsymbol{v}$ is integrated over, the free energy can be evaluated by doing the sum in Eq. (145) over either set of nine roots, instead of over all 18, and multiplying the sum by 2.

The lowest free energy state is determined minimizing the free energy given in Eq. (145) with respect to the gap parameter Δ and with respect to $\boldsymbol{q}_2$ and $\boldsymbol{q}_3$. One could also determine self-consistently the values of μ_e, μ_3, and μ_8 which ensure electrical and color neutrality. Moreover, one could allow $\Delta_2 \neq \Delta_3$ and minimize with respect to the two gap parameters separately. However, in the results that we present in the next section we fix $\Delta_2 = \Delta_3 = \Delta$, $\mu_e = M_s^2/(4\mu)$ and $\mu_3 = \mu_8 = 0$, as is correct for small Δ.

2. Ginzburg-Landau analysis

As discussed for the two-flavor case, the GL expansion allows us to determine the gap parameter and the free energy for a generic crystalline structure. We discuss the GL results for various crystalline phases in Sec. III.C; in the present section we restrict to the case of the condensate reported in Eq. (134). In the three-flavor case the GL expansion is controlled by the ratio $\Delta/\Delta_{\mathrm{CFL}} \approx \Delta/\delta\mu$ and is reliable in the vicinity of a second-order transition; this restriction implies that pairing does not significantly change any number density, and thus one can assume $\mu_3 = \mu_8 = 0$ and $\mu_e \approx M_s^2/4\mu$ as in the normal phase. We briefly comment in Sec. III.B.5 on the latter approximation.

For the condensate in Eq. (134), the GL expansion of the free energy is given by (Casalbuoni, Gatto, Ippolito *et al.*, 2005; Mannarelli, Rajagopal, and Sharma, 2006)

$$\Omega = \Omega_n + \sum_{I=1}^{3}\left(\alpha_I\Delta_I^2 + \frac{\beta_I}{2}\Delta_I^4 + \sum_{J\neq I}\frac{\beta_{IJ}}{2}\Delta_I^2\Delta_J^2\right) + O(\Delta^6), \tag{147}$$

which can be seen as an extension of the $\mathcal{O}(\Delta^4)$ two-flavor GL free energy, [cf. Eq. (47)] to the three-flavor case. We neglect the sextic (and higher-order) terms because for the simple inhomogeneous condensates considered here the quartic terms are positive. Note that, in contrast to the two-flavor case, the presence of three Δ_I's requires the introduction of various coefficients with indices referring to the particular condensate Δ_I. In particular, the term proportional to β_{IJ}, with $I \neq J$, corresponds to the interaction term between different condensates.

Using the HDET formalism, it has been shown by Casalbuoni, Gatto, Ippolito *et al.* (2005) that α_I and β_I have the same formal expression derived in the GL analysis of the two-flavor FF structure. This means that

$$\alpha_I \equiv \alpha_{\rm FF}(q_I, \delta\mu_I), \qquad \beta_I \equiv \beta_{\rm FF}(q_I, \delta\mu_I), \tag{148}$$

with $\alpha_{\rm FF}$ defined in Eq. (48) [with $\Delta_{\rm 2SC} \to 2^{1/3}\Delta_{\rm CFL}$, for replacing the 2SC gap parameter with the CFL gap parameter; cf. Eq. (96) with Eq. (146)] and $\beta_{\rm FF}$ defined in Eq. (50). We indicate with $\delta\mu_I$ the chemical potential difference between quark whose flavor is not I, e.g., $2\delta\mu_1 = \mu_d - \mu_s$. In the weak-coupling limit the chemical potential differences are the same of the unpaired phase, thus from Eq. (130) one obtains

$$\delta\mu_1 = -\mu_e, \qquad \delta\mu_2 = -\delta\mu_3 = -\frac{\mu_e}{2}. \tag{149}$$

For the interaction term between different condensates, it turns out that

$$\beta_{12} = -\frac{\mu^2}{4\pi^2}\int\frac{d\boldsymbol{v}}{4\pi}\frac{1}{(i\epsilon - 2\boldsymbol{q}_1\cdot\boldsymbol{v} - 2\delta\mu_1)(i\epsilon - 2\boldsymbol{q}_2\cdot\boldsymbol{v} - 2\delta\mu_2)}, \tag{150}$$

and β_{13} is obtained from β_{12} by changing $\boldsymbol{q}_2 \to \boldsymbol{q}_3$ and $\mu_s \leftrightarrow \mu_d$; in a similar way β_{23} is obtained from β_{12} by changing $\boldsymbol{q}_1 \to \boldsymbol{q}_3$ and $\mu_s \leftrightarrow \mu_u$. These are the only terms in which a dependence of the free energy from the relative orientation of the $\boldsymbol{q}_I$ can arise at this order.

One should fix the norms q_I and the relative orientation of the three vectors $\boldsymbol{q}_I$ by a minimization procedure. This is a complex task requiring the simultaneous minimization of the free energy with respect to many parameters. What is usually done to circumvent this complication is to propose different definite structures for the $\boldsymbol{q}_I$, selecting among them the one with the lowest free energy. In the present simple case we can do something better, using the angle ϕ between $\boldsymbol{q}_2$ and $\boldsymbol{q}_3$ as a variational parameter. Indeed, it has been found by Casalbuoni, Gatto, Ippolito *et al.* (2005) that the energetically favored solution corresponds to $\Delta_1 = 0$ and $\Delta_2 \approx \Delta_3$ and clearly in this case the free energy is independent of $\boldsymbol{q}_1$. As to the norms q_2 and q_3, since we work in the GL approximation, it is possible to neglect the $\mathcal{O}(\Delta^2)$ terms in the minimization of Ω. Thus, one has that $\partial\alpha_I/\partial q_I = 0$ for $I = 2, 3$, which is identical to the condition for two flavors giving the result $q_I = z_q^{-1}|\delta\mu_I|$, with z_q defined in Eq. (87). Considering this condition and Eq. (149) one has that

$$|\delta\mu_2| = |\delta\mu_3| \equiv \delta\mu, \qquad |\boldsymbol{q}_2| = |\boldsymbol{q}_3| \equiv q, \tag{151}$$

therefore implies that the u-s and d-u quark pairs momenta have the same modulus. A pictorial representation of the Fermi surfaces and pairing regions for this simple configuration is reported in Fig. 15 for two different values of ϕ.

Given Eq. (151) and taking $\Delta_1 = 0$, the free energy including up to $\mathcal{O}(\Delta^4)$ terms can be written as

$$\Omega = \Omega_n + 2\alpha_{\rm FF}\Delta^2 + (\beta_{\rm FF} + \beta_{23})\Delta^4, \tag{152}$$

where $\alpha_{\rm FF} \equiv \alpha_{\rm FF}(q, \delta\mu)$, $\beta_{\rm FF} \equiv \beta_{\rm FF}(q, \delta\mu)$, and

$$\Delta \equiv \Delta_2 = \Delta_3, \tag{153}$$

is the only independent gap parameter. Minimizing the free energy expression with respect to Δ we obtain for values of $\delta\mu$, where $\alpha_{\rm FF}$ is negative, the solution

$$\Delta^2 = \frac{|\alpha_{\rm FF}|}{\beta_{\rm FF} + \beta_{23}}, \tag{154}$$

and the free energy at the minimum is given by

$$\Omega = \Omega_n - \frac{\alpha_{\rm FF}^2}{\beta_{\rm FF} + \beta_{23}}, \tag{155}$$

which still depends on the angle ϕ by β_{23}.

3. Testing the Ginzburg-Landau approximation

We are now able to evaluate the gap parameter and the free energy for the "crystalline" color superconducting phase

$$\Delta_{ij}^{\alpha\beta} = \Delta(e^{2iq\boldsymbol{n}_2\cdot\boldsymbol{x}}\varepsilon^{\alpha\beta 2}\epsilon_{ij2} + e^{2iq\boldsymbol{n}_3\cdot\boldsymbol{x}}\varepsilon^{\alpha\beta 3}\epsilon_{ij3}), \tag{156}$$

with and without the GL approximation (Mannarelli, Rajagopal, and Sharma, 2006); here we have written $\boldsymbol{q}_2 = q\boldsymbol{n}_2$ and $\boldsymbol{q}_3 = q\boldsymbol{n}_3$. In Fig. 13 we report the results obtained for $\mu = 500$ MeV and $\Delta_{\rm CFL} = 25$ MeV. Calculations are made varying M_s, but we plot quantities versus M_s^2/μ because the most important effect of a nonzero M_s is the splitting between the d, u, and s Fermi momenta given in Eq. (130). We report the results for four values of the angle between $\boldsymbol{n}_2$ and $\boldsymbol{n}_3$: $\phi = 0$, $2\pi/3$, $7\pi/8$, and $31\pi/32$. The lines correspond to the GL analysis, with Δ and $\Omega - \Omega_n$ determined from Eqs. (154) and (155), respectively, using Eq. (148) to relate $\alpha_{\rm FF}$ to $\delta\mu_I$ and hence to M_s^2/μ. The points correspond to the NJL calculation without the GL expansion, hereafter full NJL, obtained by minimizing the free energy of Eq. (145) with respect to Δ.

For all values of the angle ϕ, both the full NJL calculation and the GL expansion have a second-order transition to the normal phase at $M_s^2/\mu \simeq 151$ MeV, clearly visible in the left panel of Fig. 13, corresponding to $\delta\mu \simeq 0.75\Delta_{\rm CFL}$. In the GL calculation the independence of the critical value of $\delta\mu$ on ϕ occurs because the location of the phase transition depends

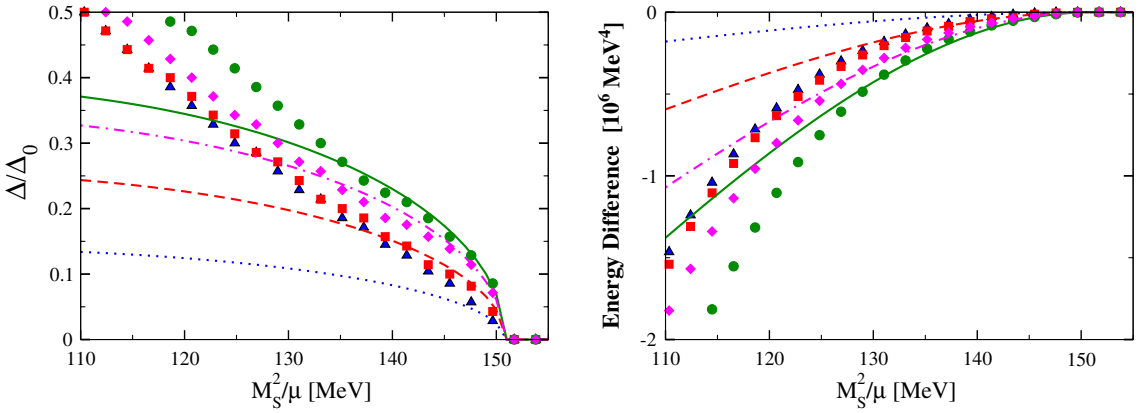

FIG. 13 (color online). Plot of Δ/Δ_0 (left panel), with $\Delta_0 = \Delta_{\mathrm{CFL}}$, and the free energy relative to neutral noninteracting quark matter (right panel) as a function of M_s^2/μ for four values of the angle ϕ between $\boldsymbol{q}_2$ and $\boldsymbol{q}_3$. The various lines correspond to the calculations done in the GL approximation whereas dots correspond to the NJL calculation, done without making a GL approximation. The solid lines and circles correspond to $\phi = 0$, the dash-dotted lines, and diamonds correspond to $\phi = 2\pi/3$, the dashed lines and squares correspond to $\phi = 7\pi/8$, the dotted lines and triangles correspond to $\phi = 31\pi/32$. From Mannarelli, Rajagopal, and Sharma, 2006.

only on α_I, which is independent of ϕ. Near the phase transition, where $\Delta/\Delta_{\mathrm{CFL}}$ and hence $\Delta/\delta\mu$ are small, there is good agreement between the full NJL calculation and the GL approximation, as expected. When the GL approximation breaks down, it does so conservatively, underpredicting both Δ and $|\Omega - \Omega_n|$. Furthermore, even considering a situation in which the GL approximation has broken down quantitatively, it correctly predicts the qualitative feature that at all values of M_s^2/μ the favored crystal structure is that with $\phi = 0$. Therefore, the GL approximation is useful as a qualitative guide even in a case in which it has broken down quantitatively.

It is evident from Fig. 13 that the extent of the regime in which the GL approximation is quantitatively reliable is strongly ϕ dependent. In the best case, which it turns out is $\phi = 0$, the results of the GL calculation are in good agreement with those of the full NJL calculation as long as $\Delta/\Delta_{\mathrm{CFL}} \lesssim 0.25$, corresponding to $\Delta/\delta\mu \lesssim 0.35$. For larger ϕ, the GL approximation yields quantitatively reliable results only for much smaller Δ. For example, with $\phi = 31\pi/32$ the GL calculation gives results in quantitative agreement with the full NJL calculation only for $\Delta/\Delta_{\mathrm{CFL}} \lesssim 0.04$, corresponding to $\Delta/\delta\mu \lesssim 0.05$ (Mannarelli, Rajagopal, and Sharma, 2006).

A remarkable result is that the free energy of the favored phase, corresponding to $\boldsymbol{n}_2 = \boldsymbol{n}_3$, has a lower free energy of the CFL and gCFL phases in the window (Casalbuoni, Gatto, Ippolito *et al.* 2005; Mannarelli, Rajagopal, and Sharma, 2006)

$$128 \lesssim \frac{M_s^2}{\mu} \lesssim 151 \text{ MeV}, \tag{157}$$

in which the GL expansion of the free energy for the favored structure is in excellent agreement with the result of the full NJL calculation; see the right panel of Fig. 13. This result strongly motivates the study of more complicated crystalline structures employing the GL approximation.

Note that the range in Eq. (157) has been obtained considering the fixed value of the gap parameter $\Delta_{\mathrm{CFL}} = 25$ MeV. However, the CFL gap parameter and the constituent strange quark mass should depend on μ. We discuss this point in Sec. III.C.1 considering the dependence of both Δ_{CFL} and M_s on μ within a NJL model.

We can now get a deeper insight about the favored orientation of the $\boldsymbol{q}_I$ from the analysis of β_{23}. As explained, this is the only term in the GL expansion that depends on the relative orientation between $\boldsymbol{n}_2$ and $\boldsymbol{n}_3$ and can be rewritten as

$$\beta_{23} = \frac{\mu^2}{\pi^2 \delta\mu^2} I(\phi), \tag{158}$$

where

$$I(\phi) = \Re e \int \frac{d\Omega}{4\pi} \frac{-1}{(i\epsilon - z_q^{-1}\boldsymbol{v}\cdot\boldsymbol{n}_2 - 1)(i\epsilon - z_q^{-1}\boldsymbol{v}\cdot\boldsymbol{n}_3 + 1)} \tag{159}$$

can be evaluated numerically and the result is plotted in Fig. 14 showing that the minimum value occurs at $\phi = 0$, that is, for $\boldsymbol{n}_1 = \boldsymbol{n}_2$, in agreement with the fact that the

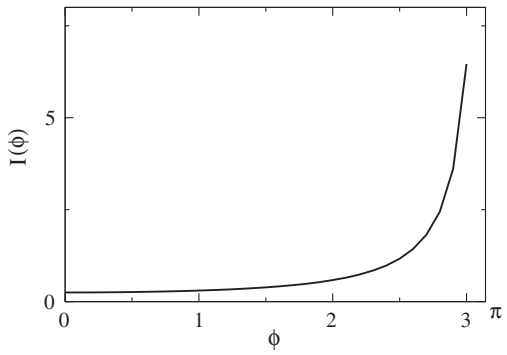

FIG. 14. $I(\phi)$, defined in Eq. (159), vs the angle ϕ between the wave vectors $\boldsymbol{q}_2$ and $\boldsymbol{q}_3$. This function is proportional to the free energy cost for having overlap between ribbons associated with different wave vectors. For $\boldsymbol{q}_2$ parallel to $\boldsymbol{q}_3$, corresponding to $\phi = 0$, there is no overlap between ribbons and no free energy cost has to be paid. The free energy cost diverges for perfectly overlapping ribbons, corresponding to $\phi = \pi$.

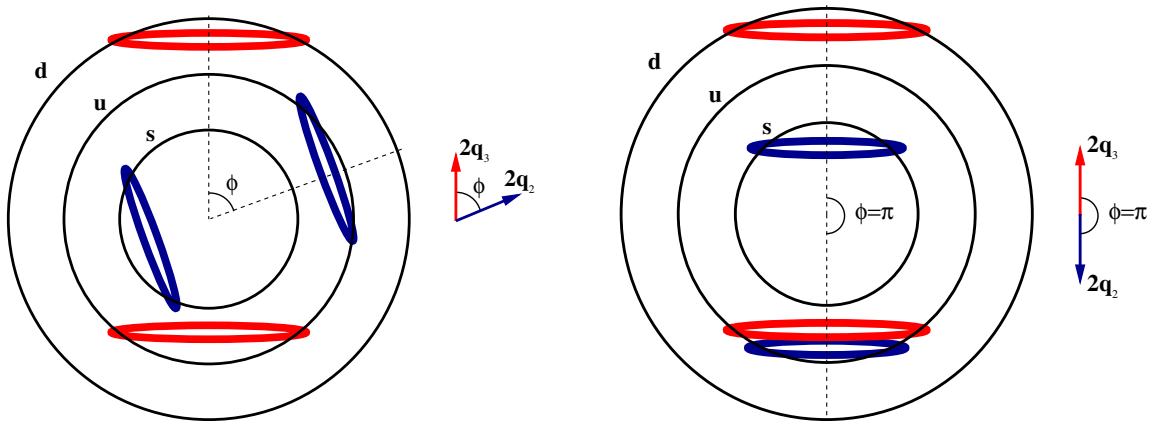

FIG. 15 (color online). Sketch showing where on the Fermi surfaces pairing occurs for condensates in which $\boldsymbol{q}_2$ and $\boldsymbol{q}_3$ are at an angle ϕ. The light gray ribbons on the d and u Fermi surfaces indicate those quarks that contribute the most to the $\langle ud\rangle$ condensate with gap parameter Δ_3 and wave vector $\boldsymbol{q}_3$, which points upward in both panels. The dark gray ribbons on the u and s Fermi surfaces indicate those quarks that contribute most to the $\langle us\rangle$ condensate with gap parameter Δ_2 and wave vector $\boldsymbol{q}_2$. For descriptive reasons, in the left panel the case $\phi = 70^\circ$ is shown, and in the right panel the antipodal case, with the two vectors pointing in opposite directions. We exaggerated the splitting between the Fermi surfaces, relative to the values used in the calculations reported in Sec. III.B.

configuration that minimizes $I(\phi)$ does as well minimize the free energy; see Eq. (155). We note that although $I(\phi)$ is an increasing function of ϕ it depends very slightly on the angle except close to the value $\phi = \pi$, i.e., when the two vectors are antiparallel and $I(\phi)$ diverges.

Although the divergence of β_{23} at $\phi = \pi$ is not physically relevant, since it is not the value that minimizes the free energy, it is worth considering this case to gain a qualitative understanding of the behavior of the GL approximation. We see in Fig. 15 that there are two pairing rings on the up quark Fermi surface, because some up quarks pair with down quarks forming Cooper pairs with wave vector $2\boldsymbol{q}_3$ and other up quarks pair with strange quarks forming Cooper pairs with wave vector $2\boldsymbol{q}_2$. However, as shown in the right panel of Fig. 15, if $\phi = \pi$ the two pairing rings on the up quark Fermi surface are close to being coincident. In the weak-coupling limit in which $\delta\mu/\mu \to 0$ (and $\Delta_{\mathrm{CFL}} \to 0$ with $\delta\mu/\Delta_{\mathrm{CFL}}$ fixed) these two rings become precisely coincident. We attribute the divergence in β_{23} to the fact that antiparallel wave vectors pay an infinite free energy price and hence are forbidden, because of the coincidence of these two pairing rings. In contrast, if $\phi = 0$, the two pairing rings on the up Fermi surface are as far apart as they can be, and β_{23} and the free energy of the state are minimized. This qualitative understanding also highlights that it is only in the strict GL and weak-coupling limits that the cost of choosing antiparallel wave vectors diverges. If $\Delta/\delta\mu$ is small but nonzero, the pairing regions are ribbons on the Fermi surfaces instead of lines. And if $\delta\mu/\mu$ is small but not taken to zero (as of course is the case in Fig. 15) then the two ribbons on the up Fermi surface will have slightly different diameter, as the figure indicates. This means that we expect that if we do a calculation at small but nonzero $\Delta_{\mathrm{CFL}} \sim \delta\mu$, and do not make a GL expansion, we should find some free energy penalty for choosing $\phi = \pi$, but not a divergent one. This is indeed the result that one obtains without using the GL expansion; see Fig. 13. These results also explain why the breakdown of the GL expansion in Fig. 13 happens for very small values of Δ for $\phi \approx \pi$, while only for larger values of Δ for $\phi = 0$. Indeed, increasing ϕ from 0 to π, the β_{23} term in the GL expansion increases, and therefore the radius of convergence of the GL expansion decreases.

A more quantitative study of the radius of convergence of the GL approximation would require evaluating (at least) the Δ^6 terms, whose coefficients we generically call γ. Because we are working in the vicinity of a point where $\alpha_I = 0$, the first estimator of the radius of convergence that we can construct comes by requiring $\gamma\Delta^6 \lesssim (\beta_I + \beta_{23})\Delta^4$. Thus, the results of the comparison in Fig. 13 are not conclusive on this point, but they certainly indicate that the radius of convergence in Δ decreases with increasing ϕ, and tends toward zero for $\phi \to \pi$.

4. Chromomagnetic stability of the three-flavor crystalline phase

Given that the three-flavor CCSC phase in Eq. (156) is thermodynamically favored with respect to the CFL and normal phases, it remains to be proven that it is chromomagnetically stable. This issue has been discussed within the GL expansion by Ciminale *et al.* (2006). It has been shown that gauging the NJL Lagrangian the Meissner masses of gluons are real and positive, meaning that this phase is chromomagnetically stable. To properly take into account gluons, the HDET Lagrangian has to be extended to include nonlocal terms arising from the integration over the negative energy fields (Casalbuoni Fabiano *et al.*, 2002; Casalbuoni *et al.*, 2003), obtaining in momentum space

$$\mathcal{L} = \psi^{\alpha\dagger}_{i,v}(\ell)\left(V\cdot\ell^{\alpha\beta}_{ij} + \mu^{\alpha\beta}_{ij} + P_{\mu\nu}\left[\frac{\ell_\mu\ell_\nu}{\tilde{V}\cdot\ell + 2\mu}\right]^{\alpha\beta}_{ij}\right)\psi^{\beta}_{j,v}(\ell), \tag{160}$$

where

$$(\ell^\mu)^{\alpha\beta}_{ij} = \ell^\mu\delta_{ij}\delta^{\alpha\beta} - g_s A_a T^{\alpha\beta}_a \delta_{ij} \tag{161}$$

and

$$P^{\mu\nu} = g^{\mu\nu} - \frac{(V^\mu \tilde{V}^\nu + \tilde{V}^\mu V^\nu)}{2}. \tag{162}$$

In the HDET there is an infinite series of effective vertices suppressed by increasing powers of $1/\mu$, describing the coupling between gluons and quarks. These interaction vertices arise from the expansion of the nonlocal term in the square bracket of (160). For the leading-order evaluation of the gluon self-energy two vertices are relevant: the one-gluon coupling to two quarks (three-body vertex, coupling $\sim g_s$); and the two-gluon coupling to two quarks (four-body vertex, coupling $\sim g_s^2$). These two vertices originate from the terms in Eq. (160) with one and two momenta ℓ, respectively. One may naively think that the contribution to the gluon self-energy due to the four-body vertex would be negligible with respect to the contribution arising from the three-body vertex, because of the $1/\mu$ suppression. Instead, the two vertices lead to the two one-loop diagrams shown in Fig. 16, whose contribution to the Meissner mass are clearly of the same order $g_s^2\mu^2$. Remarkably, these are the only order g_s^2 contributions to the Meissner mass not suppressed in the $\mu \to \infty$ limit; see Casalbuoni, Gatto *et al.* (2002b) for more details.

In more detail, the four-body coupling gives rise to the tadpolelike Feynman diagram, in Fig. 16(a), contributing $g_s^2\mu^2/(2\pi^2)$ to the Meissner mass. This contribution is momentum independent, is the same for all the eight gluons, and is the same one has in the CFL phase. The three-body coupling gives rise to the charmlike Feynman diagram, in Fig. 16(b), contributing

$$i\Pi^{\mu\nu}_{ab}(x,y) = -\mathrm{Tr}[iS(x,y)iH^\mu_a iS(y,x)iH^\nu_b] \tag{163}$$

to the polarization tensor. Here the trace is over all internal indexes; $S(x,y)$ is the quark propagator, and

$$H^\mu_a = i\frac{g_s}{2}\begin{pmatrix} iV^\mu T_a & 0 \\ 0 & -i\tilde{V}^\mu T^*_a \end{pmatrix} \tag{164}$$

is the vertex matrix in the HDET formalism.

The Meissner masses are defined in terms of the gluon self-energy in momentum space [see Eq. (37)], and in this case the mass matrix of gluons in the adjoint sector $a = 3, 8$ is not diagonal. Therefore we introduce the two linear combinations

$$\begin{aligned} \tilde{A}_{i3} &= \cos\theta_i A_{i3} + \sin\theta_i A_{i8}, \\ \tilde{A}_{i8} &= -\sin\theta_i A_{i3} + \cos\theta_i A_{i8}, \end{aligned} \tag{165}$$

which are eigenstates of the mass matrix. In Eq. (165) the subscript i denotes the spatial component of the gluon field; it is easily shown that the mixing angle satisfies

$$\tan 2\theta_i = \frac{2\mathcal{M}^2_{ii,38}}{\mathcal{M}^2_{ii,33} - \mathcal{M}^2_{ii,88}}; \tag{166}$$

the corresponding Meissner masses are the eigenvalues of the matrix

$$\begin{pmatrix} \mathcal{M}^2_{ij,33} & \mathcal{M}^2_{ij,38} \\ \mathcal{M}^2_{ij,38} & \mathcal{M}^2_{ij,88} \end{pmatrix}, \tag{167}$$

which turn out to be positive and are reported in Fig. 17.

On the left panel of Fig. 17 we report the longitudinal (i.e., zz) components of the squared Meissner masses against M_s^2/μ, in units of the CFL squared Meissner mass (Rischke, 2000a; Son and Stephanov, 2000b), at the $\mathcal{O}(\Delta^4)$; on the right panel the results for the transverse (i.e., xx) squared Meissner masses are given.

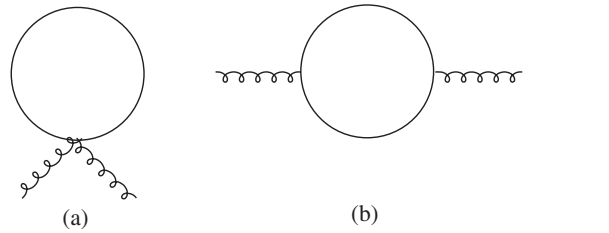

FIG. 16. (a) Tadpolelike diagram and (b) charmlike diagram contributing to the gluon masses in the HDET. The curly lines correspond to the gluon fields; the solid lines correspond to the positive energy quark fields; see Eq. (136). The interaction vertices can be obtained from the expansion of the effective Lagrangian in Eq. (160), including terms of order $1/\mu$.

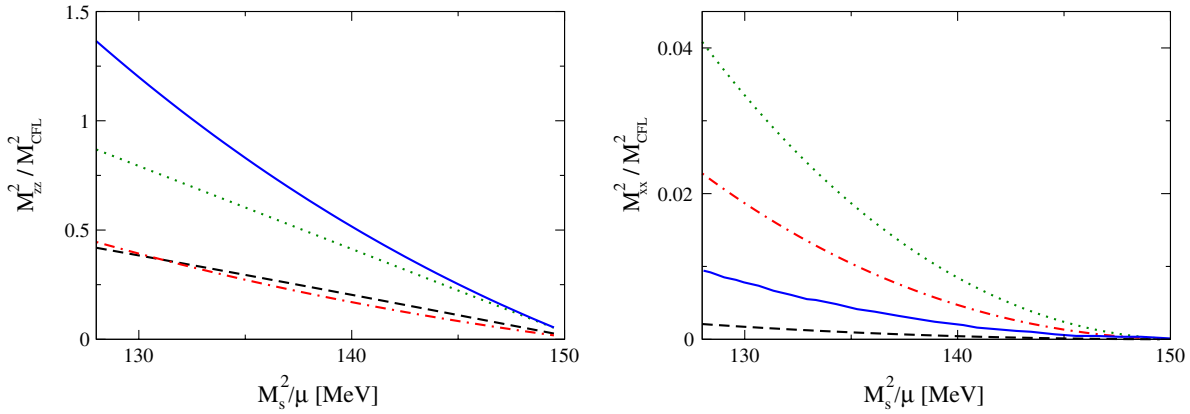

FIG. 17 (color online). Squared Meissner masses of the gluons $\tilde{A}_3$ (solid line), A_6 (dotted line), $\tilde{A}_8$ (dashed black line), and A_1 (dot-dashed line), in units of the CFL squared Meissner mass, vs M_s^2/μ. Left panel: longitudinal masses. Right panel: transverse masses. Adapted from Ciminale *et al.*, 2006.

These results are the analogs of those obtained in the two-flavor case by Giannakis and Ren (2005b). Note that the transverse mass of $\tilde{A}_8$, although positive, is almost zero, being 3 orders of magnitude smaller than the other ones. The conclusion is that the three-flavor condensate in Eq. (156) has no chromomagnetic instability, at least within the GL approximation. The results of Ciminale *et al.* (2006) have not been extended to more complicated structures, however, for a generic CCSC structure the Meissner tensor should be positive definite for small values of Δ, since it is additive with respect to different terms of order Δ^2 in the GL expansion (Giannakis and Ren, 2005b). These considerations suggest that the CCSC phase can be a good candidate in removing the chromomagnetic instability of the homogeneous gapless CSC phases of QCD.

5. Influence of $\mathcal{O}(1/\mu)$ corrections

Since the Meissner masses have been determined including the $\mathcal{O}(1/\mu)$ corrections in the HDET Lagrangian, for a consistent calculation it is necessary considering the effect of $\mathcal{O}(1/\mu)$ corrections on the gap parameters and the free energy (Casalbuoni *et al.*, 2006). These corrections amount to a shift of the strange quark Fermi momentum to lower values with respect to the corresponding chemical potential

$$p_s^F \simeq \mu_s - \frac{M_s^2}{2\mu_s} - \frac{1}{2\mu}\left(\frac{M_s^2}{2\mu}\right)^2, \tag{168}$$

and thus increasing the difference between the u and s strange chemical potential, without affecting the u-d chemical potential difference. Therefore (neglecting corrections proportional to μ_3 and μ_8 which are of order Δ^6) one has that

$$\delta\mu_2 = \frac{1}{2}\left[\mu_e - \frac{M_s^2}{2\mu} - \frac{1}{3\mu}\left(\frac{M_s^2}{2\mu}\right)^2\right], \qquad \delta\mu_3 = \frac{\mu_e}{2}, \tag{169}$$

and $|\delta\mu_2| > |\delta\mu_3|$ [neglecting $\mathcal{O}(1/\mu)$ corrections one would get $|\delta\mu_2| = |\delta\mu_3|$ as in Eq. (149); indeed in this limit $\mu_e = M_s^2/4\mu$]. The results for the splitting of chemical potentials are reported in the left panel of Fig. 18, together with the result obtained in the large μ limit.

As a consequence of the $\mathcal{O}(1/\mu)$ corrections, the two gap parameters are not equal and $\Delta_2 < \Delta_3$, as shown in the right panel of Fig. 18. This effect is akin to the one considered in the gCFL phase (see Fig. 12), but in that case the chromomagnetic instability prevented the splitting of the gap parameters. The effect of the corrections considered here is to enlarge the LOFF window, as can be seen from the right panel of Fig. 18. Neglecting $\mathcal{O}(1/\mu)$ corrections the crystalline phase was characterized by one gap, and by condensation in two channels: u-s and u-d. Including $\mathcal{O}(1/\mu)$ corrections there is pairing in both channels only for small values of M_s^2/μ, but the crystalline phase extends to larger values of M_s^2/μ, where only $\Delta_3 \neq 0$ and therefore there is no u-s pairing. This phase is the two-flavor FF phase, with a chemical potential difference determined by the ratio of the strange quark mass to the average quark chemical potential.

C. Ginzburg-Landau analysis of crystalline structures

As in the two-flavor case, more complicated crystalline structure can be considered and analyzed by the GL expansion (Rajagopal and Sharma, 2006). The most general two-flavor CCSC condensate was given in Eq. (45) and in the three-flavor case it can be extended to

$$\langle 0|\psi_{iL}^{\alpha}\psi_{jL}^{\beta}|0\rangle = -\langle 0|\psi_{iR}^{\alpha}\psi_{jR}^{\beta}|0\rangle \propto \sum_{I=1}^{3}\varepsilon^{\alpha\beta I}\epsilon_{ijI}\sum_{\boldsymbol{q}_I^m\in\{\boldsymbol{q}_I\}}\Delta_{I,\boldsymbol{q}_I^m}e^{2i\boldsymbol{q}_I^m\cdot\boldsymbol{x}}. \tag{170}$$

This condensate is antisymmetric in color (α,β), spin, and flavor (i,j) indices, and can be viewed as well as a generalization of the CFL ansatz. As in two-flavor quark matter, we consider the simplified case with $\Delta_{I,\boldsymbol{q}_I^m} \equiv \Delta_I$ independent of $\boldsymbol{q}_I^m$. The resulting condensate is the one reported in Eq. (7), where each gap parameter has a periodic modulation in space corresponding to a crystalline structure. For example, Δ_2 is associated with a crystal due to u-s pairing

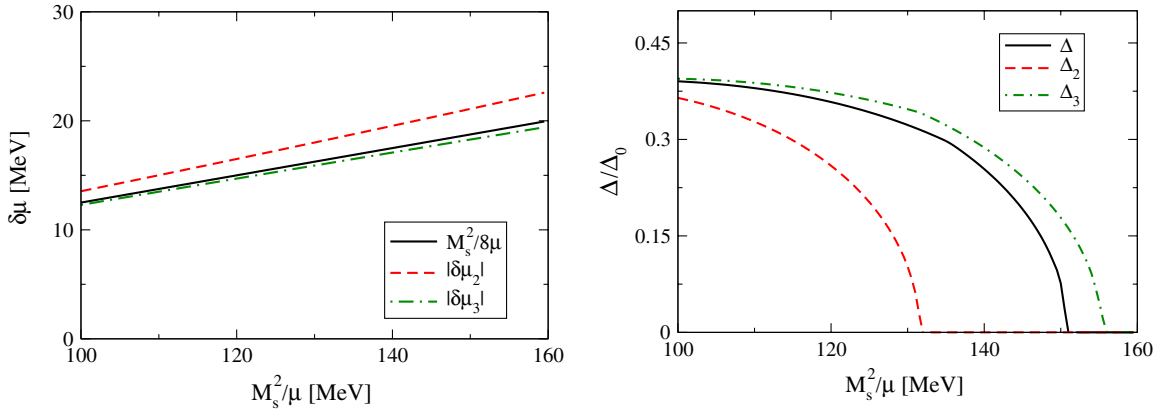

FIG. 18 (color online). Left panel: Quark chemical potential difference as a function of M_s^2/μ. The dashed line corresponds to $|\delta\mu_2|$ and the dash-dotted line corresponds to $|\delta\mu_3|$; their common value $M_s^2/(8\mu)$, obtained neglecting $\mathcal{O}(1/\mu)$ corrections, corresponds to the solid black line. Right panel: Gap parameters as a function of M_s^2/μ. The solid black line represents the solution $\Delta = \Delta_2 = \Delta_3$ obtained neglecting $\mathcal{O}(1/\mu)$ corrections; the dashed and dash-dotted lines represent, respectively, Δ_2 and Δ_3 and are obtained including $\mathcal{O}(1/\mu)$ corrections. All gap parameters are normalized to the CFL gap $\Delta_0 = \Delta_{\mathrm{CFL}} = 25$ MeV. Adapted from Casalbuoni *et al.*, 2006.

which is described by the vectors $\boldsymbol{q}_2^m$, where m is the index which identifies the elements of the set $\{\boldsymbol{q}_2\}$. This means that the $\boldsymbol{q}_2^m$'s are the reciprocal vectors which define the crystal structure of the u-s condensate.

Even within this simplified case, self-consistent computations based on Eq. (7) are very complicated. As a consequence, several additional assumptions and simplifications have been used by Rajagopal and Sharma (2006). As discussed in the previous section, the pairing between d and s quarks can been neglected; this is a very reasonable approximation, since the difference of chemical potentials between d and s quarks is approximately twice the imbalance of chemical potentials between u-s and u-d. Therefore, $\Delta_1 = 0$, and one can take $\Delta_2 = \Delta_3$, neglecting $\mathcal{O}(1/\mu)$ corrections. As a further simplification, only crystalline structures with wave vectors $\{\boldsymbol{q}_2^m\}$ and $\{\boldsymbol{q}_3^m\}$ with equal modulus are considered. This means that any phase is determined by one gap parameter, by the modulus of the total pair momentum q, and by the sets of unit vectors which determine the two crystalline structures. The corresponding pairing ansatz simplifies to

$$\begin{aligned}\langle 0|\psi_{iL}^{\alpha}\psi_{jL}^{\beta}|0\rangle &= -\langle 0|\psi_{iR}^{\alpha}\psi_{jR}^{\beta}|0\rangle \\ &\propto \Delta\sum_{I=2}^{3}\varepsilon^{\alpha\beta I}\epsilon_{ijI}\sum_{\boldsymbol{n}_I^m\in\{\boldsymbol{n}_I\}} e^{2iq\boldsymbol{n}_I^m\cdot\boldsymbol{x}}. \end{aligned} \tag{171}$$

Finally, Rajagopal and Sharma (2006) consider only structures which are exchange symmetric, which means that $\{\boldsymbol{n}_2\}$ and $\{\boldsymbol{n}_3\}$ can be exchanged by some combination of rotations and reflections applied simultaneously to all wave vectors.

The thermodynamic potential within the GL expansion up to the sextic order in the gap parameters is given by a generalization of Eq. (47) [see also Eqs. (147) and (152)], that is,

$$\begin{aligned}\Omega = \Omega_n &+ \left[P\alpha(|\Delta_2|^2+|\Delta_3|^2)+\frac{\beta}{2}(|\Delta_2|^4+|\Delta_3|^4)\right. \\ &\left.+\frac{\gamma}{3}(|\Delta_2|^6+|\Delta_3|^6)\right] \\ &+\left[\frac{\beta_{23}}{2}|\Delta_2|^2|\Delta_3|^2+\frac{\gamma_{233}}{3}|\Delta_2|^2|\Delta_3|^4+\frac{\gamma_{322}}{3}|\Delta_2|^4|\Delta_3|^2\right] \\ &+\mathcal{O}(\Delta^8), \end{aligned} \tag{172}$$

where we have explicitly diversified Δ_2 and Δ_3 as a means to show the interaction between the condensates in the u-d and u-s channels. The coefficients α, β, and γ in the first square bracket are the same coefficients computed for the two-flavor case by Bowers and Rajagopal (2002). The terms in the second square bracket are peculiar of the three-flavor case. In the numerical computations the free energy is minimized with respect to Δ and for any crystalline structure considered it is found that the thermodynamic potential is always bounded from below. Therefore, it is possible to compute the numerical value of Δ and the value of the free energy density at the minimum.

Among the many crystalline structures considered by Rajagopal and Sharma (2006), two of them have been found to have the lowest free energy: they are called the CubeX and 2Cube45z structures. In the CubeX crystal each set contains four vectors, that is, $\{\boldsymbol{n}_2\}=\{\boldsymbol{n}_2^1,\boldsymbol{n}_2^2,\boldsymbol{n}_2^3,\boldsymbol{n}_2^4\}$ and $\{\boldsymbol{n}_3\}=\{\boldsymbol{n}_3^1,\boldsymbol{n}_3^2,\boldsymbol{n}_3^3,\boldsymbol{n}_3^4\}$ with

$$\begin{aligned}\boldsymbol{n}_2^1 &= \sqrt{\frac{1}{3}}(1,1,1) = -\boldsymbol{n}_2^2, \qquad \boldsymbol{n}_2^3 = \sqrt{\frac{1}{3}}(-1,-1,1) = -\boldsymbol{n}_2^4, \\ \boldsymbol{n}_3^1 &= \sqrt{\frac{1}{3}}(-1,1,1) = -\boldsymbol{n}_3^2, \qquad \boldsymbol{n}_3^3 = \sqrt{\frac{1}{3}}(1,-1,1) = -\boldsymbol{n}_3^4. \end{aligned}$$

Thus, the vectors of each set point to the vertices of a rectangle; the eight vectors together point toward the vertices of a cube. In the 2Cube45z crystal, $\{\boldsymbol{n}_2\}$ and $\{\boldsymbol{n}_3\}$ each contains eight wave vectors, pointing to the corners of a cube; the two cubes are rotated by 45° about the z axis. The computation of Rajagopal and Sharma (2006) shows that the CubeX crystal is favored over all considered structures in the range

$$2.9\Delta_{\mathrm{CFL}} < \frac{M_s^2}{\mu} < 6.4\Delta_{\mathrm{CFL}}; \tag{173}$$

similarly for the 2Cube45z crystal it is found that it is energetically favored for

$$6.4\Delta_{\mathrm{CFL}} < \frac{M_s^2}{\mu} < 10.4\Delta_{\mathrm{CFL}}. \tag{174}$$

Putting together the above results, the CCSC phase is favored with respect to the homogeneous CFL, gCFL, and unpaired phases in the range

$$2.9\Delta_{\mathrm{CFL}} < \frac{M_s^2}{\mu} < 10.4\Delta_{\mathrm{CFL}}. \tag{175}$$

The above condition can be translated to a condition on μ only if the constituent strange quark mass as a function of μ is known. This topic will be discussed in the next section.

We remark that from the quantitative point of view, the result in Eq. (175) should be taken with care. The GL expansion is reliable only if the gap parameter Δ is small, compared to $\delta\mu$. On the other hand, the numerical results of Rajagopal and Sharma (2006) show that, within this expansion, the ratio $\Delta/\delta\mu$ turns out to be of order 1. This clearly signals that the results lie beyond the validity of the expansion itself. Moreover, the coefficients in the expansion in Eq. (172) depend on the microscopic model. Therefore, Eq. (175) is certainly model dependent. Nevertheless, the qualitative picture which arises in Rajagopal and Sharma (2006) seems to be quite robust: the crystalline superconductor has lower free energy with respect to the single-plane-wave state. This conclusion seems reasonable and model independent: in fact, the phase space for pairing in the case of CubeX and 2Cube45z is larger than the one corresponding to the single-plane-wave structure; this suggests that the free energy gain for multiple plane waves is larger than the one obtained for the single-plane-wave state.

1. LOFF window in the QCD phase diagram

It is important to identify, within a self-consistent computation, the range of chemical potential in which the CCSC phase is expected to be thermodynamically favored. This would correspond to a chemical potential LOFF window in Fig. 2. Then, using an appropriate equation of state this chemical potential window can be translated into a density window. So far we reported the LOFF window in terms of M_s^2/μ for the two-plane-waves structure and the favored crystalline phases, respectively. For translating this window to a window in μ, it is necessary to consider the chemical potential dependence of both the CFL gap parameter and of the constituent quark masses. This investigation has been started by Ippolito, Nardulli, and Ruggieri (2007) considering vanishing temperature. They computed the in-medium quark masses self-consistently within a NJL model and the CFL gap was evaluated in the chiral limit by means of Eq. (146), where the considered hard momentum cutoff is taken as $\delta = \Lambda - \mu$. Ippolito, Nardulli, and Ruggieri (2007) considered $\Lambda \simeq 643$ MeV with a corresponding NJL coupling constant $G(\Lambda) \simeq 13.2\ \mathrm{GeV}^{-2}$.

In the simple case of two plane waves, Eq. (156), the state with $\boldsymbol{n}_2 = \boldsymbol{n}_3$ is energetically favored in the range given in Eq. (157) This range has been obtained for a fixed value of the CFL gap parameter. Considering the dependence of the CFL gap on the chemical potential given in Eq. (146) and the results for the constituent strange quark mass $M_s(\mu)$ computed by Ippolito, Nardulli, and Ruggieri (2007), that range can be transformed in

$$4.8\Delta_{\mathrm{CFL}}(\mu) \lesssim \frac{M_s(\mu)^2}{\mu} \lesssim 7.6\Delta_{\mathrm{CFL}}(\mu), \tag{176}$$

and then to the quark chemical potential window

$$467 \lesssim \mu \lesssim 488\ \mathrm{MeV}. \tag{177}$$

Therefore, there exists a small but finite window in μ in which the structure (156) has a lower free energy than both gCFL quark matter and normal quark matter.

One might expect that such a small window is considerably enlarged in more complicated CCSC phases. As discussed in the previous section, the analysis of Rajagopal and Sharma (2006) shows that more complicated crystalline structures are favored in the interval reported in Eq. (175), which used the self-consistent treatment of Ippolito, Nardulli, and Ruggieri (2007) transforms in

$$442 \lesssim \mu \lesssim 515\ \mathrm{MeV}. \tag{178}$$

This result is certainly model dependent, however it shows that the actual extension of the LOFF window in Fig. 2 might not be very large. Therefore, it is likely that the CCSC phase occupies only a fraction of the quark core of hybrid compact stars. We discuss this topic in Sec. IV.D.

D. Shear modulus and Nambu-Goldstone modes

The three-flavor CCSC phase has several low-energy excitations; besides gapless quasifermions, there are the bosonic modes related to the spontaneous breaking of translational symmetry, the three phonons, of the chiral symmetry, the eight pseudoscalar NGBs, and to the breaking of $\mathrm{U}(1)_B$ symmetry, the so-called H phonon. The phonon Lagrangian for the two-flavor CCSC phase has been discussed in Sec. II.F; here we extend the results to the three-flavor case (Mannarelli, Rajagopal, and Sharma, 2007) deriving the low-energy coefficients of the GL expansion from a NJL-like model. Regarding the eight pseudoscalar NGBs, we briefly discuss the results of Anglani *et al.* (2007) obtained for the three-flavor CCSC phase.

1. Phonons effective action and shear modulus

According to the basic theory of elastic media (Landau and Lifshits, 1959), the elastic moduli are related to the potential energy cost of small deformations of the crystal. Therefore, the evaluation of the shear modulus requires knowledge of the low-energy Lagrangian for the displacement fields (Mannarelli, Rajagopal, and Sharma, 2007). Since the three condensates that characterize the crystalline phase can oscillate independently, three are three sets of displacement fields $\boldsymbol{u}_I(x)$. Thus, we can extend the definition of the phonon fields in Eq. (97) by

$$\Delta_I(\boldsymbol{x}) \to \Delta_I^u(x) = \Delta_I(\boldsymbol{x} - \boldsymbol{u}_I(x)), \tag{179}$$

and the Lagrangian that includes fluctuation on the top of the mean field solution can be written as

$$\mathcal{L} = \frac{1}{2}\bar{\chi}\begin{pmatrix} i\partial + \mu & \Delta^u(x) \\ \bar{\Delta}^u(x) & (i\partial - \mu)^T \end{pmatrix}\chi + \frac{1}{16G}\,\mathrm{tr}[(\bar{\Delta}^u)^T\Delta^u], \tag{180}$$

where tr represents the trace over color, flavor, and Dirac indices.

To find the low-energy effective action describing the phonons and the gapless fermionic excitations, one should integrate out the high-energy fermion fields. The procedure is detailed in Mannarelli, Rajagopal, and Sharma (2007), where the effective action is derived starting from a NJL-like microscopic model. The final form of the effective action of the phonon fields is given by

$$\begin{aligned} i\mathcal{S}[\boldsymbol{u}] &= \log(Z[\boldsymbol{u}]) \\ &= i\int d^4x \left[\frac{1}{16G}\,\mathrm{tr}[(\bar{\Delta}^u)^T\Delta^u]\right] + \frac{1}{2}\,\mathrm{Tr}_{\mathrm{ng}}\,\log\,(S^{-1}), \end{aligned} \tag{181}$$

where $\mathrm{Tr}_{\mathrm{ng}}$ stands for the trace over the Nambu-Gorkov, color, flavor, and Dirac indices and a further trace over a set of functions on space-time containing all energy modes. The full inverse propagator is given by

$$S^{-1} = \begin{pmatrix} i\partial + \mu & \Delta^u(x) \\ \bar{\Delta}^u(x) & (i\partial - \mu)^T \end{pmatrix}, \tag{182}$$

and it includes interactions of the phonon fields.

For the crystal structures CubeX and 2Cube45z, the full inverse propagator cannot be inverted, so a GL expansion has

been performed in order to obtain the effective action for the phonon field, first separating the full inverse propagator into the free part S_0^{-1} and a part containing the condensate Σ, as follows: $S^{-1} = S_0^{-1} + \Sigma$, where

$$S_0^{-1} = \begin{pmatrix} i\partial + \not{\mu} & 0 \\ 0 & (i\partial - \not{\mu})^T \end{pmatrix} \tag{183}$$

and

$$\Sigma = \begin{pmatrix} 0 & \Delta^u(\boldsymbol{x}) \\ \bar{\Delta}^u(\boldsymbol{x}) & 0 \end{pmatrix}. \tag{184}$$

Then, one can expand the term $\log(S^{-1})$ that appears on the right-hand side of Eq. (181) as

$$\begin{aligned} \mathrm{Tr}_{\mathrm{ng}}[\log(S_0^{-1} + \Sigma)] = \mathrm{Tr}_{\mathrm{ng}}(\log\, S_0^{-1}) + \mathrm{Tr}_{\mathrm{ng}}(S_0\Sigma) \\ - \tfrac{1}{2}\mathrm{Tr}_{\mathrm{ng}}(S_0\Sigma)^2 + \cdots. \end{aligned} \tag{185}$$

The $\mathrm{Tr}_{\mathrm{ng}}(\log\, S_0^{-1})$ term is related to the free energy of unpaired (normal) quark matter. Furthermore, it is easily found that only even powers of $(S_0\Sigma)$ contribute to the trace over Nambu-Gorkov indices. Expanding the effective action in powers of $\phi_I^m = 2\boldsymbol{q}^m \cdot \boldsymbol{u}_I$ and including the first nontrivial quadratic term, which is calculated to order Δ^2, one obtains

$$\mathcal{S}^{\phi^2\Delta^2} = \sum_I \sum_{\boldsymbol{q}_I^m} \int \frac{d^4k}{(2\pi)^4} \phi_I^m(k)\phi_I^m(-k)\Delta_I^*\Delta_I \mathcal{P}_I^m(k), \tag{186}$$

where $k = k_2 - k_1$ is the four-momentum of the phonon and

$$\begin{aligned} \mathcal{P}_I^m(k) = i\sum_{\substack{j\neq k \\ \neq I}} \int \frac{d^4p}{(2\pi)^4} \\ \times \mathrm{Tr}\left[\frac{1}{(\not{p} + \not{q}_I{}^m + \not{k}_1 + \not{\mu}_j)(\not{p} - \not{q}_I{}^m + \not{k}_2 - \not{\mu}_k)}\right. \\ \left. - \frac{1}{(\not{p} + \not{q}_I{}^m + \not{\mu}_j)(\not{p} - \not{q}_I{}^m - \not{\mu}_k)}\right], \end{aligned} \tag{187}$$

where the trace is over Dirac indices. Integrating Eq. (187) one obtains

$$\begin{aligned} \mathcal{S}^{\Delta^2}[\boldsymbol{u}] = \frac{1}{2}\int d^4x \sum_I \kappa_I \sum_{\boldsymbol{n}_I^m} [\partial_0(\boldsymbol{n}_I^m \cdot \boldsymbol{u}_I)\partial_0(\boldsymbol{n}_I^m \cdot \boldsymbol{u}_I) \\ - (\boldsymbol{n}_I^m \cdot \partial)(\boldsymbol{n}_I^m \cdot \boldsymbol{u}_I)(\boldsymbol{n}_I^m \cdot \partial)(\boldsymbol{n}_I^m \cdot \boldsymbol{u}_I)], \end{aligned} \tag{188}$$

where

$$\kappa_I \equiv \frac{2\mu^2|\Delta_I|^2}{\pi^2(1 - z_q^2)}, \tag{189}$$

with z_q defined in Eq. (87). This action generalizes Eq. (99) to the three-flavor case and is the LO low-energy effective action valid for phonons in any CCSC phase, indeed it has a general expression depending on the $\boldsymbol{n}_I^m$ vectors. Only terms of the second order in derivatives and the phonon fields are reported, but higher-order terms can be obtained in a similar way.

In Eq. (188) there are no terms that "mix" the different $\boldsymbol{u}_I(k)$, meaning that at this order the displacement of the various crystals can be considered separately. This follows from the fact that the Lagrangian conserves particle number for every flavor of quarks, which corresponds to symmetry under independent global phase rotations of quark fields of the three flavors, meaning independent phase rotations of the three Δ_I's. The effective action should be invariant under these rotations and hence Δ_I can only occur in the combination $\Delta_I^*\Delta_I$. Since the effective action has been obtained up to the second order in the gap parameters Δ_I's, the mixing terms do not appear; mixing between different fluctuations can only appear in higher-order terms, e.g., by terms such as $\mu^2|\Delta_I\Delta_J|^2\partial\boldsymbol{u}_I\partial\boldsymbol{u}_J/\delta\mu^2$.

The coefficients κ_I determine the potential energy cost of a fluctuation and therefore are related to the shear modulus. In particular, Mannarelli, Rajagopal, and Sharma (2007) found that for the two favored structures, 2Cube45z and CubeX, the shear modulus is a 3×3 nondiagonal matrix in coordinate space with entries given by

$$\nu_{\mathrm{CQM}} = 2.47\ \mathrm{MeV/fm^3}\left(\frac{\Delta}{10\ \mathrm{MeV}}\right)^2\left(\frac{\mu}{400\ \mathrm{MeV}}\right)^2. \tag{190}$$

Considering typical values of the quark chemical potential in the range

$$350 < \mu < 500\ \mathrm{MeV} \tag{191}$$

and

$$5\ < \Delta < 25\ \mathrm{MeV}, \tag{192}$$

one has that

$$0.47 < \nu_{\mathrm{CQM}} < 24\ \mathrm{MeV/fm^3}. \tag{193}$$

The standard neutron star crust, which is a conventional crystal of positively charged ions immersed in a fluid of electrons (and, at sufficient depth, a fluid of neutrons), has a shear modulus given by (Strohmayer *et al.*, 1991; Mannarelli, Rajagopal, and Sharma, 2007)

$$0.092 < \nu_{\mathrm{NM}} < 23\ \mathrm{keV/fm^3}, \tag{194}$$

thus, the crystalline quark matter is more rigid than the conventional neutron star crust by at least a factor of 20–1000. Note that the three-flavor CCSC phase is also a superfluid, by picking a phase its order parameter does indeed break the quark-number $\mathrm{U}(1)_B$ symmetry spontaneously. These results demonstrate that this superfluid phase of matter is at the same time a rigid solid and a superfluid.

2. Goldstone modes

The superfluid property of the CCSC phase derives from the existence of a massless NGB associated with the breaking of $\mathrm{U}(1)_B$. Actually, the crystalline condensate breaks the same global (and local) symmetries of the CFL phase (Alford, Rajagopal, and Wilczek, 1999), leaving unbroken a global symmetry group: $\mathrm{SU}(3)_{c+L+R} \times Z_2$; see Eq. (3). Therefore, there are nine NGBs due to the spontaneous breaking of

$U(1)_B$ and of the chiral symmetry, but only the $U(1)_B$ boson (H phonon) is massless. Indeed, the pseudoscalars associated with chiral symmetry have mass, because this group is explicitly broken by quark mass terms and by chemical potential differences.

Similar to the phonons described in the previous section, the NGBs discussed here describe the fluctuations of the condensate; see, e.g., Eguchi (1976). The pseudo-NGBs are related to fluctuations in flavor space, while the H phonon ϕ describes fluctuations in baryonic number. The form of the low-energy Lagrangian describing both phonons and the H phonon can be determined from symmetry arguments alone following the discussion by Leutwyler (1997) and Son (2005); see also Cirigliano, Reddy, and Sharma (2011). Here we focus on the microscopic derivation of the H phonon Lagrangian and introduce it by means of the transformation $\psi \to U^\dagger \psi$ with $U = \exp\{i\varphi/f_\varphi\}$, where f_φ is its decay constant. Taking into account the unitary rotations, the HDET Lagrangian takes the form (Anglani *et al.*, 2007)

$$\mathcal{L} = \frac{1}{2}\int \frac{d\Omega}{4\pi}\chi_A^\dagger \begin{pmatrix} [V\cdot\ell + \delta\mu_A(\boldsymbol{v}))\delta_{AB}] & -\Xi^\star_{BA} \\ -\Xi_{AB} & [V\cdot\ell - \delta\mu_A(-\boldsymbol{v})]\delta_{AB} \end{pmatrix}\chi_B, \tag{195}$$

where all quantities have been defined in Sec. III.B.1 [see Eq. (143)], except Ξ_{AB}, which is given by

$$\Xi_{AB} = \Delta_I^\star(\boldsymbol{x})\mathrm{Tr}[\epsilon_I (F_A U^\dagger)^T \varepsilon^I F_B U^\dagger], \tag{196}$$

with $\epsilon_I \equiv \epsilon_{ijI}$ and $\varepsilon^I \equiv \varepsilon^{\alpha\beta I}$.

Expanding the Lagrangian in the scalar field one derives three-body and four-body interaction vertices. At the leading order in Δ these couplings provide the dominant contribution to the H phonon self-energy. We encountered similar interaction terms in the evaluation of the Meissner masses of gluons discussed in Sec. III.B.4. As in that case the two leading contributions are given by the tadpolelike and charmlike Feynman diagrams reported, in Figs. 16(a) and 16(b), respectively, but with the gluon lines replaced by H phonon lines. Technically the calculation is very similar to the one sketched in Sec. III.B.4 and the result is that the charmlike diagram contributes to the self-energy by

$$\mathcal{S}_{\text{c.l.}} = -i\frac{2}{f_\varphi^2}\sum_{I=2}^{3}\Delta_I^2\sum_{\boldsymbol{q}_I^m}\int\frac{d^4k}{(2\pi)^4}\varphi(-k)\varphi(k)\mathcal{P}_I^m(k_0,\boldsymbol{k}), \tag{197}$$

with $k = (k_0, \boldsymbol{k})$ and $\mathcal{P}_I^m(k_0,\boldsymbol{k})$ corresponds to the HDET version of Eq. (187),

$$\begin{aligned}\mathcal{P}_I^m(k_0,\boldsymbol{k}) &= -2\mu^2\int\frac{d\Omega}{4\pi}\int\frac{dp_0 d\xi}{(2\pi)^4}\\ &\times\left[\frac{1}{(\tilde V\cdot\ell + \delta\mu - \boldsymbol{q}_I^m\cdot\boldsymbol{v})[V\cdot(\ell+k)+\delta\mu-\boldsymbol{q}_I^m\cdot\boldsymbol{v}]}\right.\\ &\left.+\frac{1}{(V\cdot\ell-\delta\mu-\boldsymbol{q}_I^m\cdot\boldsymbol{v})[\tilde V\cdot(\ell+k)-\delta\mu-\boldsymbol{q}_I^m\cdot\boldsymbol{v}]}\right]\\ &+\delta\mu\to-\delta\mu.\end{aligned} \tag{198}$$

The tadpolelike contribution is given by

$$\mathcal{S}_{\text{t.l.}} = i\frac{2}{f_\phi^2}\sum_{I=2}^{3}\Delta_I^2\sum_{\boldsymbol{q}_I^m}\int\frac{d^4k}{(2\pi)^4}\varphi(-k)\varphi(k)\mathcal{P}_I^m(k_0=0,\boldsymbol{k}=0). \tag{199}$$

We do not provide further details of the calculation which can be found in Anglani *et al.* (2007), and we only quote the final result valid at small momenta

$$\mathcal{L}_\varphi(k) = \tfrac{1}{2}\varphi(-k)[k_0^2\mathcal{I}_0 - k_i k_j V_{ij}]\varphi(k), \tag{200}$$

where

$$\begin{aligned}\mathcal{I}_0 &= -\frac{\mu^2}{\pi^2 f_\varphi^2}\sum_{I=2}^{3}\Delta_I^2\sum_{\boldsymbol{q}_I^m}\Re e\\ &\times\int\frac{d\Omega}{4\pi}\frac{1}{(\delta\mu-\boldsymbol{q}_I^m\cdot\boldsymbol{v}+i0^+)^2}+(\delta\mu\to-\delta\mu),\end{aligned} \tag{201}$$

$$\begin{aligned}V_{ij} &= -\frac{\mu^2}{\pi^2 f_\varphi^2}\sum_{I=2}^{3}\Delta_I^2\sum_{\boldsymbol{q}_I^m}\Re e\\ &\times\int\frac{d\Omega}{4\pi}\frac{\boldsymbol{v}_i\boldsymbol{v}_j}{(\delta\mu-\boldsymbol{q}_I^m\cdot\boldsymbol{v}+i0^+)^2}+(\delta\mu\to-\delta\mu).\end{aligned} \tag{202}$$

Specializing these results to the case $\Delta_2 = \Delta_3 = \Delta$, $|\boldsymbol{q}_2^a| = |\boldsymbol{q}_3^a| = q$, and requiring canonical normalization of the Lagrangian in Eq. (200), leads to

$$f_\varphi^2 = \frac{4P\mu^2}{\pi^2}\frac{z_q^2\Delta^2}{\delta\mu^2(1-z_q^2)}, \tag{203}$$

where P is the number of plane waves comprising each crystal (we assume that the number of plane waves in the two crystals are equal). Upon substituting this result in to Eq. (202), and specializing it to $P = 1$, we find $V_{ij} = [\mathrm{diag}(0,0,1)]_{ij}$, where we have chosen $\boldsymbol{q}_2$ and $\boldsymbol{q}_3$ along the positive z axis. For the two cubic structures corresponding to the values $P = 4$ (CubeX) and $P = 8$ (2Cube45z) we find $V_{ij} = \delta_{ij}/3$, i.e., the velocity is isotropic and has the value $1/\sqrt{3}$.

The extension of the above procedure to the octet of pseudo-NGBs is straightforward; see Anglani *et al.* (2007). Here we just recall that one of the important result is that the

squared masses of the pseudo-NGBs are always positive, thus kaon condensation for the considered CCSC phases is excluded, at least at the order Δ^2.

As we see in the next sections, it is of astrophysical interest the study of rotating quark matter. In particular, in Sec. IV.B we see how superfluid vortices may influence the spinning evolution of compact stars. The response of the crystalline phase to rotation should indeed result in the formation of vortices. The naive expectation is the formation of $\mathrm{U}(1)_B$ vortices (Forbes and Zhitnitsky, 2002; Iida and Baym, 2002), but non-Abelian vortices (Auzzi *et al.*, 2003; Hanany and Tong, 2003) might be energetically favored (Balachandran, Digal, and Matsuura, 2006; Eto, Nitta, and Yamamoto, 2010).

IV. ASTROPHYSICS

The artificial creation of the low-temperature and high-density conditions appropriate for testing the properties of color superconductors is one of the challenging aims of high-energy experiments (Klahn, Blaschke, and Weber, 2012). To date, however, the unique *laboratory* in which these extreme conditions can be realized is the core of a compact stellar object (CSO). (Note that even if the relevant densities and low-temperature conditions were reached in a terrestrial laboratory, the conditions realized in a CSO are different from those produced in an accelerator, because in the former case quark matter is long lived, charge neutral, and in β equilibrium.) In the inner core of a CSO the extremely high densities and low temperatures may favor the transition from nuclear to quark matter (Ivanenko and Kurdgelaidze, 1965, 1969; Collins and Perry, 1975; Baym and Chin, 1976) and in turn, to the color superconducting (CSC) phase. Indeed, if matter is compressed at densities about a factor of 5 larger than the density of an ordinary nucleus, a simple geometrical reasoning suggests that baryons are likely to lose their identity and dissolve into deconfined quarks (Weber, 1999). In this case compact (hybrid) stars featuring quark cores would exist providing a window on the properties of QCD at high baryon densities. Assuming that deconfined matter is present, it should be in a CSC phase because its critical temperature (in weak coupling) is given by $T_c \simeq 0.57\Delta$, and as we have seen in the previous sections $\Delta \sim 5$–100 MeV, although lower values of the gap parameter, of the order of keV up to few MeV, can be realized in the spin-1 single flavor pairing phase (Alford, Rajagopal, and Wilczek, 1998; Schafer, 2000b; Schmitt, Wang, and Rischke, 2002; Alford *et al.*, 2003; Buballa, Hosek, and Oertel, 2003; Schmitt, 2005). In any case, for the greatest part of the compact star lifetime, the temperature is much lower than this critical temperature and the CSC state is thermodynamically favored.

Clearly, the basic question is whether gravity in the interior of CSOs is able to compress matter to such extreme densities. This question is still open, but some progress has been made in recent years. In particular, recent astronomical observations of very massive CSOs (Demorest *et al.*, 2010) seem to disfavor this possibility (Logoteta *et al.*, 2012), but the results depend on the poorly known equation of state (EOS) of matter at high density, and the possibility that hybrid stars of about $2M_\odot$ have a quark-matter core (Alford, Braby *et al.*, 2005; Bonanno and Sedrakian, 2012) or a crystalline color superconducting (CCSC) core (Ippolito *et al.*, 2008) cannot be excluded.

Besides the stellar mass, the presence of deconfined quark matter in the interior of a CSO can be probed by a number of astrophysical observables linked to the microscopic properties of CSC matter. In particular, the mass-radius relation, various transport properties, the r-mode evolution, glitches, and very strong magnetic fields are under scrutiny for ruling in or out CSC matter. Unfortunately, the available observational data do not allow us to infer in a unique way the internal structures of CSOs, but the investigation of the astrophysical signatures can help to pave the path connecting theoretical models to astronomical observations. In the following we present a brief state-of-the-art of some astrophysical implications related to the presence of CCSC matter in CSOs.

A. Gravitational waves

As reported in Sec. III.D the CCSC phase is extremely rigid, with a shear modulus larger than the standard neutron star crust by at least a factor 20. The existence of such a rigid core within compact stars may have a variety of observable consequences. A large deformation of the core, initially produced, for example, by magnetic fields not aligned with the rotation axis, can be sustained by the rigid structure provided by the crystalline condensate. If the deformation of the core is in a shape that has a nonzero quadrupole moment and if this axis-asymmetric mass distribution is not compensated by the overlying nuclear envelope, the spinning CSO would efficiently emit gravitational waves (Haskell *et al.*, 2007; Lin, 2007). The size of the distortion of the mass distribution can be measured by the equatorial ellipticity

$$\epsilon = \frac{I_{xx} - I_{yy}}{I_{zz}}, \tag{204}$$

which is defined in terms of the star principal moments of inertia. Standard neutron stars are expected to have maximum ellipticity of the order of $\epsilon_{\max} \approx 10^{-6}$, meaning that this is the largest deformation sustainable by the crust before breaking. For the three-flavor crystalline phases considered in Sec. III.D, deformed to the maximum extent allowed by the shear modulus, the maximum equatorial ellipticity sustainable could be as large as $\epsilon_{\max} \approx 10^{-2}$ (Haskell *et al.*, 2007; Lin, 2007). Different models of exotic stars composed of quark clusters (Xu, 2003) have a magnitude of the maximum ellipticity which is smaller than the CCSC phase by 2 orders of magnitude (Owen, 2005).

The gravitational waves emitted by an optimally oriented compact star spinning at a frequency ν would produce a strain on Earth-based interferometric detectors (such as LIGO, VIRGO, GEO600, and TAMA300) given by

$$h_0 = \frac{16\pi^2 G}{c^2}\frac{\epsilon I_{zz}\nu^2}{r}, \tag{205}$$

where G is the gravitational constant and r is the distance. If the standard value $I_{zz} = 10^{38}$ kg m^2 is assumed, Eq. (205) can be used to relate the ellipticity to the spinning frequency and

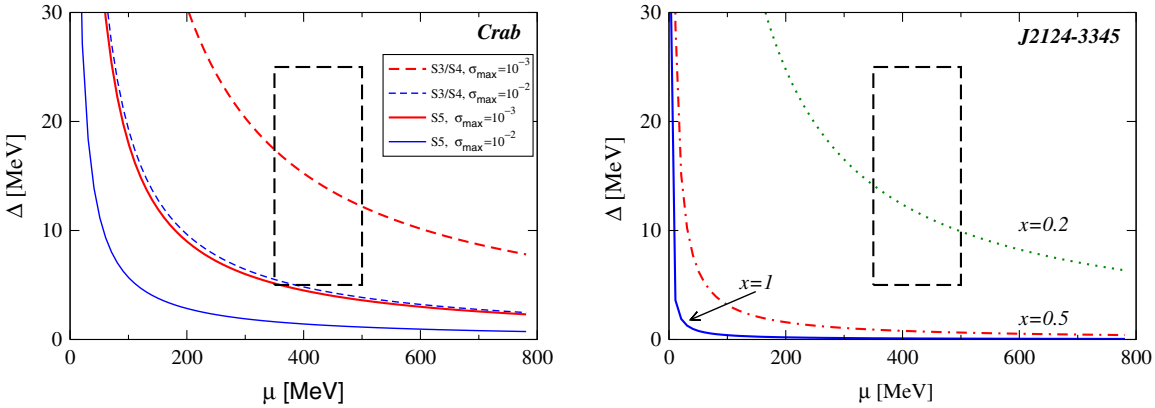

FIG. 19 (color online). Exclusion plots in the Δ-μ plane for the Crab (left panel) and the pulsar J2124-3358 (right panel) obtained assuming that these stars have mass $M = 1.4M_{\odot}$, radius $R = 10$ km, uniform mass distribution, and are maximally strained. The area above each line is excluded by the corresponding model. The rectangular box is the theoretically allowed region of μ and Δ for the CCSC phase; see Mannarelli, Rajagopal, and Sharma (2007). Left panel: The dashed lines correspond to the results of Lin (2007) which considers the S3/S4 LIGO data of the Crab pulsar, for the case $\sigma_{\max} = 10^{-3}$ (upper heavy dashed line) and $\sigma_{\max} = 10^{-2}$ (lower dashed line) and assuming that the whole star consists of maximally strained crystalline color superconducting matter. The solid lines have been determined using Eq. (7) of Lin (2007), but with the S5 LIGO data (Abbott *et al.*, 2010) and considering the case of $\sigma_{\max} = 10^{-3}$ (upper heavy solid line) and $\sigma_{\max} = 10^{-2}$ (lower solid line). Right panel: Dependence of the exclusion region on the size of the crystalline core for the pulsar J2124-3358 obtained using the S5 LIGO data (Abbott *et al.*, 2010) and considering the case of $\sigma_{\max} = 10^{-3}$. The three lines correspond to different values of $x = R_c/R$, where R_c is the radius of the crystalline color superconducting core.

distance. The LIGO nondetection of gravity waves from nearby neutron stars already limits the parameter space of CCSC matter. A first analysis of CSOs which include the crystalline phase was made by Haskell *et al.* (2007) and Lin (2007) using the results of the S3/S4 LIGO scientific run (Abbott *et al.*, 2007) and by Knippel and Sedrakian (2009) using the results of the S5 LIGO scientific run (Abbott *et al.*, 2008) on gravitational wave emission from the Crab neutron star. This is a young neutron star, first observed in the year 1054, which is a pulsating emitter of electromagnetic radiation (generically known as pulsars). In Fig. 19 we present the exclusion plots for the Crab (left panel) and the pulsar J2124-3358 (right panel), assuming maximum strain and that these stars are constituted by incompressible and uniformly distributed matter. The dashed lines on the left panel are those obtained by Lin (2007) for the Crab pulsar using the S3/S4 LIGO data assuming that the whole star is in the crystalline color superconducting phase. We determined the solid lines using the S5 LIGO data of Abbott *et al.* (2010). The parameter space appears to be extremely reduced and even more severe constraints can be obtained from the pulsar J2124-3358, which leads to the exclusion plots reported in the right panel of Fig. 19.

Unfortunately, the maximum deformation of a star depends as well on the breaking strain $\sigma_{\max}$, which measures the largest shear stress deformation sustainable by a rigid body before breaking. For standard neutron stars it is assumed that $10^{-5} \leq \sigma_{\max} \leq 10^{-2}$. The results shown on the left panel of Fig. 19 have been obtained with $\sigma_{\max} = 10^{-3}$ (upper dashed line) and $\sigma_{\max} = 10^{-2}$ (lower dashed line). The plots on the right panel are instead obtained assuming $\sigma_{\max} = 10^{-3}$ and considering three different values of $x = R_c/R$, where R_c is the CCSC core radius. For lower values of $\sigma_{\max}$ the various curves would move up. It is important to remark that there seems to be little motivation for assuming that the breaking strain of the CCSC phase be of the order discussed above, because the breaking mechanism (if it exists) of the crystalline pattern of CCSC matter is still unknown.

From Fig. 19 we infer that the S5 LIGO data give some hints about the properties of quark matter (under the assumption discussed above), because if it is present it should have a breaking strain $\sigma_{\max} \leq 10^{-3}$ and that if $\sigma_{\max} \sim 10^{-3}$, it is unlikely that the pulsar J2124-3358 is a crystalline quark star; although, it could still contain a small crystalline quark core. With Advanced LIGO and Virgo detectors the spin-down limit on gravitation waves (GW) emission from known CSOs will reach $\epsilon \approx 10^{-5}$, and objects with ellipticity of the order of 10^{-6} would be detectable up to the Galactic center (Palomba, 2012). These observation will put even more severe limitations the parameters of the crystalline phases and on the EOS of highly compressed matter.

Different constraints on the CCSC phase can be obtained from the study of r-mode oscillations, which, if not damped, would lead to a rapid slowdown of a spinning compact star by emission of gravitational waves (Andersson, 1998; Friedman and Morsink, 1998). The analysis of Rupak and Jaikumar (2012) shows that a quark star with a CCSC crust can provide sufficiently large damping for preventing the growth of these oscillations even for rapidly rotating CSOs.

B. Glitches

The rigidity of the crystalline phase may also be put in relation with the anomalies in the frequency of rotation of CSOs observed as pulsars (Alford, Bowers, and Rajagopal, 2001; Mannarelli, Rajagopal, and Sharma, 2007). Pulsars steadily spin down, because they lose rotational energy by emitting electromagnetic radiation, but occasionally the angular velocity at the crust of the star suddenly spins up in a dramatic event called a glitch. Pulsar glitches are rare events

first observed in the Vela pulsar (Radhakrishnan and Manchester, 1969; Reichley and Downs, 1969) and the Crab pulsar (Boynton *et al.*, 1969; Richards *et al.*, 1969) which manifest in a variety of sizes (Espinoza *et al.*, 2011), with an activity changing with time and peaking for pulsars with a characteristic age of about 10 kyr. Although a number of models have been proposed including two-fluid models (Baym *et al.*, 1969; Anderson and Itoh, 1975; Alpar, 1977) and "crust-quake" models (Ruderman, 1969; Baym and Pines, 1971) [for a review of early models see Ruderman (1972)], these phenomena still remain to be well understood, and their underlying mechanism is not yet completely clear.

The standard explanation of pulsar glitches (Anderson and Itoh, 1975; Alpar, 1977) requires the presence of two basic ingredients: a superfluid in some region of the star and a rigid structure that can pin the vortex lines without deforming when the vortices are under tension. The spinning superfluid is indeed threaded by superfluid vortex lines with quantized circulation and, as the crust of the spinning pulsar slowly loses angular momentum by radiation emission, the superfluid vortices tend to move toward the surface of the star to compensate the rotational energy bias. The reason is that the angular momentum of a superfluid is proportional to the density of vortices and therefore the only way in which a superfluid can reduce the rotational energy is by *vortex creep* toward the boundary of the superfluid region. But vortex lines are topological objects and if they are pinned to a rigid structure they cannot move outward and therefore the superfluid cannot spin down. Thus, as time passes, the frequency lag between the superfluid component of the star and the rest of the star increases. This state persists until the stress exerted by the pinned vortices on the rigid structure reaches a critical value, equal to the pinning force. Then, there is a sudden avalanche in which many vortices unpin from their original sites, move outward, in part reaching the superfluid boundary and in part repinning. Both processes reduce the angular momentum of the superfluid component, meaning that the rest of the star, including in particular the surface whose angular velocity is observed, speeds up.

The two above-mentioned basic ingredients are both present in the CCSC matter, indeed the crystalline phases are rigid as well as superfluid. Since the core of superfluid vortices consists of unpaired matter, it is reasonable to expect that the superfluid vortex lines will have lower free energy if they are centered along the intersections of the nodal planes of the underlying crystal structure, i.e., along lines along which the condensate vanishes even in the absence of a vortex. An estimate of the pinning force on vortices within CCSC quark matter (Mannarelli, Rajagopal, and Sharma, 2007) indicates that it is comparable to that on neutron superfluid vortices within a conventional neutron star crust (Alpar, Anderson, Pines, and Shaham, 1984; Alpar, Pines, Anderson, and Shaham, 1984). Although the basic requirements for explaining glitches are both present, several issues remain to be addressed and a great deal of theoretical work remains before the hypothesis that pulsar glitches originate within a CCSC core is developed fully enough to allow it to confront the observational data. The road map for achieving this goal includes the following: the explicit construction of a vortex line on the top of the crystalline pattern; the understanding of the pinning mechanism and the calculation of the corresponding pinning force; the investigation of the mechanism which allows angular momentum transfer between the CCSC core and the crust, presumably by means of the common electron fluid or by coupling through the magnetic field.

The same mechanism outlined above might work for a star with a CFL inner core and an outer core in the CCSC phase. In this case superfluid vortices lying in the CFL phase are pinned to the periodic structure of the CCSC phase.

C. Cooling and Urca processes

Neutron stars cool down by neutrino emission and photon emission, the latter dominating at late ages ($t \gtrsim 10^6$ yr). The cooling rate of a CSO may give information on its interior constitution, because different phases of hadronic matter cool down in a rather different way; see, e.g., Pethick (1992) for a brief review.

After a very short epoch, when the temperature of a compact star is of the order of $\sim 10^{11}$ K and neutrinos are trapped in the stellar core (Shapiro and Teukolsky, 1983; Prakash *et al.*, 2001; Steiner, Reddy, and Prakash, 2002; Ruester *et al.*, 2006b), the temperature drops and the mean free path of neutrinos becomes larger than the star radius. Then, the neutrinos emitted from any part of the neutron star are free to escape and the cooling is governed by the following differential equation:

$$\frac{dT}{dt} = -\frac{L_\nu + L_\gamma}{V_n c_V^n + V_q c_V^q} = -\frac{V_n \varepsilon_\nu^n + V_q \varepsilon_\nu^q + L_\gamma}{V_n c_V^n + V_q c_V^q}, \tag{206}$$

where T is the inner temperature at time t and L_ν and L_γ are, respectively, neutrino and photon luminosities, i.e., heat losses per unit time; with c_V^n and ε_ν^n (c_V^q and ε_ν^q) we denote the specific heat and the emissivity of nuclear matter (quark matter). Here it is assumed that the specific heats and emissivities do not depend on the local value of the density and thus the pertinent volumes of nuclear matter V_n and quark matter V_q factorize. In principle, for obtaining the heat loss one should integrate the density dependent quantities over the corresponding volume. In our simplified treatment we neglect this dependence, considering toy models of CSOs with a constant density. Although this approximation is rather rough, especially for nuclear matter, it serves to show the qualitative effect due to the presence of the crystalline phase. We assume, as well, a common inner temperature T, which is appropriate for sufficiently old compact stars (Lattimer *et al.*, 1994); see, e.g., Ho, Glampedakis, and Andersson (2012) for a recent discussion.

Since the mean free path of photons is very short, the luminosity by photon emission is a surface effect and can be estimated by the black-body expression

$$L_\gamma \simeq 4\pi R^2 \sigma T_s^4, \tag{207}$$

where R is the radius of the star, σ is the Stefan-Boltzmann constant, and the surface temperature is given by

$$T_s \simeq 0.87 \times 10^6 \left(\frac{g_s}{10^{14}\ \mathrm{cm/s^2}}\right)^{1/4} \left(\frac{T_b}{10^8\ \mathrm{K}}\right)^{0.55} \mathrm{K}, \quad (208)$$

(Gudmundsson, Pethick, and Epstein, 1982; Page *et al.*, 2004), where $T_b \simeq T$ is the temperature at the basis of the stellar envelope and $g_s = G_N M/R^2$ is the surface gravity. The above relation between T_s and T_b holds for CSOs with a standard crust. In the following we always assume that the matter at the basis of the envelope consists of nuclear matter with deconfined matter eventually present within the core of the star.

For the neutrino luminosity, one has to consider the relevant weak processes. When kinematically allowed, direct Urca processes are the most efficient cooling mechanism for a CSO in the early stage of its lifetime (Shapiro and Teukolsky, 1983). However, the neutrino emission via the (nuclear) direct Urca processes $n \to p + e + \bar{\nu}_e$ and $e^- + p \to n + \nu_e$ is only allowed for certain EOS (Lattimer *et al.*, 1991) having a sufficiently large proton abundance to guarantee energy-momentum conservation (Chiu and Salpeter, 1964; Bahcall and Wolf, 1965). Therefore, considering nuclear matter, only modified Urca processes are in general considered, where a bystander particle allows energy-momentum conservation. The resulting cooling is less rapid and the emissivity turns out to be

$$\varepsilon_\nu^{\mathrm{n}} = (1.2 \times 10^4\ \mathrm{erg\,cm^{-3}\ s^{-1}}) \left(\frac{n}{n_0}\right)^{2/3} \left(\frac{T}{10^7\ \mathrm{K}}\right)^8, \quad (209)$$

much smaller than the emission rate $\varepsilon_\nu^n \sim T^6$ due to direct Urca processes (Shapiro and Teukolsky, 1983). Here n is the number density and $n_0 = 0.16\ \mathrm{fm}^{-3}$ is the nuclear equilibrium density.

These considerations apply to stars containing standard nuclear matter; faster cooling can be determined by the presence of a pion condensate (Bahcall and Wolf, 1965; Maxwell *et al.*, 1977; Muto and Tatsumi, 1988) or a kaon condensate (Brown *et al.*, 1988). If the central region of the star consists of deconfined quark matter direct Urca processes involving quarks, i.e., the processes $d \to u + e^- + \bar{\nu}_e$ and $u + e^- \to d + \nu_e$ may take place and largely contribute to the cooling rate. It has been shown by Iwamoto (1980, 1981, 1982) that quark direct Urca processes are kinematically allowed and the corresponding emission rate for massless quarks is of the order $\alpha_s T^6$, where α_s is the strong coupling constant. This result is valid if quark matter is a normal Fermi liquid, but in the CSC phase the expression above is not correct because quarks form Cooper pairs and fermionic excitations are gapped. If the color superconductor is cold (i.e., $T \ll T_c$) and homogeneous (i.e., the quasiparticle gap Δ does not depend on the spatial coordinate), the corresponding neutrino emissivity and specific heat are suppressed by a factor $e^{-\Delta/T}$. This suppression is particularly strong in the CFL phase, because Δ is large and all quarks are paired.

However, the ground state of quark matter in realistic conditions might not be the CFL phase, but a phase with a less symmetric pairing pattern. In this case not all quarks form Cooper pairs, with unpaired quarks giving the leading contribution to the neutrino emissivity. It is also possible that the temperature of the CSO is close to T_c, in that case the emissivity of quark matter is not exponentially suppressed (Jaikumar, Roberts, and Sedrakian, 2006). In the following we evaluate the contribution of the CCSC phase to the neutrino emissivity and specific heat showing how the cooling curve is modified.

1. Neutrino emissivity

The transition rate for the β decay of a down quark d_α, of color $\alpha = r, g, b$, into an up quark u_α

$$d_\alpha(p_1) \to \bar{\nu}_e(p_2) + u_\alpha(p_3) + e^-(p_4), \quad (210)$$

is

$$W_{\mathrm{fi}} = V(2\pi)^4 \delta^4(p_1 - p_2 - p_3 - p_4) |\mathcal{M}|^2 \prod_{i=1}^4 \frac{1}{2E_i V}, \quad (211)$$

where V is the available volume and $\mathcal{M}$ is the invariant amplitude. Neglecting quark masses the squared invariant amplitude averaged over the initial spins and summed over spins in the final state is

$$|\mathcal{M}|^2 = 64 G_F^2 \cos^2\theta_c (p_1 \cdot p_2)(p_3 \cdot p_4), \quad (212)$$

where G_F is the Fermi constant and θ_c is the Cabibbo angle; we neglect the strange-quark β decay whose contribution is smaller by a factor of $\tan^2\theta_c$. Since for relatively aging stars there is no neutrino trapping, the neutrino momentum and energy are both of the order T. The magnitude of the other momenta is of the order of the corresponding Fermi momenta $p_1 \sim p_F^1 \sim \mu$, $p_3 \sim p_F^3 \sim \mu$ and $p_4 \sim p_F^4 \sim \mu_e$, which is smaller, but still sizable (see the discussion in Sec. III). It follows that the momentum conservation can be implemented neglecting $\boldsymbol{p}_2$ and one can depict the three-momentum conservation for the decay (210) as a triangle (Iwamoto, 1980, 1981, 1982) having for sides $\boldsymbol{p}_1, \boldsymbol{p}_3$ and $\boldsymbol{p}_4$. It follows that we can approximate

$$(p_1 \cdot p_2)(p_3 \cdot p_4) \simeq E_1 E_2 E_3 E_4 (1 - \cos\theta_{12})(1 - \cos\theta_{34}), \quad (213)$$

where E_j are the energies and θ_{12} (θ_{34}) is the angle between momenta of the down quark and the neutrino (between the up quark and the electron).

In the CSC phase one has to take into account that the neutrino emissivity

$$\begin{aligned}\varepsilon_\nu^{\mathrm{q}} &= \sum_{\alpha=r,g,b} \varepsilon_\nu^\alpha \\ &= \sum_{\alpha=r,g,b} \frac{2}{V} \left[\prod_{i=1}^4 \int \frac{d^3 p_i}{(2\pi)^3}\right] E_2 W_{\mathrm{fi}} n(\boldsymbol{p}_1)[1 - n(\boldsymbol{p}_3)] \\ &\quad \times [1 - n(\boldsymbol{p}_4)] B_{d_\alpha}^2(\boldsymbol{p}_1) B_{u_\alpha}^2(\boldsymbol{p}_3) \end{aligned} \quad (214)$$

depends on the Bogolyubov coefficients B_{u_α} and B_{d_α} which are functions of the quasiparticle dispersion laws (Alford,

Jotwani *et al.*, 2005). In Eq. (214) the quark thermal equilibrium Fermi distributions

$$n(\boldsymbol{p}_j) = (1 + e^{[E_j(\boldsymbol{p}_j)-\mu_j]/T})^{-1} \tag{215}$$

appear because strong and electromagnetic processes establish thermal equilibrium much faster than weak interactions. The overall factor of 2 in Eq. (214) takes into account the electron capture process.

The cooling of the CCSC matter with condensate (156) was studied by Anglani *et al.* (2006), and in this case the largest contribution to the emissivity stems from the phase space region around the quark gapless modes, while the relevant momentum for the electron is its Fermi momentum, thus we have that

$$\int d^3p_1 \int d^3p_3 \int d^3p_4 \approx \int \mu_e^2 dp_4 d\Omega_4 P_1^2 dp_1 d\Omega_1 P_3^2 dp_3 d\Omega_3, \tag{216}$$

with $d\Omega_j = \sin\vartheta_j d\vartheta_j d\phi_j$ and P_1 (P_3) is the quark down (quark up) momentum where the corresponding quasiparticle energy vanishes. The gapless momenta P_1 and P_3 depend on the angle ϑ_j that quark momenta form with the pair momentum $\boldsymbol{q}$. The integral expression in Eq. (214) can be simplified expanding around the gapless modes $E_j(p) \simeq \mu_j + v_j(p - P_j)$ (for $j = 1$ and 3), with the quasiparticle velocity given by

$$v_j = \left.\frac{\partial E_j}{\partial p}\right|_{p=P_j}. \tag{217}$$

In the three-flavor case the dispersion law of each quasiparticle has from one to three gapless modes, thus one has to expand the corresponding dispersion laws around each gapless momentum.

Using the above approximations the neutrino emissivity for each pair of gapless momenta P_1, P_3, can be written as

$$\varepsilon_\nu^\alpha \simeq \frac{G_F^2 \cos^2\theta_c \mu_e^2 T^6}{32\pi^8} \mathcal{I} \prod_{j=1}^{4} \int d\Omega_j \frac{P_1^2 P_3^2 B_{d_\alpha}^2(P_1) B_{u_\alpha}^2(P_3)}{|v_1||v_3|} \times \delta^{(3)}(\boldsymbol{p}_1 - \boldsymbol{p}_3 - \boldsymbol{p}_4 - \boldsymbol{q})(1 - \cos\theta_{12})(1 - \cos\theta_{34}), \tag{218}$$

where $\mathcal{I} = 457\pi^6/5040$. Some of the angular integrations appearing in Eq. (218) can be performed analytically [see Anglani *et al.* (2006) for more details], and the numerical computation can be reduced observing that, even if each quasiparticle dispersion law is characterized by various gapless momenta, not all of them satisfy the conservation of momentum $\boldsymbol{p}_1 - \boldsymbol{p}_3 - \boldsymbol{p}_4 - \boldsymbol{q} = 0$.

From Eq. (218) one can deduce that the largest contribution to the emissivity is due to blue quarks, that is, to the process in Eq. (210) with $\alpha = b$. The reason is that according to the Ginzburg-Landau analysis of Casalbuoni, Gatto, Ippolito *et al.*, (2005), the gap parameter Δ_1 vanishes and therefore the down blue quark is ungapped [see the discussion after Eq. (133)]. Quarks of different flavor or color are instead gapped; neglecting $\mathcal{O}(1/\mu)$ corrections (see Sec. III.B.5) one has $\Delta_2 = \Delta_3 = \Delta$. The dispersion of down blue quarks is $E_1(p) = p$, with gapless momentum $P_1 \simeq \mu$ independent of ϑ_1, mixing coefficient $B_{d_b}(P_1) = 1$, and $v_1 = 1$. The up blue quark is instead paired and has two gapless momenta depending on ϑ_3; see Anglani *et al.* (2006) for an explicit expression. Of these two gapless momenta one satisfies the momentum conservation and thus the decay of a down blue quark in an up blue quark is not suppressed with respect to the analogous decay in unpaired quark matter, giving the leading contribution to the emissivity. The contributions of quarks with red and green colors can be treated in a similar way, but for these colors neither the down nor the up quarks are unpaired and the corresponding processes are thus suppressed. The sum of the contributions of all quarks turns out to be

$$\varepsilon_\nu \approx 4.3 \times 10^{13} \left(\frac{T}{10^7\ \mathrm{K}}\right)^6 \mathrm{erg\,cm^{-3}s^{-1}}, \tag{219}$$

and is comparable with the emissivity of unpaired quark matter; see, e.g., Iwamoto (1982).

2. Specific heats

As discussed in Sec. II.D for the two-flavor case, at low temperature the largest contribution to the specific heat is determined by the fermionic quasiparticles. The specific heat of the three-flavor crystalline phase is given by the same formal expression given in Eq. (73), but with the quasiparticle dispersion laws of the three-flavor CCSC phase. The computation can be simplified following the same reasoning used above: the contributions of gapped modes are exponentially suppressed and each gapless mode contributes by a factor $\propto T$. This result follows from the evaluation of the integral in Eq. (73); employing the saddle point method and assuming that the quasiparticle dispersion laws are linear close the gapless momenta. Then the angular integral can also be simplified because the dispersion laws are gapless only in a restricted angular region. The numerical analysis confirms the above results; see Anglani *et al.* (2006) for a discussion and an expression of the specific heat.

For unpaired nuclear matter and unpaired quark matter the contribution of each fermionic species can be given by the fermionic ideal gas result

$$c_V = \frac{T}{3} P^F \sqrt{m^2c^2 + (P^F)^2}, \tag{220}$$

where m and P^F are the appropriate fermionic mass and Fermi momentum, respectively. For unpaired nuclear matter, the three species are neutrons, protons, and electrons with Fermi momenta evaluated as in neutral matter in weak equilibrium (Shapiro and Teukolsky, 1983)

$$P_n^F \simeq (340\ \mathrm{MeV})\left(\frac{n}{n_0}\right)^{1/3}, \qquad P_p^F = P_e^f \simeq (60\ \mathrm{MeV})\left(\frac{n}{n_0}\right)^{2/3}. \tag{221}$$

For unpaired quarks, considering electric neutrality and weak equilibrium, the nine quark species have Fermi momenta independent of color given by $P_d^F = \mu + M_s^2/12\mu$, $P_u^F = \mu - M_s^2/6\mu$ and $P_s^F = \mu - 5M_s^2/12\mu$; see the discussion in Sec. III.

3. Cooling by neutrino emission

For evaluating the effect on the compact star cooling of the CCSC phase we consider three different toy models comprising neutral and β equilibrated matter (Anglani *et al.*, 2006). Model I is a star consisting of unpaired "nuclear" matter (neutrons, protons, and electrons) with mass $M = 1.4M_\odot$ (where $M_\odot$ is the solar mass), radius $R = 12$ km, and uniform number density $n = 1.5n_0$. Model II is a star containing a core of radius $R_c = 5$ km of unpaired quark matter with $\mu = 500$ MeV, with an outer part of unpaired nuclear matter with uniform density n. Assuming a star mass $M = 1.4M_\odot$ from the solution of the Tolman-Oppenheimer-Volkov (TOV) equations (Oppenheimer and Volkoff, 1939; Tolman, 1939) one gets a star radius $R = 10$ km. Model III is a compact star containing a core of electric and color neutral three-flavor quark matter in the CCSC phase with gap parameter given in Eq. (156), with $\Delta \simeq 6$ MeV, $\mu = 500$ MeV, and $M_s^2/\mu = 140$ MeV. The outer part of the star is made of unpaired nuclear matter. Since the value of the gap parameter in the model III is small, the radius of the CSO and the quark core do not differ appreciably from those of a star with a core of unpaired quark matter, i.e., $R_c = 5$ km and $R = 10$ km (also in these cases $M = 1.4M_\odot$).

In Fig. 20 the cooling curves of the surface temperature are shown as a function of time for the various star models. For unpaired quark matter the coupling $\alpha_s \simeq 1$ is used, corresponding to $\mu = 500$ MeV and $\Lambda_{\rm QCD} = 250$ MeV. The use of perturbative QCD at such small momentum scales is, however, questionable. Therefore the results for model II should be considered with some caution and the curve is plotted only to allow a comparison with the other models. The similarity between the dashed curve and the dotted curve follows from the fact that in the CCSC phase the quasiparticle dispersion laws are linear and gapless, so that the scaling laws $c_V \sim T$ and $\varepsilon_\nu \sim T^6$ are analogous to those of the unpaired quark matter. Thus, the two models cannot easily be distinguished. From this figure we can see that stars with a CCSC core (or an unpaired quark core) cool down faster than ordinary neutron stars. In particular, for $10^3 < t < 10^6$ yr the cooling is dominated by the neutrino emission and one has that for model I, $T \sim t^{-1/6}$, while $T \sim t^{-1/4}$ for models II and III. At later times photon emission dominates and the three cooling curves move closer.

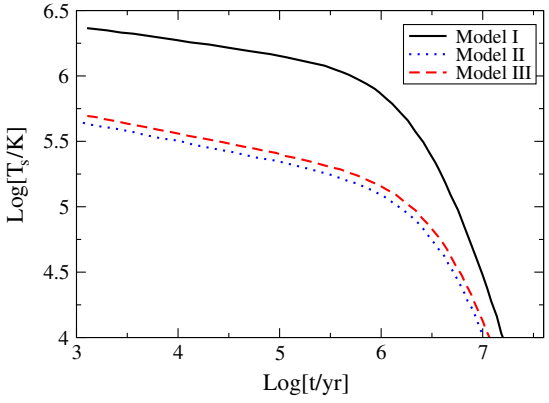

FIG. 20 (color online). Surface temperature, in Kelvin, as a function of time, in years, for various models of compact stars (Anglani *et al.*, 2006). Model I is a neutron star of nuclear matter with uniform density $n = 0.24$ fm^{-3} and radius $R = 12$ km; model II corresponds to a star with $R = 10$ km, having an outer part of nuclear matter and a core of radius $R_c = 5$ km of unpaired quark matter; model III is like model II, but in the core there is quark matter in a crystalline phase, see the text for more details. For all stars $M = 1.4M_\odot$ and the temperature at $t = 1$ yr was set to $T = 10^9$ K. Parameters for the core are $\mu = 500$ MeV and $M_s^2/\mu = 140$ MeV. Adapted from Anglani *et al.*, 2006.

Similar results, with a more refined analysis, have been obtained by Hess and Sedrakian (2011), where a more realistic EOS is used to model compact stars with different masses. Their results are reported in Fig. 21. The models considered have an envelope of standard nuclear matter, cooling by the modified Urca process and neutral current bremsstrahlung processes, and a core of quark matter comprising a two-flavor inhomogeneous phase, cooling by the direct Urca process. The solid curve corresponds to standard nuclear matter; the other curves correspond to hybrid stars with a quark core of different radii. In order to reproduce, with a hybrid model, the measured surface temperatures of compact stars, the BCS-like pairing between u and d blue quarks has to be included, with a pairing gap Δ_b of the order of 0.1 MeV. In this case models with a quark core radius $R_c \lesssim 1$ km seem to be in good agreement with part of the observational data.

All these results have interesting phenomenological consequences because observational measurements on the cooling of compact stars are being accumulated at an increasing rate. Some data indicate that stars with an age in the range 10^3–10^4 years have a temperature significantly smaller than expected on the basis of the modified Urca processes; see Fig. 21. It is difficult, however, to infer, from these data, predictions on the star composition, as theses stars may have different masses. But, quite recently, the thermal evolution of the neutron star in Cassiopeia A (Heinke and Ho, 2010; Shternin *et al.*, 2011), corresponding to the + sign in Fig. 21, has been observed [note that we do not report in Fig. 21 the detailed observational data of Heinke and Ho (2010) and Shternin *et al.* (2011)] and explained as an effect of neutron superfluidity (Page *et al.*, 2004, 2011; Shternin *et al.*, 2011). From Fig. 21 we see that models with a LOFF-like two-flavor pairing seem to fail to reproduce the initial observed values of age-temperature of this compact star. However, it has been recently shown that the rapid cooling of Cassiopeia A might be explained as a phase transition from a gapped to a gapless (possibly crystalline) phase in a two-flavor CSC (Sedrakian, 2013). The caveat is that the considered CSO should have a mass $\simeq 2M_\odot$. It would be interesting to check whether the observed behavior can be reproduced with the thermodynamically favored CCSC phase, for which, however, the identification of the quasiparticle dispersion laws is still lacking.

The rapid cooling of neutron superfluids determined in Page *et al.* (2004, 2011) and Shternin *et al.* (2011) is due to the difermion pair-breaking effect, which enhances the emissivity

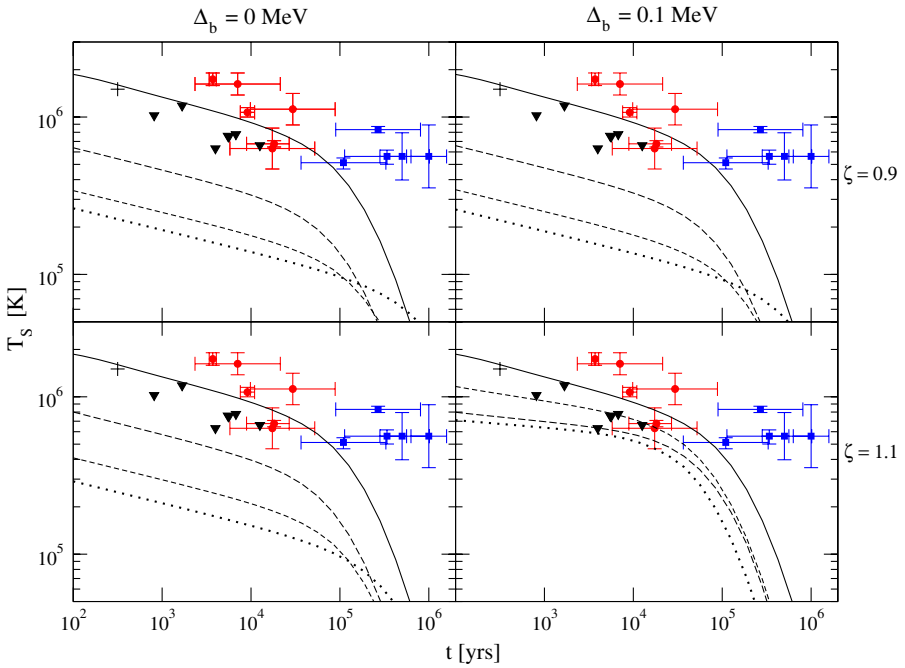

FIG. 21 (color online). Surface temperature, in Kelvin, as a function of time, in years, for various models of compact stars comprising a two-flavor LOFF phase between u and d red and green quarks, with gap parameter Δ, and pairing between u and d blue quarks, with gap parameter Δ_b. Various values of the central density ρ_c of $\zeta = \Delta/\delta\mu$ and Δ_b are considered. The solid curve refers to a model with no quark matter, central density $5.1\rho_{14}$, where $\rho_{14} = 10^{14}$ g cm^{-3}, corresponding to a star with $M \simeq 0.54 M_\odot$. The long dashed curve corresponds to a model with $\rho_c = 10.8\rho_{14}$, $M \simeq 1.91 M_\odot$, and a quark core with radius $R_c \simeq 0.68$ km. The short dashed curve corresponds to a model with $\rho_c = 11.8\rho_{14}$, $M \simeq 1.93 M_\odot$, and $R_c \simeq 3.41$ km. The dotted curve corresponds to a model with $\rho_c = 21.0\rho_{14}$, $M \simeq 2.05 M_\odot$, and $R_c \simeq 6.77$ km. The symbols correspond to the observational data points [see Hess and Sedrakian (2011) for an explanation]; here we only remark that the + sign on the top left corner corresponds to Cassiopeia A (Heinke and Ho, 2010; Shternin *et al.*, 2011). From Hess and Sedrakian, 2011.

of nuclear matter. The presence of CCSC matter has a very similar effect. Indeed, the fast cooling of relatively young compact stars with a CCSC core should be a consequence of the scaling laws for neutrino emissivity and specific heat, which in turn strongly depend on the existence of gapless points (Anglani *et al.*, 2006; Hess and Sedrakian, 2011), present at the edge of the pairing regions in momentum space. Since this property is typical of any CCSC phase, independently of detailed form of the condensate, when a CCSC core nucleates inside a compact star it should be followed by a rapid cooling, pretty much as the formation of a neutron superfluid determines the rapid cooling of a young neutron star.

Although the above-reported analysis is not conclusive, because a detailed treatment of the thermodynamically favored CCSC phase is still missing, some qualitative assessments can be made from the obtained results. Slow cooling is typical of stars containing only nonsuperfluid standard nuclear matter or of stars with a uniform CSC phase (like CFL); the observed cooling rate of the neutron star in Cassiopeia A (Heinke and Ho, 2010; Shternin *et al.*, 2011) seems to disfavor both possibilities, leaving superfluid nuclear matter and CCSC matter as candidate phases. The latter possibility is compatible with the result that for intermediate densities the quark normal state and the CFL phase are less favored than the CCSC phase in a certain range of values of the quark chemical potential.

Note that the results reported above do not properly take into account the heat transport inside the compact star. It would be interesting to include in the analysis the various transport mechanisms to have detailed simulations of the CSO cooling; see, e.g., Ho, Glampedakis, and Andersson (2012).

D. Mass-radius relation

Since any phase transition leads to a softening of the EOS (Lattimer and Prakash, 2001; Haensel, 2003), at one time it was thought that hybrid stars (having a quark matter core and an envelope of baryonic matter) should have mass $M \lesssim 1.7 M_\odot$; see, e.g., Alford and Reddy (2003), Buballa *et al.* (2004), and Maieron *et al.* (2004). For CSOs with larger masses, the deconfinement phase transition from baryonic to quark matter would reduce the central pressure to the point of instability toward black hole formation, unless some repulsive interaction between quarks prevents the collapse.

Some evidence for massive neutron stars with $M \sim 2M_\odot$ has been inferred from various astronomical observations: a compact star may exist in the LMXB (low mass x-ray binary) 4U 1636-536 with $(2.0 \pm 0.1) M_\odot$ (Barret, Olive, and Miller, 2005). A measurement on the pulsar PSR B1516+02B in the Globular Cluster M5 gave $M = (2.08 \pm 0.19) M_\odot$ (Freire *et al.*, 2008). The millisecond pulsar J1614-2230 has a mass $(1.97 \pm 0.04) M_\odot$ accurately measured by Shapiro delay

(Demorest *et al.*, 2010). Although these observations seem to disfavor the presence of quark matter (Logoteta *et al.*, 2012), the details of a stability analysis depend on the theoretical model employed for the description of the hadronic phase, deconfinement, and the CSC matter. We show below that in the presence of the crystalline phase large masses can indeed be reached (Ippolito *et al.*, 2008). The drawback, as we see, is that if $M \simeq 2M_\odot$ CSOs have a CCSC core, then ordinary $M \simeq 1.4M_\odot$ CSOs are unlikely to have a CCSC core.

Since a first principles calculation of the high-density EOS is not feasible, the description of quark matter relies on several different models including the MIT bag model, the NJL model, and the chromodielectric model. The results obtained within these three models may differ in a sizable way, and do as well depend on the detailed form of the model considered. Recent phenomenological studies of hybrid stars based on the MIT bag model were carried out using a generic parametrization of the quark matter EOS in Alford, Braby *et al.* (2005) and it was shown that hybrid stars may actually "masquerade" as neutron stars. Alford, Braby *et al.* (2005) parametrized nonperturbative QCD corrections to the EOS of the Fermi gas in a rather general way, considering a Taylor expansion of the pressure in terms of μ^2; for a different approach see Fraga, Pisarski, and Schaffner-Bielich (2001). Taking into account these corrections, stable hybrid stars containing CFL quark matter may exist with maximum mass of about $2M_\odot$.

Various studies of very massive hybrid stars within the three-flavor NJL model displayed a general instability toward collapse into a black hole (Buballa *et al.*, 2004). Stable stars featuring the 2SC phase were obtained with typical maximum masses $M \sim 1.7M_\odot$ assuming reasonable values of the constituent quark masses (Shovkovy, Hanauske, and Huang, 2003) or by replacing the hard NJL cutoffs by soft form factors with parameters fitted to a certain set of data (Grigorian, Blaschke, and Aguilera, 2004; Blaschke *et al.*, 2007). Heavier objects can be obtained if a repulsive vector interaction is introduced in the NJL Lagrangian (Klahn *et al.*, 2007; Bonanno and Sedrakian, 2012; Orsaria *et al.*, 2013), which makes the EOS stiffer, but at the same time, reducing the amount of deconfined quark matter in the core of the star, or with no pure quark matter at all (Orsaria *et al.*, 2013), i.e., with a core comprising a mixed phase of quarks and hadrons.

Another source of uncertainty comes from the nuclear EOS at high densities, which can be constructed starting from a number of different principles (Weber, 1999; Sedrakian, 2007) and a large number of EOS have been proposed for hybrid star configurations. In the analysis of the considered EOS, presented below only the stiffest were found to be admissible for phase equilibrium between nuclear and CCSC matter.

The inclusion of hyperonic matter in the EOS of compact stars although reasonable is certainly troublesome, because the nucleon-hyperon and hyperon-hyperon interactions are not well known, even though some progress has been done mainly by lattice simulations (Aoki *et al.*, 2012). Hyperons would certainly soften the EOS (Glendenning and Kettner, 2000), making the comparison with the observed $2M_\odot$ of some CSOs problematic (Lattimer and Prakash, 2007).

1. Matching the equation of state

The self-consistent computation of the strange quark mass given in Ippolito, Nardulli, and Ruggieri (2007) allows the evaluation of pressure as a function of the quark chemical potential μ. Thus, varying the quark chemical potential, the phase equilibrium between the confined and the CSC phase can be constructed.

A possible normalization of the quark pressure in the NJL model is obtained by requiring that the pressure vanishes at zero density and temperature (Buballa and Oertel, 1999; Sandin and Blaschke, 2007). In the terminology of the MIT bag model, this is equivalent to a subtraction of the bag constant from the thermodynamic potential (Alford, Braby *et al.*, 2005). Since the value of the bag constant is related to confinement, which is absent in the NJL model, it appears reasonable changing its value, and hence the normalization of the pressure. The simplest option is to consider the case of a constant shift in the asymptotic value of the pressure; an alternative is the use of form factors for the bag constant (Grigorian, Blaschke, and Aguilera, 2004).

Regarding the matching between the nuclear and quark matter EOS, it can be performed in the *strong coupling* limit, corresponding to $G_D/G_S = 1$ (Ruester *et al.*, 2005; Sandin and Blaschke, 2007) [see Eq. (15) and the discussion after Eq. (29)]. The transition from the confined phase to quark matter happens at the baryonic chemical potential at which the pressures of the two phases are equal, meaning that the chemical potential curves $P(\mu)$ for these phases cross. At intermediate coupling and weak coupling, corresponding, respectively, to $G_D/G_S \sim 0.75$ and $G_D/G_S \lesssim 0.7$, the $P(\mu)$ curves for nuclear and quark matter do not cross; the models are thus incompatible, meaning that they cannot describe the desired transition between nuclear and quark matter.

In the following we discuss two simple models of CSOs (Ippolito *et al.*, 2008). In the first model, hereafter named nuclear, we consider standard nuclear matter described by the Dirac-Brueckner-Hartree-Fock theory. The selected EOS is the hardest one in the collection of Weber (1999) and Weber, Negreiros, and Rosenfield (2007). The second model, hereafter model A, has the same low-density EOS of nuclear matched at an interface via the Maxwell construction to the high-density EOS of CCSC matter. In order to achieve this matching the zero density pressure is shifted by an amount $\delta p = 10\ \mathrm{MeV/fm^3}$. This is equivalent to a variation of the bag constant. Another possibility is to set $\delta p = 0$, but varying the value of the constituent masses of the light quarks in the fit of the parameters of the NJL model; for small values of the light quark masses the matching between quark and nuclear equations of state is facilitated (Buballa *et al.*, 2004).

Note that because of the Maxwell construction of the deconfinement phase transition, there is a jump in the density at constant pressure as illustrated in the left panel of Fig. 22.

2. Results for nonrotating configurations

Given the EOS, the spherically symmetric solutions of Einstein's equations for nonrotating self-gravitating fluids are obtained by the TOV equations. For simplicity we only discuss the two nonrotating configurations corresponding to the Model A and nuclear; see Ippolito *et al.* (2008) for different

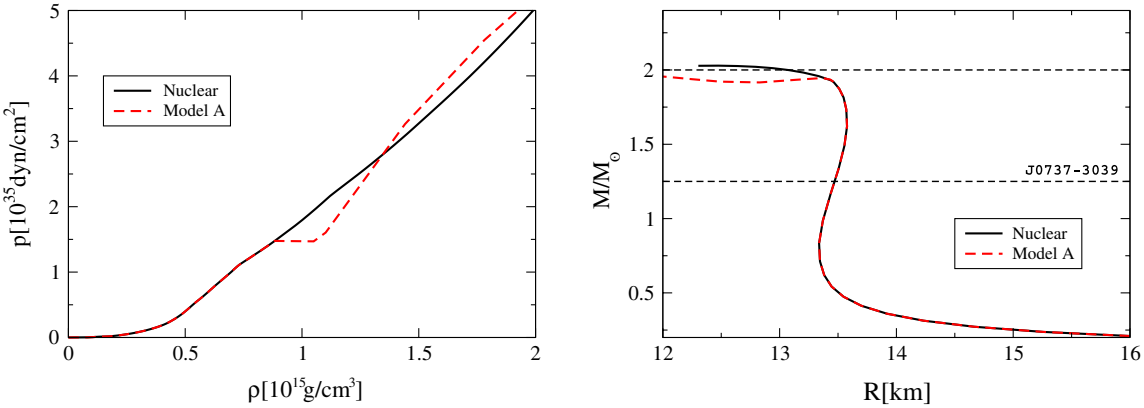

FIG. 22 (color online). Left panel: Pressure vs matter density for the two considered models. The solid black line labeled nuclear refers to the EOS based on the Dirac-Brueckner-Hartree-Fock approach (Weber, 1999; Weber, Negreiros, and Rosenfield, 2007). The dashed line corresponds to model A. The EOS of model A has the low-density EOS corresponding to nuclear and the high-density EOS obtained by a NJL model describing CCSC matter. At the deconfinement phase transition there is a jump in the density at constant pressure. Right panel: Mass-radius diagram for nonrotating configurations. The dashed lines correspond to the lower pulsar mass bound from J0737-3039 and the $2M_\odot$ upper bound from various astronomical observations.

models including rotation. A generic feature of the TOV solutions is the existence of a maximum mass for any EOS; as the central density is increased beyond the value corresponding to the maximum mass, the star becomes unstable toward collapse to a black hole. One criterion for the stability of a sequence of configurations is the requirement that $dM/d\rho_c > 0$, meaning that the mass of the star should be an increasing function of the central density. At the point of instability the fundamental (pulsation) modes become unstable. If stability is regained at higher central densities, the modes by which the stars become unstable toward the eventual collapse belong to higher-order harmonics.

The right panel of Fig. 22 shows that for configurations constructed from the nuclear EOS, the stable sequence extends up to a maximum mass of the order $2M_\odot$; the value of the maximum mass is large, since the chosen EOS is stiff. The hybrid configurations branch off from the nuclear configurations when the central density reaches that of the deconfinement phase transition. We also report the astronomical bounds on the masses of CSOs (horizontal dashed lines). The upper bound corresponds to $M = 2M_\odot$, while the lower bound to a mass of about $(1.249 \pm 0.001)M_\odot$ inferred from the millisecond binary J0737-3039 (Lyne *et al.*, 2004). Note that both the hybrid stars and their nuclear counterparts have masses and radii within these bounds. However, the hybrid configurations are more compact than their nuclear counterparts, i.e., they have smaller radii. Contrary to the case of self-bound quark stars (Alcock, Farhi, and Olinto, 1986), whose radii could be much smaller than the radii of purely nuclear stars, the differences between the radii of hybrid and nuclear stars are small and cannot be used to distinguish these two classes by means of current astronomical observations. A remarkable result is that although the hybrid model A is roughly consistent with the bound of $M \sim 2M_\odot$, it should be noted that canonical $1.4M_\odot$ CSOs will be purely nuclear if they are described by this model. According to the presented analysis when the CCSC matter appears the star first gets unstable and then it becomes stable only at higher values of the central density [corresponding to the so-called third family compact stars (Gerlach, 1968; Glendenning and Kettner, 2000; Schertler *et al.*, 2000)]. Moreover, only sufficiently massive CSOs, with mass $M \gtrsim 1.8M_\odot$, can contain a fraction of quark matter. Different hybrid EOS constructed in a similar way lead to analogous results (Ippolito *et al.*, 2008).

V. CONCLUSION

The investigation of the properties of matter in extreme conditions is one of the most fascinating and challenging frontiers in high-energy physics. The aim is to understand the fundamental properties of matter when the relevant degrees of freedom are deconfined quarks and gluons. According to QCD, cold and dense matter at asymptotic densities should be in the color superconducting (CSC) phase, with quarks forming Cooper pairs.

Ongoing research in cold and dense quark matter is now confronting astrophysical data, allowing us to exclude some CSC models and/or to restrict the parameter space of some phases. The most important consideration for a comparison with the astrophysical data is certainly that the conditions realized in compact stellar objects may determine a mismatch between the Fermi momenta of quarks, disfavoring the homogeneous CSC phases, and favoring less symmetric diquark pairing.

In this review, we focused on the inhomogeneous CSC phases, chiefly on the crystalline color superconducting (CCSC) phase. This phase might be the CSC phase realized in the core of compact stars, if deconfined quark matter is present, because it allows pairing between quarks on mismatched Fermi surfaces.

First proposed in the two-flavor case by Alford, Bowers, and Rajagopal (2001), the CCSC phase has been studied by many for both two- and three-flavor quark matter. We reported on the various results obtained showing that nowadays it is a well-developed subject with several open problems and fascinating applications to compact star astrophysics. In this

respect, this phase of matter has very appealing features, residing in its extraordinary properties. The CCSC is characterized by a periodic modulation of the condensate which is extremely resistant to deformations. Thus, compact stars featuring CCSC matter may sustain large "mountains," meaning that spinning compact stars might be strong sources of gravitational waves. Moreover, since the three-flavor CCSC phase is also superfluid, when rotating it will develop quantized vortices which might be pinned to the periodic condensate, thus it satisfies the basic requirements for explaining stellar glitches. Finally, we also discussed how the presence of CCSC matter might influence the mass-radius relation and the cooling curve of a compact star, although in this case the presence of a crystalline modulation appears to be less relevant.

Whether the CCSC phase will stand the test of the increasing observational data on compact stellar objects it is still unclear. It seems to us that among the astrophysical data, probably those on stellar glitches and those provided by the next-generation gravitational wave detectors might give the most stringent constraints on the CCSC matter. However, to properly confront the astrophysical data, we still need to understand several fundamental properties of the CCSC phase. Among the open issues, we remark that the individuation of the favored crystalline structure does so far rely on a Ginzburg-Landau (GL) expansion. Although the GL analysis does certainly give useful qualitative information on the favored periodic modulations, the resulting gap parameter and free energy are under poor quantitative control. Moreover, in order to study stellar glitches, an understanding of superfluid vortices in CCSC matter has to be developed. So far only an order of magnitude estimate of the pinning force has been obtained, which is not enough for a full description of the vortex dynamics and the associated stellar spinning evolution.

LIST OF SYMBOLS AND ABBREVIATIONS

For clarity we report below a list of the review's most used acronyms and symbols.

bcc:	Body-centered cube
BCS:	Bardeen-Cooper-Schrieffer
BEC:	Bose-Einstein condensate
CCSC:	Crystalline color superconducting
CFL:	Color-flavor locked
CC:	Chandrasekhar-Clogston
CSC:	Color superconducting
CSO:	Compact stellar object
EOS:	Equation of state
fcc:	Face-centered cube
FF:	Fulde-Ferrell
GL:	Ginzburg-Landau
GW:	Gravitational waves
HDET:	High-density effective theory
LO:	Larkin-Ochinnikov
LOFF:	Larkin-Ochinnikov-Fulde-Ferrell
NGB:	Nambu-Goldstone boson
NJL:	Nambu-Jona–Lasinio
QCD:	Quantum chromodynamics
QGP:	Quark-gluon plasma
TOV:	Tolman-Opennheimer-Volkoff
2SC:	Two-flavor color superconducting
gCFL:	Gapless color-flavor locked
g2SC:	Gapless two-flavor color superconducting
a, b:	Adjoint color indices
i, j, k:	Flavor indices
s, t:	Spin indices
G_D:	Quark-quark coupling constant
G_S:	Quark-antiquark coupling constant
P^F:	Fermi momentum
M_s:	Constituent strange quark mass
$M_\odot$:	Solar mass
α, β, γ:	Fundamental color indices
$\delta\mu$:	Chemical potential difference
$\epsilon_{i,j,k}$:	Levi-Civita symbol in flavor space
$\varepsilon^{\alpha\beta\gamma}$:	Levi-Civita symbol in color space
μ:	Quark chemical potential
μ_e:	Electron chemical potential
Δ:	Pairing gap
Ω:	Free energy

ACKNOWLEDGMENTS

The review has benefitted from long-standing and insightful discussion with Giuseppe Nardulli. We thank M. G. Alford, K. Fukushima, A. Sedrakian, and R. Sharma for useful suggestions. We thank A. Sedrakian for providing us with the data points reported in Fig. 22.

REFERENCES

Abbott, B., *et al.* (LIGO Scientific Collaboration), 2007, Phys. Rev. D **76**, 042001.
Abbott, B., *et al.* (LIGO Scientific Collaboration), 2008, Astrophys. J. **683**, L45.
Abbott, B., *et al.* (Virgo Collaboration), 2010, Astrophys. J. **713**, 671.
Abuki, H., 2003, Prog. Theor. Phys. **110**, 937.
Abuki, H., D. Ishibashi, and K. Suzuki, 2012, Phys. Rev. D **85**, 074002.
Abuki, H., and T. Kunihiro, 2006, Nucl. Phys. **A768**, 118.
Alcock, C., E. Farhi, and A. Olinto, 1986, Astrophys. J. **310**, 261.
Alford, M. G., 2001, Annu. Rev. Nucl. Part. Sci. **51**, 131.
Alford, M. G., J. Berges, and K. Rajagopal, 1999, Nucl. Phys. **B558**, 219.
Alford, M. G., J. Berges, and K. Rajagopal, 2000a, Phys. Rev. Lett. **84**, 598.
Alford, M. G., J. Berges, and K. Rajagopal, 2000b, Nucl. Phys. **B571**, 269.
Alford, M. G., J. A. Bowers, J. M. Cheyne, and G. A. Cowan, 2003, Phys. Rev. D **67**, 054018.
Alford, M. G., J. A. Bowers, and K. Rajagopal, 2001, Phys. Rev. D **63**, 074016.

Alford, M. G., M. Braby, M. W. Paris, and S. Reddy, 2005, Astrophys. J. **629**, 969.
Alford, M. G., P. Jotwani, C. Kouvaris, J. Kundu, and K. Rajagopal, 2005, Phys. Rev. D **71**, 114011.
Alford, M. G., A. Kapustin, and F. Wilczek, 1999, Phys. Rev. D **59**, 054502.
Alford, M. G., C. Kouvaris, and K. Rajagopal, 2004, Phys. Rev. Lett. **92**, 222001.
Alford, M. G., C. Kouvaris, and K. Rajagopal, 2005, Phys. Rev. D **71**, 054009.
Alford, M. G., and K. Rajagopal, **2002**, J. High Energy Phys. 06 031.
Alford, M. G., K. Rajagopal, and F. Wilczek, 1998, Phys. Lett. B **422**, 247.
Alford, M. G., K. Rajagopal, and F. Wilczek, 1999, Nucl. Phys. **B537**, 443.
Alford, M. G., and S. Reddy, 2003, Phys. Rev. D **67**, 074024.
Alford, M. G., A. Schmitt, K. Rajagopal, and T. Schafer, 2008, Rev. Mod. Phys. **80**, 1455.
Alford, M. G., and Q.-h. Wang, 2005, J. Phys. G **31**, 719.
Alford, M. G., and Q.-h. Wang, 2006, J. Phys. G **32**, 63.
Allton, C. R., S. Ejiri, S. J. Hands, O. Kaczmarek, F. Karsch, E. Laermann, and C. Schmidt, 2003, Phys. Rev. D **68**, 014507.
Alpar, M. A., 1977, Astrophys. J. **213**, 527.
Alpar, M. A., P. W. Anderson, D. Pines, and J. Shaham, 1984, Astrophys. J. **278**, 791.
Alpar, M. A., D. Pines, P. W. Anderson, and J. Shaham, 1984, Astrophys. J. **276**, 325.
Amore, P., M. C. Birse, J. A. McGovern, and N. R. Walet, 2002, Phys. Rev. D **65**, 074005.
Anderson, P. W., and N. Itoh, 1975, Nature (London) **256**, 25.
Andersson, N., 1998, Astrophys. J. **502**, 708.
Anglani, R., R. Gatto, N. D. Ippolito, G. Nardulli, and M. Ruggieri, 2007, Phys. Rev. D **76**, 054007.
Anglani, R., M. Mannarelli, and M. Ruggieri, 2011, New J. Phys. **13**, 055002.
Anglani, R., G. Nardulli, M. Ruggieri, and M. Mannarelli, 2006, Phys. Rev. D **74**, 074005.
Aoki, S., *et al.* (HAL QCD Collaboration), 2012, arXiv:1206.5088.
Auzzi, R., S. Bolognesi, J. Evslin, K. Konishi, and A. Yung, 2003, Nucl. Phys. **B673**, 187.
Bahcall, J. N., and R. A. Wolf, 1965, Phys. Rev. Lett. **14**, 343.
Bailin, D., and A. Love, 1979, J. Phys. A **12**, L283.
Bailin, D., and A. Love, 1984, Phys. Rep. **107**, 325.
Balachandran, A., S. Digal, and T. Matsuura, 2006, Phys. Rev. D **73**, 074009.
Bardeen, J., L. N. Cooper, and J. R. Schrieffer, 1957a, Phys. Rev. **106**, 162.
Bardeen, J., L. N. Cooper, and J. R. Schrieffer, 1957b, Phys. Rev. **108**, 1175.
Barret, D., J.-F. Olive, and M. C. Miller, 2005, Mon. Not. R. Astron. Soc. **361**, 855.
Barrois, B. C., 1977, Nucl. Phys. **B129**, 390.
Baym, G., and S. A. Chin, 1976, Phys. Lett. **62B**, 241.
Baym, G., C. Pethick, D. Pines, and M. Ruderman, 1969, Nature (London) **224**, 872.
Baym, G., and D. Pines, 1971, Ann. Phys. (N.Y.) **66**, 816.
Beane, S. R., P. F. Bedaque, and M. J. Savage, 2000, Phys. Lett. B **483**, 131.
Bedaque, P. F., H. Caldas, and G. Rupak, 2003, Phys. Rev. Lett. **91**, 247002.
Bedaque, P. F., and T. Schafer, 2002, Nucl. Phys. **A697**, 802.
Berges, J., and K. Rajagopal, 1999, Nucl. Phys. **B538**, 215.
Blaschke, D., D. Gomez Dumm, A. G. Grunfeld, T. Klahn, and N. N. Scoccola, 2007, Phys. Rev. C **75**, 065804.
Bonanno, L., and A. Sedrakian, 2012, Astron. Astrophys. **539**, A16.
Bowers, J. A., J. Kundu, K. Rajagopal, and E. Shuster, 2001, Phys. Rev. D **64**, 014024.
Bowers, J. A., and K. Rajagopal, 2002, Phys. Rev. D **66**, 065002.
Boynton, P. E., E. J. Groth III, R. B. Partridge, and D. T. Wilkinson, 1969, IAU Circulars **2179**, 1.
Brown, G. E., K. Kubodera, D. Page, and P. Pizzochero, 1988, Phys. Rev. D **37**, 2042.
Brown, W. E., J. T. Liu, and H.-C. Ren, 2000, Phys. Rev. D **61**, 114012.
Buballa, M., 2005, Phys. Rep. **407**, 205.
Buballa, M., J. Hosek, and M. Oertel, 2003, Phys. Rev. Lett. **90**, 182002.
Buballa, M., F. Neumann, M. Oertel, and I. Shovkovy, 2004, Phys. Lett. B **595**, 36.
Buballa, M., and D. Nickel, 2010, Acta Phys. Pol. Supp. **3**, 523.
Buballa, M., and M. Oertel, 1999, Phys. Lett. B **457**, 261.
Bulaevskĭ, L. N., 1973, Sov. Phys. JETP **37**, 1133.
Bulgac, A., and M. M. Forbes, 2008, Phys. Rev. Lett. **101**, 215301.
Bulgac, A., M. M. Forbes, and A. Schwenk, 2006, Phys. Rev. Lett. **97**, 020402.
Carlson, J., and S. Reddy, 2005, Phys. Rev. Lett. **95**, 060401.
Carter, G. W., and D. Diakonov, 1999, Phys. Rev. D **60**, 016004.
Casalbuoni, R., M. Ciminale, R. Gatto, G. Nardulli, and M. Ruggieri, 2006, Phys. Lett. B **642**, 350.
Casalbuoni, R., M. Ciminale, M. Mannarelli, G. Nardulli, M. Ruggieri, and R. Gatto, 2004, Phys. Rev. D **70**, 054004.
Casalbuoni, R., F. De Fazio, R. Gatto, G. Nardulli, and M. Ruggieri, 2002, Phys. Lett. B **547**, 229.
Casalbuoni, R., Z.-y. Duan, and F. Sannino, 2000, Phys. Rev. D **62**, 094004.
Casalbuoni, R., E. Fabiano, R. Gatto, M. Mannarelli, and G. Nardulli, 2002, Phys. Rev. D **66**, 094006.
Casalbuoni, R., and R. Gatto, 1999, Phys. Lett. B **464**, 111.
Casalbuoni, R., R. Gatto, N. Ippolito, G. Nardulli, and M. Ruggieri, 2005, Phys. Lett. B **627**, 89.
Casalbuoni, R., R. Gatto, M. Mannarelli, and G. Nardulli, 2001, Phys. Lett. B **511**, 218.
Casalbuoni, R., R. Gatto, M. Mannarelli, and G. Nardulli, 2002a, Phys. Rev. D **66**, 014006.
Casalbuoni, R., R. Gatto, M. Mannarelli, and G. Nardulli, 2002b, Phys. Lett. B **524**, 144.
Casalbuoni, R., R. Gatto, M. Mannarelli, G. Nardulli, M. Ruggieri, and S. Stramaglia, 2003, Phys. Lett. B **575**, 181.
Casalbuoni, R., R. Gatto, M. Mannarelli, G. Nardulli, and M. Ruggieri, 2005, Phys. Lett. B **605**, 362.
Casalbuoni, R., R. Gatto, and G. Nardulli, 2001, Phys. Lett. B **498**, 179.
Casalbuoni, R., and G. Nardulli, 2004, Rev. Mod. Phys. **76**, 263.
Castorina, P., M. Grasso, M. Oertel, M. Urban, and D. Zappala, 2005, Phys. Rev. A **72**, 025601.
Chandrasekhar, B. S., 1962, Appl. Phys. Lett. **1**, 7.
Chin, C., R. Grimm, P. Julienne, and E. Tiesinga, 2010, Rev. Mod. Phys. **82**, 1225.
Chiu, H.-Y., and E. E. Salpeter, 1964, Phys. Rev. Lett. **12**, 413.
Ciminale, M., G. Nardulli, M. Ruggieri, and R. Gatto, 2006, Phys. Lett. B **636**, 317.
Cirigliano, V., S. Reddy, and R. Sharma, 2011, Phys. Rev. C **84**, 045809.
Clogston, A. M., 1962, Phys. Rev. Lett. **9**, 266.
Collins, J. C., and M. J. Perry, 1975, Phys. Rev. Lett. **34**, 1353.

Cooper, L. N., 1956, Phys. Rev. **104**, 1189.
de Gennes, P. G., 1966, *Superconductivity of Metals and Alloys* (Benjamin, New York).
Demorest, P., T. Pennucci, S. Ransom, M. Roberts, and J. Hessels, 2010, Nature (London) **467**, 1081.
Eguchi, T., 1976, Phys. Rev. D **14**, 2755.
Espinoza, C. M., A. G. Lyne, B. W. Stappers, and M. Kramer, 2011, Mon. Not. R. Astron. Soc. **414**, 1679.
Eto, M., M. Nitta, and N. Yamamoto, 2010, Phys. Rev. Lett. **104**, 161601.
Evans, N. J., J. Hormuzdiar, S. D. H. Hsu, and M. Schwetz, 2000, Nucl. Phys. **B581**, 391.
Evans, N. J., S. D. H. Hsu, and M. Schwetz, 1999, Phys. Lett. B **449**, 281.
Ferrer, E. J., and V. de la Incera, 2007, Phys. Rev. D **76**, 114012.
Fodor, Z., and S. D. Katz, 2002, Phys. Lett. B **534**, 87.
Forbes, M. M., and A. R. Zhitnitsky, 2002, Phys. Rev. D **65**, 085009.
Forbes, M. M., E. Gubankova, W. Liu Vincent, and F. Wilczek, 2005, Phys. Rev. Lett. **94**, 017001.
Fraga, E. S., R. D. Pisarski, and J. Schaffner-Bielich, 2001, Phys. Rev. D **63**, 121702.
Frautschi, S. C., 1980, *Hadronic Matter at Extreme Energy Density*, Ettore Majorana International Science Series Vol. 2 (Springer, New York).
Freire, P. C. C., A. Wolszczan, M. van den Berg, and J. W. T. Hessels, 2008, Astrophys. J. **679**, 1433.
Friedman, J. L., and S. M. Morsink, 1998, Astrophys. J. **502**, 714.
Fromm, M., J. Langelage, S. Lottini, and O. Philipsen, **2012**, J. High Energy Phys. 01 042.
Fukushima, K., 2005, Phys. Rev. D **72**, 074002.
Fukushima, K., 2006, Phys. Rev. D **73**, 094016.
Fukushima, K., C. Kouvaris, and K. Rajagopal, 2005, Phys. Rev. D **71**, 034002.
Fulde, P., and R. A. Ferrell, 1964, Phys. Rev. **135**, A550.
Gatto, R., and M. Ruggieri, 2007, Phys. Rev. D **75**, 114004.
Gerlach, U. H., 1968, Phys. Rev. **172**, 1325.
Giannakis, I., D.-f. Hou, and H.-C. Ren, 2005, Phys. Lett. B **631**, 16.
Giannakis, I., and H.-C. Ren, 2005a, Phys. Lett. B **611**, 137.
Giannakis, I., and H.-C. Ren, 2005b, Nucl. Phys. **B723**, 255.
Giorgini, S., L. P. Pitaevskii, and S. Stringari, 2008, Rev. Mod. Phys. **80**, 1215.
Glendenning, N. K., and C. Kettner, 2000, Astron. Astrophys. **353**, L9.
Gorbar, E., 2000, Phys. Rev. D **62**, 014007.
Gorbar, E. V., M. Hashimoto, and V. Miransky, 2007, Phys. Rev. D **75**, 085012.
Gorbar, E. V., M. Hashimoto, V. Miransky, and I. Shovkovy, 2006, Phys. Rev. D **73**, 111502.
Gorbar, E. V., M. Hashimoto, and V. A. Miransky, 2006a, Phys. Lett. B **632**, 305.
Gorbar, E. V., M. Hashimoto, and V. A. Miransky, 2006b, Phys. Rev. Lett. **96**, 022005.
Gradshteyn, I. S., and I. M. Ryzhik, 1980, *Table of Integrals, Series and Products* (Academic Press, New York).
Grigorian, H., D. Blaschke, and D. N. Aguilera, 2004, Phys. Rev. C **69**, 065802.
Gross, D. J., and A. Neveu, 1974, Phys. Rev. D **10**, 3235.
Gubankova, E., M. Mannarelli, and R. Sharma, 2010, Ann. Phys. (N.Y.) **325**, 1987.
Gubankova, E., A. Schmitt, and F. Wilczek, 2006, Phys. Rev. B **74**, 064505.
Gubankova, E., W. Vincent Liu, and F. Wilczek, 2003, Phys. Rev. Lett. **91**, 032001.
Gubbels, K., and H. Stoof, 2012, arXiv:1205.0568.
Gudmundsson, E. H., C. J. Pethick, and R. I. Epstein, 1982, Astrophys. Lett. **259**, L19.
Haensel, P., 2003, in *Equation of State of Dense Matter and Maximum Mass of Neutron Stars*, EAS Publications Series Vol. 7, edited by C. Motch and J.-M. Hameury, p. 249.
Hanany, A., and D. Tong, **2003**, J. High Energy Phys. 07 037.
Haskell, B., N. Andersson, D. I. Jones, and L. Samuelsson, 2007, Phys. Rev. Lett. **99**, 231101.
He, L., M. Jin, and P. Zhuang, 2007, Phys. Rev. D **75**, 036003.
Heinke, C. O., and W. C. G. Ho, 2010, Astrophys. J. **719**, L167.
Hess, D., and A. Sedrakian, 2011, Phys. Rev. D **84**, 063015.
Ho, W. C. G., K. Glampedakis, and N. Andersson, 2012, Mon. Not. R. Astron. Soc. **422**, 2632.
Hong, D. K., 2001, Acta Phys. Pol. B **32**, 1253.
Hong, D. K., 2005, arXiv:hep-ph/0506097.
Hong, D. K., V. A. Miransky, I. A. Shovkovy, and L. C. R. Wijewardhana, 2000, Phys. Rev. D **61**, 056001.
Hong, D. K., 2000a, Phys. Lett. B **473**, 118.
Hong, D. K., 2000b, Nucl. Phys. **B582**, 451.
Hsu, S. D., 2000, arXiv:hep-ph/0003140.
Huang, M., and I. Shovkovy, 2003, Nucl. Phys. **A729**, 835.
Huang, M., and I. A. Shovkovy, 2004a, Phys. Rev. D **70**, 051501.
Huang, M., and I. A. Shovkovy, 2004b, Phys. Rev. D **70**, 094030.
Huxley, A. D., C. Paulson, O. Laborde, J. L. Tholence, D. Sanchez, A. Junod, and R. Calemczuk, 1993, J. Phys. Condens. Matter **5**, 7709.
Iida, K., and G. Baym, 2002, Phys. Rev. D **66**, 014015.
Iida, K., and K. Fukushima, 2006, Phys. Rev. D **74**, 074020.
Iida, K., T. Matsuura, M. Tachibana, and T. Hatsuda, 2004, Phys. Rev. Lett. **93**, 132001.
Ippolito, N., M. Ruggieri, D. Rischke, A. Sedrakian, and F. Weber, 2008, Phys. Rev. D **77**, 023004.
Ippolito, N. D., G. Nardulli, and M. Ruggieri, **2007**, J. High Energy Phys. 04 036.
Ivanenko, D., and D. F. Kurdgelaidze, 1969, Lett. Nuovo Cimento **2**, 13.
Ivanenko, D. D., and D. F. Kurdgelaidze, 1965, Astrophysics **1**, 251.
Iwamoto, N., 1980, Phys. Rev. Lett. **44**, 1637.
Iwamoto, N., 1981, Neutrino Processes in Dense Matter, Ph.D. thesis (Illinois University, Urbana-Champaign).
Iwamoto, N., 1982, Ann. Phys. (N.Y.) **141**, 1.
Jaikumar, P., C. D. Roberts, and A. Sedrakian, 2006, Phys. Rev. C **73**, 042801.
Kaplan, D., and S. Reddy, 2002, Phys. Rev. D **65**, 054042.
Ketterle, W., and M. W. Zwierlein, 2008, Nuovo Cimento Riv. Ser. **31**, 247.
Kiriyama, O., 2006, Phys. Rev. D **74**, 114011.
Kiriyama, O., D. Rischke, and I. Shovkovy, 2006, Phys. Lett. B **643**, 331.
Klahn, T., D. Blaschke, F. Sandin, C. Fuchs, A. Faessler, H. Grigorian, G. Röpke, and J. Trümper, 2007, Phys. Lett. B **654**, 170.
Klahn, T., D. Blaschke, and F. Weber, 2012, Phys. Part. Nucl. Lett. **9**, 484.
Knippel, B., and A. Sedrakian, 2009, Phys. Rev. D **79**, 083007.
Kojo, T., R. D. Pisarski, and A. Tsvelik, 2010, Phys. Rev. D **82**, 074015.
Kryjevski, A., 2008, Phys. Rev. D **77**, 014018.
Kryjevski, A., and T. Schfer, 2005, Phys. Lett. B **606**, 52.
Kundu, J., and K. Rajagopal, 2002, Phys. Rev. D **65**, 094022.

Landau, L. D., and E. M. Lifshits, 1959, *Theory of Elasticity*, edited by L. D. Landau and E. M. Lifshits, Addison-Wesley Physics Books (Addison-Wesley, London).
Larkin, A. I., and Y. N. Ovchinnikov, 1964, Zh. Eksp. Teor. Fiz. **47**, 1136.
Lattimer, J. M., and M. Prakash, 2001, Astrophys. J. **550**, 426.
Lattimer, J. M., and M. Prakash, 2007, Phys. Rep. **442**, 109.
Lattimer, J. M., M. Prakash, C. J. Pethick, and P. Haensel, 1991, Phys. Rev. Lett. **66**, 2701.
Lattimer, J. M., K. A. van Riper, M. Prakash, and M. Prakash, 1994, Astrophys. J. **425**, 802.
Le Bellac, M., 2000, *Thermal Field Theory*, Cambridge Monographs on Mathematical Physics (Cambridge University Press, Cambridge, England).
Leibovich, A. K., K. Rajagopal, and E. Shuster, 2001, Phys. Rev. D **64**, 094005.
Leutwyler, H., 1997, Helv. Phys. Acta **70**, 275.
Lin, L.-M., 2007, Phys. Rev. D **76**, 081502.
Liu, W. V., and F. Wilczek, 2003, Phys. Rev. Lett. **90**, 047002.
Logoteta, D., C. Providencia, I. Vidana, and I. Bombaci, 2012, Phys. Rev. C **85**, 055807.
Lyne, A. G., *et al.*, 2004, Science **303**, 1153.
Maieron, C., M. Baldo, G. F. Burgio, and H. J. Schulze, 2004, Phys. Rev. D **70**, 043010.
Mannarelli, M., G. Nardulli, and M. Ruggieri, 2006, Phys. Rev. A **74**, 033606.
Mannarelli, M., K. Rajagopal, and R. Sharma, 2006, Phys. Rev. D **73**, 114012.
Mannarelli, M., K. Rajagopal, and R. Sharma, 2007, Phys. Rev. D **76**, 074026.
Matsuda, Y., and H. Shimahara, 2007, J. Phys. Soc. Jpn. **76**, 051005.
Maxwell, O., G. E. Brown, D. K. Campbell, R. F. Dashen, and J. T. Manassah, 1977, Astrophys. J. **216**, 77.
McLerran, L., and R. D. Pisarski, 2007, Nucl. Phys. **A796**, 83.
Muther, H., and A. Sedrakian, 2002, Phys. Rev. Lett. **88**, 252503.
Muto, T., and T. Tatsumi, 1988, Prog. Theor. Phys. **79**, 461.
Nardulli, G., 2002, Riv. Nuovo Cimento **25N3**, 1.
Nickel, D., 2009, Phys. Rev. D **80**, 074025.
Nickel, D., and M. Buballa, 2009, Phys. Rev. D **79**, 054009.
Oppenheimer, J. R., and G. M. Volkoff, 1939, Phys. Rev. **55**, 374.
Orsaria, M., H. Rodrigues, F. Weber, and G. Contrera, 2013, Phys. Rev. D **87**, 023001.
Owen, B. J., 2005, Phys. Rev. Lett. **95**, 211101.
Page, D., J. M. Lattimer, M. Prakash, and A. W. Steiner, 2004, Astrophys. J. Suppl. Ser. **155**, 623.
Page, D., M. Prakash, J. M. Lattimer, and A. W. Steiner, 2011, Phys. Rev. Lett. **106**, 081101.
Palomba, C., *et al.* (LIGO Scientific Collaboration and Virgo Collaboration), 2012, arXiv:1201.3176.
Pao, C.-H., S.-T. Wu, and S.-K. Yip, 2006, Phys. Rev. B **73**, 132506.
Partridge, G. B., W. Li, R. I. Kamar, Y.-a. Liao, and R. G. Hulet, 2006, Science **311**, 503.
Pethick, C. J., 1992, Rev. Mod. Phys. **64**, 1133.
Pisarski, R. D., and D. H. Rischke, 2000a, Phys. Rev. D **61**, 074017.
Pisarski, R. D., and D. H. Rischke, 2000b, Phys. Rev. D **61**, 051501.
Polchinski, J., 1992, arXiv:hep-th/9210046.
Prakash, M., J. M. Lattimer, J. A. Pons, A. W. Steiner, and S. Reddy, 2001, Lect. Notes Phys. **578**, 364.
Radhakrishnan, V., and R. N. Manchester, 1969, Nature (London) **222**, 228.
Radzihovsky, L., and D. E. Sheehy, 2010, Rep. Prog. Phys. **73**, 076501.
Rajagopal, K., and R. Sharma, 2006, Phys. Rev. D **74**, 094019.
Rajagopal, K., and F. Wilczek, 2000, arXiv:hep-ph/0011333.
Rapp, R., T. Schafer, E. V. Shuryak, and M. Velkovsky, 1998, Phys. Rev. Lett. **81**, 53.
Rapp, R., T. Schafer, E. V. Shuryak, and M. Velkovsky, 2000, Ann. Phys. (N.Y.) **280**, 35.
Rapp, R., E. V. Shuryak, and I. Zahed, 2001, Phys. Rev. D **63**, 034008.
Reddy, S., and G. Rupak, 2005, Phys. Rev. C **71**, 025201.
Reichley, P. E., and G. S. Downs, 1969, Nature (London) **222**, 229.
Richards, D. W., G. H. Pettengill, J. A. Roberts, C. C. Counselman, and J. Rankin, 1969, IAU Circulars **2181**, 1.
Rischke, D. H., 2000a, Phys. Rev. D **62**, 054017.
Rischke, D. H., 2000b, Phys. Rev. D **62**, 034007.
Rischke, D. H., 2004, Prog. Part. Nucl. Phys. **52**, 197.
Rischke, D. H., and I. A. Shovkovy, 2002, Phys. Rev. D **66**, 054019.
Rischke, D. H., D. T. Son, and M. A. Stephanov, 2001, Phys. Rev. Lett. **87**, 062001.
Rizzi, M., M. Polini, M. A. Cazalilla, M. R. Bakhtiari, M. P. Tosi, and R. Fazio, 2008, Phys. Rev. B **77**, 245105.
Roberge, A., and N. Weiss, 1986, Nucl. Phys. **B275**, 734.
Ruderman, M., 1969, Nature (London) **223**, 597.
Ruderman, M., 1972, Annu. Rev. Astron. Astrophys. **10**, 427.
Ruester, S. B., V. Werth, M. Buballa, I. A. Shovkovy, and D. H. Rischke, 2005, Phys. Rev. D **72**, 034004.
Ruester, S. B., V. Werth, M. Buballa, I. A. Shovkovy, and D. H. Rischke, 2006a, arXiv:nucl-th/0602018.
Ruester, S. B., V. Werth, M. Buballa, I. A. Shovkovy, and D. H. Rischke, 2006b, Phys. Rev. D **73**, 034025.
Rupak, G., and P. Jaikumar, 2012, arXiv:1209.4343.
Saint-James, D., G. Sarma, and E. J. Thomas, 1969, *Type II Superconductivity* (Pergamon Press, New York).
Sandin, F., and D. Blaschke, 2007, Phys. Rev. D **75**, 125013.
Sarma, G., 1963, J. Phys. Chem. Solids **24**, 1029.
Schafer, T., 2000a, Nucl. Phys. **B575**, 269.
Schafer, T., 2000b, Phys. Rev. D **62**, 094007.
Schafer, T., 2003a, Nucl. Phys. **A728**, 251.
Schafer, T., 2003b, arXiv:hep-ph/0304281.
Schafer, T., and E. V. Shuryak, 1998, Rev. Mod. Phys. **70**, 323.
Schafer, T., and F. Wilczek, 1999a, Phys. Rev. Lett. **82**, 3956.
Schafer, T., and F. Wilczek, 1999b, Phys. Lett. B **450**, 325.
Schafer, T., and F. Wilczek, 1999c, Phys. Rev. D **60**, 114033.
Schertler, K., C. Greiner, J. Schaffner-Bielich, and M. Thoma, 2000, Nucl. Phys. **A677**, 463.
Schmitt, A., 2005, Phys. Rev. D **71**, 054016.
Schmitt, A., Q. Wang, and D. H. Rischke, 2002, Phys. Rev. D **66**, 114010.
Schmitt, A., Q. Wang, and D. H. Rischke, 2004, Phys. Rev. D **69**, 094017.
Sedrakian, A., 2007, Prog. Part. Nucl. Phys. **58**, 168.
Sedrakian, A., 2013, Astron. Astrophys. **555**, L10.
Shapiro, S. L., and S. A. Teukolsky, 1983, *Research Supported by the National Science Foundation* (Wiley-Interscience, New York), p. 663.
Sharma, R., and S. Reddy, 2008, Phys. Rev. A **78**, 063609.
Sheehy, D. E., and L. Radzihovsky, 2006, Phys. Rev. Lett. **96**, 060401.
Shin, Y.-I., C. H. Schunck, A. Schirotzek, and W. Ketterle, 2008, Nature (London) **451**, 689.
Shovkovy, I., M. Hanauske, and M. Huang, 2003, arXiv:hep-ph/0310286.
Shovkovy, I., and M. Huang, 2003, Phys. Lett. B **564**, 205.
Shovkovy, I., and L. Wijewardhana, 1999, Phys. Lett. B **470**, 189.

Shternin, P. S., D. G. Yakovlev, C. O. Heinke, W. C. G. Ho, and D. J. Patnaude, 2011, Mon. Not. R. Astron. Soc. **412**, L108.
Son, D., 2005, Phys. Rev. Lett. **94**, 175301.
Son, D. T., 1999, Phys. Rev. D **59**, 094019.
Son, D. T., 2002, arXiv:hep-ph/0204199.
Son, D. T., and M. A. Stephanov, 2000a, Phys. Rev. D **61**, 074012.
Son, D. T., and M. A. Stephanov, 2000b, Phys. Rev. D **62**, 059902.
Son, D. T., and M. A. Stephanov, 2006, Phys. Rev. A **74**, 013614.
Steiner, A. W., S. Reddy, and M. Prakash, 2002, Phys. Rev. D **66**, 094007.
Strohmayer, T., H. M. van Horn, S. Ogata, H. Iyetomi, and S. Ichimaru, 1991, Astrophys. J. **375**, 679.
Tolman, R. C., 1939, Phys. Rev. **55**, 364.
Uji, S., *et al.*, 2006, Phys. Rev. Lett. **97**, 157001.
Vanderheyden, B., and A. D. Jackson, 2000, Phys. Rev. D **62**, 094010.
F. Weber, 1999, Ed., *Pulsars as Astrophysical Laboratories for Nuclear and Particle Physics* (Institute of Physics, Bristol).
Weber, F., R. Negreiros, and P. Rosenfield, 2007, arXiv:0705.2708.
Wu, S.-T., and S. Yip, 2003, Phys. Rev. A **67**, 053603.
Xu, R.-X., 2003, Astrophys. J. **596**, L59.
Yang, K., 2005, arXiv:cond-mat/0508484.
Yang, K., 2006, arXiv:cond-mat/0603190.
Zwierlein, M. W., and W. Ketterle, 2006, arXiv:cond-mat/0603489.
Zwierlein, M. W., A. Schirotzek, C. H. Schunck, and W. Ketterle, 2006, Science **311**, 492.